

FIELD TESTING OF A CROSSFLOW  
WATER TURBINE

By

ALEJANDRO F. TONGCO

Bachelor of Science  
in Mechanical Engineering  
Collegio de San Jose-Recoletos  
Cebu City, Philippines  
1973

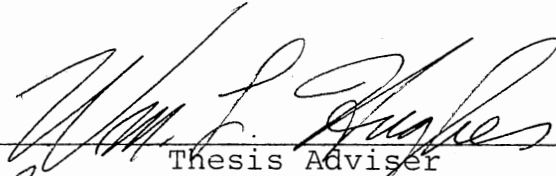
Master of Science  
University of the Philippines  
at Los Banos  
College, Laguna  
1979

Submitted to the Faculty of the  
Graduate College of the  
Oklahoma State University  
in partial fulfillment of  
the requirements for  
the Degree of  
DOCTOR OF PHILOSOPHY  
July 1988

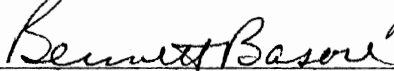
Thesis  
1988D  
T665F  
cop. 2

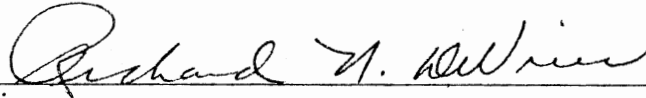
FIELD TESTING OF A CROSSFLOW  
WATER TURBINE

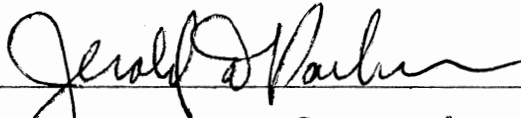
Thesis Approved:



Thesis Adviser









Dean of the Graduate College

## ACKNOWLEDGEMENT

I wish to express my deepest gratitude to all the people who assisted me in making this work a success.

To James "Fred" Myers of OSU Fire Service Training, I am most indebted. His wholehearted and enthusiastic help in all phases of the conduct of the experiment was unprecedented. His unrelenting effort made the experiment a success. Thanks a million, Fred! I wish to thank also Mr. Harold R. Mace, director of Fire Service Training, for the use of fire training equipment and facilities.

I am also thankful to my thesis adviser, Dr. William L. Hughes, for his invaluable advise and for the use of the facilities and men of his company, InEn Corporation, during the turbine's construction. Sincere thanks are due to my major adviser, Dr. Bennett L. Basore for his invaluable guidance and financial support for the thesis. Let me also thank Dr. Jerald D. Parker and Dr. Richard N. DeVries for their advisement.

The help of Ramon Laguna in data gathering is deeply appreciated. I am also grateful to Tatay, Mana, Loloy, Lina, Bebbie, and Dina for their moral and financial help.

A very special thank-you to my wife, Adele, and my children, Tara and Brent, who stood by me through all my trials and tribulations. I could never thank you enough.

## TABLE OF CONTENTS

Chapter	Page
I. INTRODUCTION. . . . .	1
Background . . . . .	1
Rationale. . . . .	5
Objectives . . . . .	5
II. REVIEW OF LITERATURE. . . . .	7
Water Turbines . . . . .	7
Power and Efficiency of Water Turbine. . .	8
Brief History and Description of the Crossflow Turbine. . . . .	9
Theory . . . . .	17
Previous Studies . . . . .	21
III. DESIGN AND CONSTRUCTION . . . . .	39
Design of the Crossflow Turbine Prototype. . . . .	39
Construction of the Turbine. . . . .	47
Construction of the Turbine Nozzle and Adapter . . . . .	60
Construction of the Prony Brake. . . . .	63
IV. INSTRUMENTATION AND TEST PROCEDURE. . . . .	67
Instrumentation. . . . .	67
Test Procedure . . . . .	73
V. RESULTS AND DISCUSSION. . . . .	78
Calculation of Total Available Head, H . .	78
Runner Performance . . . . .	84
VI. DEVELOPMENT OF A PREDICTION EQUATION. . . . .	118
Selection of Pi Terms. . . . .	118
Experimental Design and Analysis . . . . .	122
The Prediction Equation. . . . .	140
Effect of Flow Rate $Q_s$ and Number of Blades $Z$ . . . . .	142
Comparison of Theoretical and Empirical Turbine Efficiencies . . . . .	146

Chapter	Page
VII. CONCLUSIONS AND RECOMMENDATIONS . . . . .	148
BIBLIOGRAPHY . . . . .	152

## LIST OF TABLES

Table	Page
I. Nozzle Pressure Data at Various Flow Rates. . .	81
II. Performance Data for the 10-Blade Runner at 300 gpm . . . . .	99
III. Performance Data for the 10-Blade Runner at 400 gpm . . . . .	100
IV. Performance Data for the 10-Blade Runner at 500 gpm . . . . .	101
V. Performance Data for the 15-Blade Runner at 300 gpm . . . . .	102
VI. Performance Data for the 15-Blade Runner at 400 gpm . . . . .	103
VII. Performance Data for the 15-Blade Runner at 500 gpm . . . . .	104
VIII. Performance Data for the 20-Blade Runner at 300 gpm . . . . .	105
IX. Performance Data for the 20-Blade Runner at 400 gpm . . . . .	106
X. Performance Data for the 20-Blade Runner at 500 gpm . . . . .	107
XI. Performance Data for the 30-Blade Runner at 300 gpm . . . . .	108
XII. Performance Data for the 30-Blade Runner at 400 gpm . . . . .	109
XIII. Performance Data for the 30-Blade Runner at 500 gpm . . . . .	110
XIV. Summary of Turbine Efficiency Equations as a Function of Rotative Speed. . . . .	111

Table	Page
XV. Maximum Efficiency and Corresponding Optimum Rotative Speed and Velocity Coefficient of Runners at Various Flow Rates. . . . .	114
XVI. Pertinent Variables for Output Power Prediction of a Small Crossflow Turbine . . .	119
XVII. Determining the Rank of the Dimensional Matrix. . . . .	121
XVIII. Experimental Plan . . . . .	123
XIX. Data Generated Using the Empirical Efficiency Equation (Equation (5.17)) for the 15-Blade Runner at 400 gpm. . . . .	127
XX. Performance Data of the 15-Blade Runner Held at N=300 for Various Flow Rates. . . . .	130
XXI. Pi-Terms for Data In Table XX . . . . .	134
XXII. Performance Data of the 6-Blade Runner at 400 gpm. . . . .	136
XXIII. Comparison of Turbine Efficiencies From Theoretical and Empirical Formulas at N=300 rpm . . . . .	147



## LIST OF FIGURES

Figure	Page
2.1. Schematic Drawing of a Crossflow Turbine . . . . .	11
2.2. Exploded View of an Ossberger Crossflow Turbine Assembly . . . . .	12
2.3. Cross-sectional View of Two Crossflow Turbines . . . . .	13
2.4. Efficiency Curve of a Crossflow Turbine with Divided Gate. . . . .	15
2.5. Inclination of Water Jet Entering the Runner . . . . .	18
2.6. The Two Velocity Stages of a Crossflow Turbine. . . . .	19
2.7. Outer Velocity Diagrams of a Crossflow Turbine Neglecting Shock Losses. . . . .	22
2.8. Outer Velocity Diagrams of a Crossflow Turbine Taking into Account Head Loss Due to Friction on the Blades . . . . .	27
2.9. Idealized Outer Velocity Diagrams of a Crossflow Turbine . . . . .	30
2.10. Outer Velocity Diagrams of a Crossflow Turbine in Actual Flow . . . . .	32
2.11. A Modification of the Outer Velocity Diagrams of Figure 2.10 . . . . .	35
2.12. Schematic Diagram of the Flow Pattern Inside of the Runner . . . . .	36
3.1. Plan for the Side Disk of the 10-Blade Runner. . . . .	48
3.2. Plan for the Side Disk of the 15-Blade Runner. . . . .	49

Figure	Page
3.3. Plan for the Side Disk of the 20-Blade Runner. . . . .	50
3.4. Plan for the Side Disk of the 30-Blade Runner. . . . .	51
3.5. Plan for the Nozzle. . . . .	52
3.6. Plan for the Nozzle Adaptor. . . . .	53
3.7. The Finished Runners (10, 15, and 20 Blades) . . . . .	57
3.8. The 30-Blade Runner. . . . .	58
3.9. The Finished Shaft and Hubs. . . . .	59
3.10. The Finished Fire Hose Adaptor, Nozzle Adaptor and Nozzle. . . . .	61
3.11. The Assembled Fire Hose Adaptor, Nozzle Adaptor and Nozzle. . . . .	62
3.12. The Crossflow Turbine Prototype. . . . .	64
3.13. Prony Brake Assembly . . . . .	65
4.1. Firetruck as Pump in the Water Supply Network . . . . .	68
4.2. Flowmeter Readout. . . . .	70
4.3. Weighing Scale . . . . .	71
4.4. Tachometer . . . . .	72
4.5 Schematics for Power and Efficiency Determination for a Particular Runner with Z Blades and at a Particular Supply Flow Rate $Q_s$ . . . . .	74
4.6. Measurement of Rotative Speed and Torque . . . . .	75
4.7. The Crossflow Turbine in Operation . . . . .	76
4.8. An Inside View of the Operating Turbine. . . . .	77

Figure	Page
5.1. Point Location of Pitot-Static Tube at Nozzle Cross-Section (Direction of Flow is Toward the Reader) . . . . .	79
5.2. Measurement of Nozzle Cross-Section Pressures . . . . .	82
5.3. Nozzle Dynamic Head as a Function of Supply Flow Rate. . . . .	83
5.4. Efficiency as a Function of Rotative Speed for the 10-Blade Runner at 300 gpm . . . . .	87
5.5. Efficiency as a Function of Rotative Speed for the 10-Blade Runner at 400 gpm . . . . .	88
5.6. Efficiency as a Function of Rotative Speed for the 10-Blade Runner at 500 gpm . . . . .	89
5.7. Efficiency as a Function of Rotative Speed for the 15-Blade Runner at 300 gpm . . . . .	90
5.8. Efficiency as a Function of Rotative Speed for the 15-Blade Runner at 400 gpm . . . . .	91
5.9. Efficiency as a Function of Rotative Speed for the 15-Blade Runner at 500 gpm . . . . .	92
5.10. Efficiency as a Function of Rotative Speed for the 20-Blade Runner at 300 gpm . . . . .	93
5.11. Efficiency as a Function of Rotative Speed for the 20-Blade Runner at 400 gpm . . . . .	94
5.12. Efficiency as a Function of Rotative Speed for the 20-Blade Runner at 500 gpm . . . . .	95
5.13. Efficiency as a Function of Rotative Speed for the 30-Blade Runner at 300 gpm . . . . .	96
5.14. Efficiency as a Function of Rotative Speed for the 30-Blade Runner at 400 gpm . . . . .	97
5.15. Efficiency as a Function of Rotative Speed for the 30-Blade Runner at 500 gpm . . . . .	98
5.16. Relationship Between Turbine Efficiency $E$ and Supply Flow Rate $Q_s$ for Various Number of Blades $Z$ . . . . .	115

Figure	Page
5.17. Relationship Between Turbine Efficiency E and Number of Blades Z at Various Levels of Supply Flow Rate $Q_s$ . . . . .	116
5.18. Relationship Between Optimum Rotative Speed $N_o$ and Supply Flow Rate $Q_s$ for Various Number of Blades Z . . . . .	117
6.1. Relationship Between $\Pi_1$ and $\Pi_2$ , with $\Pi_3$ and $\Pi_4$ as Constants . . . . .	129
6.2. Relationship Between Runner Efficiency and Flow Rate for the 15-Blade Runner Held at 300 rpm . . . . .	132
6.3. Relationship Between $\Pi_1$ and $\Pi_3$ , with $\Pi_2$ and $\Pi_4$ as Constants . . . . .	133
6.4. Performance Curve of the 6-Blade Runner at 400 gpm . . . . .	137
6.5. Relationship Between $\Pi_1$ and $\Pi_4$ , with $\Pi_2$ and $\Pi_3$ as Constants . . . . .	139
6.6. Effect of Flow Rate on Turbine Efficiency. . . .	143
6.7. Effect of Number of Blades on Turbine Efficiency . . . . .	145

## LIST OF SYMBOLS

$A$	cross-sectional area of the nozzle
$C$	nozzle coefficient
$c$	chord length of blade
$D_1$	outside diameter of runner
$D_2$	inside diameter of runner
$E$	turbine efficiency
$E_M$	Mockmore and Merryfield's turbine efficiency
$E_D$	Durali's turbine efficiency
$E_H$	Haimerl's turbine efficiency
$E_C$	turbine efficiency derived from curve
$E_P$	predicted turbine efficiency
$E_h$	hydraulic efficiency
$E_m$	mechanical efficiency
$E_q$	volumetric efficiency
$E_{max}$	maximum turbine efficiency
$F$	brake force
$g$	acceleration due to gravity
$H$	total available head
$H_n$	average nozzle head
$H_{nd}$	average nozzle dynamic head
$H_{ns}$	average nozzle static head

$h$	distance from nozzle tip to center axis of the runner
$K$	blade constant
$K_1, K_2$	predicted turbine efficiency constants
$k_1, k_2, k_3$	constants or slopes of straight lines in the log-log space
$L$	runner length
$N$	rotational speed of runner
$N_o$	optimum rotative speed
$P_i$	input or water power
$P_o$	output or brake power
$P_{op}$	predicted output power
$P_{1-2}$	power developed in the first stage
$P_{3-4}$	power developed in the second stage
$P(1), P(2), P(3)$	coefficients in a second degree equation
$P_n$	nozzle pressure
$Q_s$	supply of flow rate of water
$Q_t$	flow rate through the turbine runner
$r$	radius of curvature of the blade
$S_o$	width of nozzle throat
$T$	torque
$t_o$	blade thickness
$t_1$	blade spacing at outer diameter
$t_2$	blade spacing at inner diameter
$U_1$	peripheral velocity of the first stage inlet
$U_2$	peripheral velocity of the first stage outlet

$U_3$	peripheral velocity of the second stage inlet
$U_4$	peripheral velocity of the second stage outlet
$U_1/V_1$	velocity coefficient
$(U_1/V_1)_o$	optimum velocity coefficient
$V_1$	absolute velocity of the first stage inlet
$V_2$	absolute velocity of the first stage outlet
$V_3$	absolute velocity of the second stage inlet
$V_4$	absolute velocity of the second stage outlet
$v_{r1}$	relative velocity of the first stage inlet
$v_{r2}$	relative velocity of the first stage outlet
$v_{r3}$	relative velocity of the second stage inlet
$v_{r4}$	relative velocity of the second stage outlet
$v_{u1}$	tangential velocity of the first stage inlet
$v_{u2}$	tangential velocity of the first stage outlet
$v_{u3}$	tangential velocity of the second stage inlet
$v_{u4}$	tangential velocity of the second stage outlet
$Z$	number of blades
$\alpha_1$	absolute velocity angle of the first stage inlet
$\alpha_2$	absolute velocity angle of the first stage outlet
$\alpha_3$	absolute velocity angle of the second stage inlet
$\alpha_4$	absolute velocity angle of the second stage outlet
$\beta_1$	relative velocity angle of the first stage inlet

$\beta_2$	relative velocity angle of the first stage outlet
$\beta_3$	relative velocity angle of the second stage inlet
$\beta_4$	relative velocity angle of the second stage outlet
$\gamma$	specific weight of water
$\delta$	nozzle entry angle
$\theta$	angle covered by blade curvature
$\mu$	dynamic viscosity of water
$\Pi$	a dimensionless group of physical quantities
$\sigma$	solidity of blades
$\phi$	a function that determines the character of the component equation
$\psi$	coefficient to account for shock losses in the blades
$\psi_1$	coefficient to account for water acceleration inside the runner
$\Omega$	angular velocity of the runner
$\ell$	length of moment arm



## CHAPTER I

### INTRODUCTION

#### Background

The energy crunch of the early 70's triggered a frantic effort by research organizations to make more efficient use of the increasingly expensive fossil fuel resources. On the other hand, alternative energy sources were vigorously searched and developed in anticipation of the declining fossil fuel supplies. Hardest hit by increasing fossil fuel costs are the developing countries which import most, if not all, of their fossil fuel needs. Majority of these countries are already very poor and further use of fossil fuels only aggravates their present low living standards.

In contrast, alternative energy sources such as solar radiation, wind, and running water are of great potential significance in developing countries. These countries are situated in the tropical regions of the earth where solar radiation and wind intensity are high. Rainfall is also high, giving these countries a continuous flow of running water all year although at times with disastrous aftermath. Tapping these natural resources for alternative energy technologies would certainly benefit the developing nation.

However, present alternative energy technologies available in developed countries demand relatively staggering costs. Solar, wind, and hydroelectric power plants have already been well-developed in the United States and in Europe but they are mostly on a grand scale and still very expensive in terms of dollar input per kW output. Hydroelectric power systems seem to be the least expensive of the three, having been developed much earlier. However, application of centralized hydropower systems in rural areas of developing countries require enormous investments in capital. Most of these turbines are more than a megawatt in capacity. Thus, turbine machinery, transmission and distribution, and installation costs are particularly high. Logistics and management are also potential problems.

Medium and small-size turbines, on the other hand, evolved together with large turbines but soon died out as dictated by the economies of scale and low fossil fuel prices. Thus research and development had focused mainly on larger hydropower systems and left behind the smaller ones.

In recent years, however, as fossil fuel prices went up, medium and small-size hydropower systems are becoming economical to build. Popularity of these turbines have been increasing recently. Hard-pressed by high fuel prices and high cost of imported turbine machinery, developing countries have started to take a keen interest on small

systems. Since the technology requirements in small systems are not as complex as in large systems, the idea of manufacturing small turbines in the developing country itself becomes a logical solution against importation. In addition, the financial burden of small systems is relatively light.

Therefore, microhydropower, as small hydropower systems are popularly known, is a novel alternative energy source. It is indeed an attractive choice for oil-importing developing countries. Utilization of microhydropower can significantly contribute to the development activities in rural areas especially those places that have been considered not economical for utility power lines to reach. Likewise, it can supply the basic electrical needs of homes, farm, shop, or small industries. This calls for a decentralization of power generation and a search for an appropriate choice of small turbine technology suited for a specific rural area situation. To accomplish this, there is a need for turbines to be fabricated in the developing country where they are to be utilized due to the relatively high cost of imported turbine machinery, spare parts and expertise. This means that local technical skill be used in the design and development of the turbine with help from the scientific and technical community. Turbine technology should be developed with local capabilities, tools, materials and based on local understanding and enthusiasm of the needs for such technology. With the turbine and its accessories

designed and constructed locally, it could create a technology base within the locality and subsequently a base for future growth and turbine manufacture endeavor on contiguous areas as well.

Specifically, the turbine design to be chosen should lend itself for easier fabrication locally with the use of simple tools and equipment. The crossflow turbine appears to be the most logical choice of design. It is a relatively small low-head turbine and can use heads of 5 feet or even less. In tropical countries, low-head streams that flow all year abound, which makes this design more suitable to those countries. The crossflow turbine is relatively easy to manufacture. A workshop with facilities to weld, drill, grind, and cut steel parts can do the job. Casting is not necessary. The turbine can be built mainly out of steel plates, and galvanized iron pipes. Other parts such as bearings, shaft, belts, and pulleys are available off-the-shelf.

The crossflow turbine has the further advantage of needing only very minimal maintenance. The runner of the turbine is so designed that when clogged during operation, it clears itself of the obstruction due to the force of outgoing water and the centrifugal force of the turning wheel. So there is less chance of blockage due to leaves, twigs, or grass and other debris. This turbine is also environmentally benign. The mixing action of the blades provides not only the generation of power but also in

reoxygenating water releases to ponds thereby providing the much needed oxygen to fish and other aquatic animals.

### Rationale

The preceding features of the crossflow turbine indicate practicality of exploring this technology for adaption. Hence, it is deemed necessary to conduct some investigations on the potential use of crossflow turbine on a small scale basis.

Although the crossflow turbine has been around for about 85 years, it is not a popular one. Like any small turbine, it has not been studied much. Only few researches are conducted regarding its development. Based on the few studies available, its performance appears to vary considerably. Experimental studies which are done in the laboratory generally show higher performance ratings. Field performance ratings are expected to be less than laboratory results. Hence, this study attempts to evaluate field performance of the turbine. Overall, the results of this study can add insight into the little known world of small crossflow turbine development.

Specifically, this study concentrates on the effect of the number of runner blades to the field performance of the turbine.

### Objectives

The general objectives of this study are the following:

1. To design and construct a small low-cost crossflow water turbine prototype with an interchangeable runner, and runners having different number of blades.
2. To evaluate the actual field performance of the turbine using each of the runner.
3. To develop a field performance prediction equation for a small crossflow turbine for a particular runner diameter.
4. To compare the turbine's field performance with previous studies from other researchers.

## CHAPTER II

### REVIEW OF LITERATURE

#### Water Turbines

A water turbine is basically a device that utilizes the energy from falling water and converts it to rotating mechanical energy. This energy, through the shaft, may either be used directly to run a mill and grinding equipment or coupled to a generator to produce electrical energy.

Water turbines fall into two general classes, impulse and reaction turbines. Impulse turbines are appropriately called free-jet turbines because of the nature of phenomena involved. Water is fed to the runner through the penstock provided at its end with the nozzle. The high velocity water jet from the nozzle strikes the runner buckets or blades causing the runner to rotate which in turn creates torque on the shaft. The water leaving the runner buckets flows around the casing and passes into the tail-race. All the available head is converted to kinetic energy at the nozzle. Any kinetic energy leaving the runner is considered lost. It is therefore essential that the buckets are designed in such a way that exit velocities are a minimum.

No draft tube is used since the runner operates under essentially atmospheric pressure and the head represented by the elevation of the unit above tailwater cannot be utilized.

Reaction turbines are called velocity-pressure turbines which account for the fact that there is pressure and velocity change across the turbine. The runner is completely submerged and both the pressure and velocity decrease from inlet to outlet of the runner. The energy absorbed is converted to kinetic or mechanical energy across the runner. A draft tube is employed so that the entire available head can be used. The distance between the runner and the tailwater level is added to the head in the nature of a suction effect.

Impulse turbines include the Pelton (tangential), Turgo (diagonal), and the Mitchell-Banki turbines (crossflow). Modern impulse turbines are generally of the Pelton type. Reaction turbines include the Francis (radial and radial-axial flow) and propeller turbines (axial-fixed blade and axial-adjustable blade).

#### Power and Efficiency of Water Turbines

The power available from a stream or falling water is a combination of volume flow rate of water and net elevation head. It is possible to produce a given amount of power with high head and low flow, low head and high flow,



or any combination of both values. The input power is given by the formula

$$P_i = \gamma Q_s H \quad (2.1)$$

where  $P_i$  is the input water power,  $\gamma$  is the specific weight of water,  $Q_s$  is the supply flow rate, and  $H$  is the total available head.

The power developed in the turbine can be determined by the use of a Prony brake or a dynamometer and a device to measure rotational speed. The power dissipated is given by

$$P_o = 2\pi TN \quad (2.2)$$

where  $P_o$  is brake power,  $T$  is the torque which is the product of the brake force and length of the moment arm, and  $N$  is the rotational speed of the turbine shaft.

The efficiency of the turbine can be calculated from

$$E = (P_o/P_i) \times 100 \text{ percent} \quad (2.3)$$

The above equations are the guiding formulas in the calculations for power and efficiency of the crossflow turbine field experiment.

### Brief History and Description of the Crossflow Turbine

The crossflow water turbine was invented in 1903 by an Australian engineer named A. G. M. Mitchell. About fifteen years later, it was further developed by Donat Banki, a

Hungarian, who made the crossflow turbine known more widely. As a result, crossflow turbines also became known as Mitchell-Banki turbines or simply, Banki turbines. In the 1920's, Ossberger Turbine Company of West Germany acquired manufacturing rights and began mass-producing the turbine. Their machines are marketed in North America by F. W. E. Stapenhorst of Point Claire, Quebec, Canada. In the United States, crossflow turbines are manufactured or supplied by companies like New Found Power Inc. of Hope Valley, Rhode Island and Canyon Industries of Deming, Washington (Volkman & Eastlake, n.d.; Alward et al. 1979). Other countries such as Nepal and Indonesia are also involved in the fabrication and implementation of crossflow turbines for several years now (Inversin, 1985).

Despite its long history, the crossflow water turbine has seen little research. Only few reports gave an account of this turbine partly because it is a relatively small water turbine (Nakase et al., 1982). Available units have capacities ranging from 1 kW to 1000 kW at a very low head of 3 feet and all the way up to 700 feet and up to 350 cfs (Johnson, 1984; Stapenhorst, 1980). Runner diameter ranges from 8 inches to 4 feet. Due to the high cost of fossil fuels, there is renewed interest in its development.

A simple crossflow turbine consists of two main parts: a nozzle and a runner (Figure 2.1). A much improved design, shown in Figure 2.2 and Figure 2.3 and represented by one of the Ossberger line of cross flow turbines, consists of a

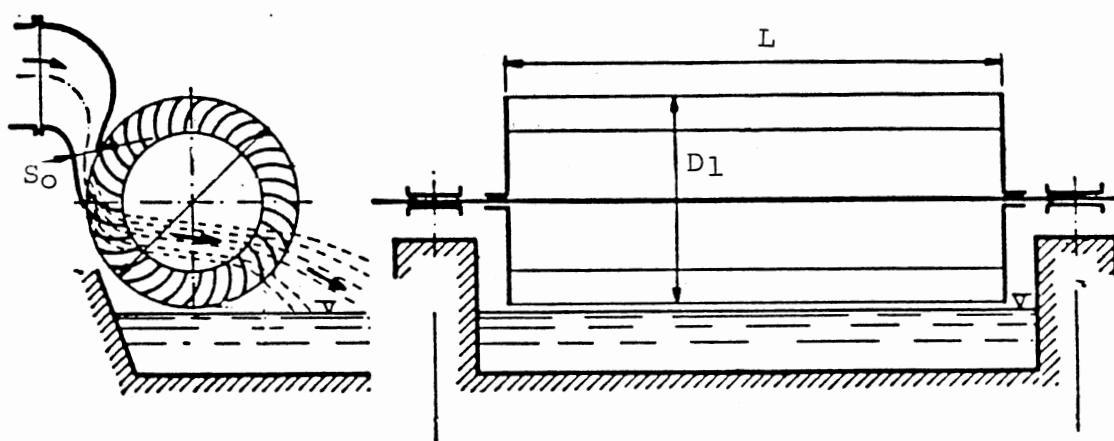


Figure 2.1. Schematic Drawing of a  
Crossflow Turbine  
(Mosonyi, 1965)

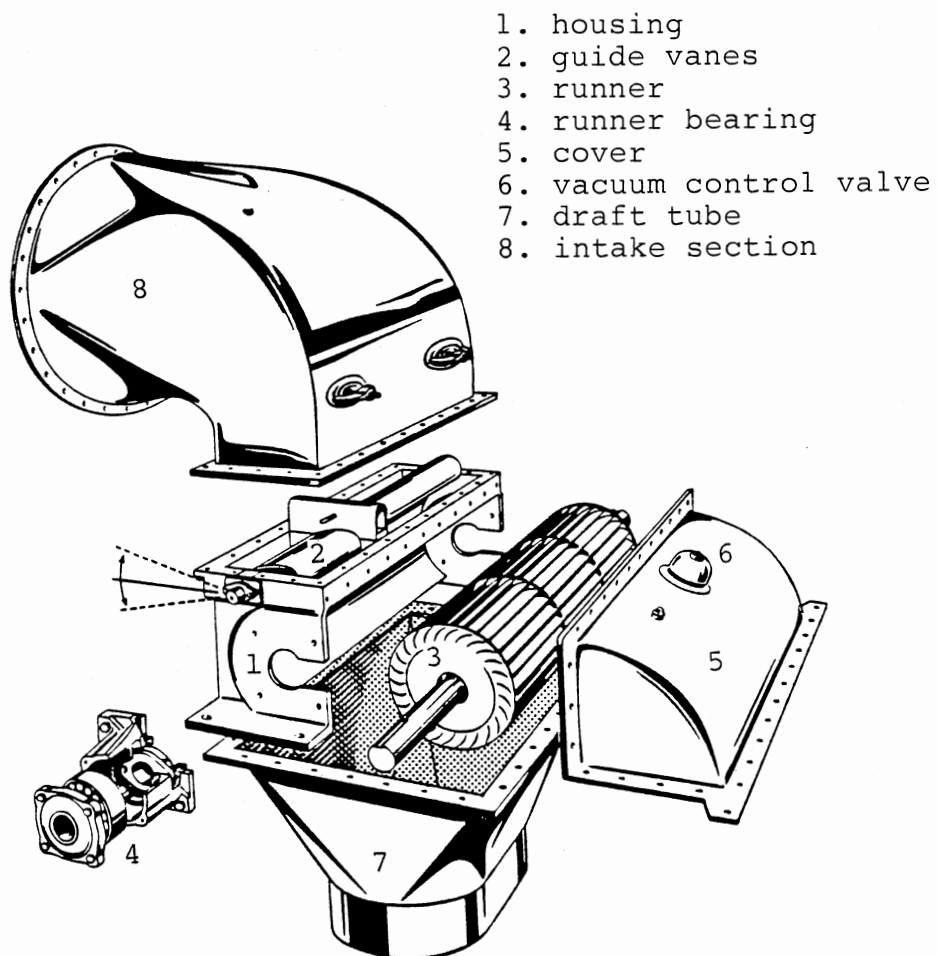
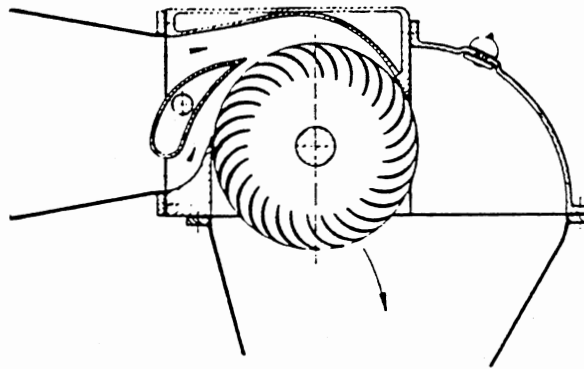
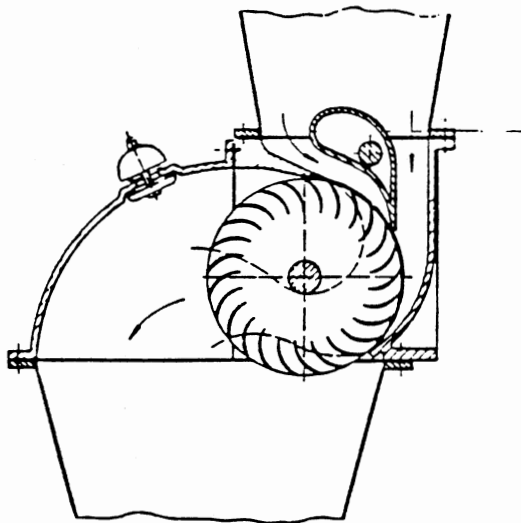


Figure 2.2. Exploded View of an Ossberger Crossflow Turbine Assembly (Stapenhorst, 1980)



Horizontal admission



Vertical admission

Figure 2.3. Cross-sectional View  
of Two Crossflow  
Turbines (Volkman,  
n.d.).

housing, guide vanes, runner and runner bearings, cover, draft tube and transition piece. The housing contains the nozzle which in turn contains the guide vanes. The nozzle converts water potential energy into kinetic energy. The nozzle is shaped to follow the runner periphery. It has a rectangular cross-sectional area which discharges the water jet at full width of the runner. The jet enters the runner blades at an angle of about 15 or 16 degrees to the tangent of the periphery of the wheel and at right angles to the shaft. The water crosses through the open interior and then from inside to outside again. Hence, the water jet coming out of the nozzle passes through the runner blades twice, developing two velocity stages. Figure 2.2 and Figure 2.3 also show the location of the guide vanes within the nozzle. The guide vane is a hydraulic-shaped flap which controls or shuts off the water flow into the turbine. The nozzle has two independently controlled guide vanes along the same nozzle width; one covering a third of the flow cross-section and the other covering the remaining two-thirds. This sub-division of the passages and controlled openings enable the turbine to operate on a wide range of gate openings and flows. The result is a flat efficiency curve over wide variation of flows. Figure 2.4 shows the consistency of the efficiency of the crossflow turbine at various gate openings. Comparing with the Francis turbine, the crossflow turbine gives relatively higher efficiency at low flow rates

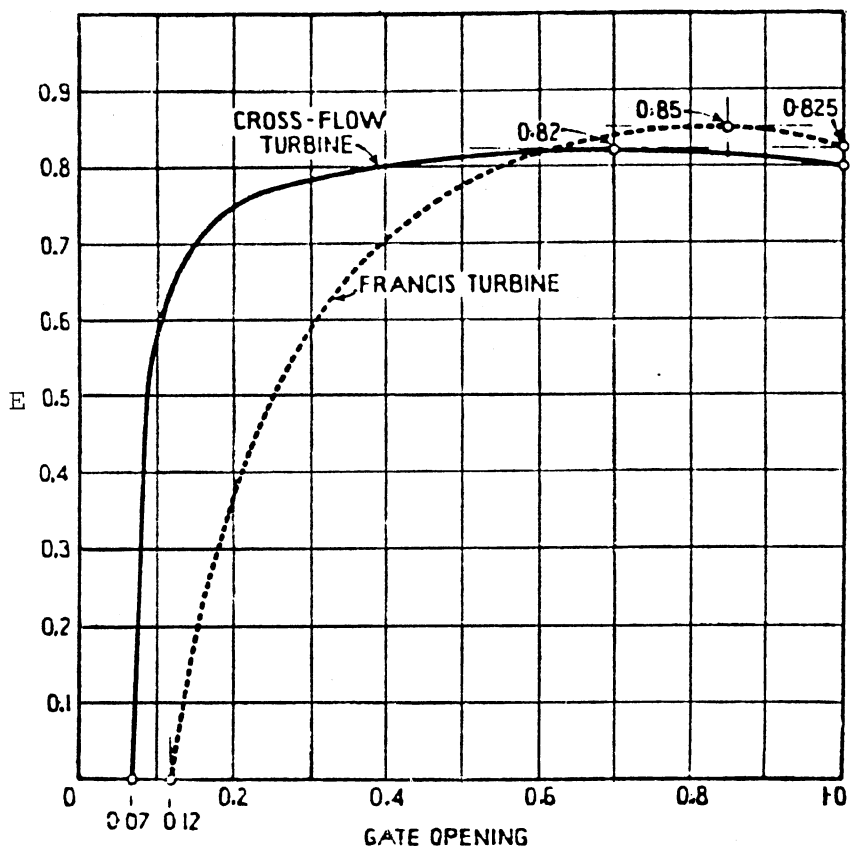


Figure 2.4. Efficiency Curve of a Crossflow Turbine with Divided Gate. The Efficiency Curve of a Francis Turbine of similar Size is Shown Dotted for Comparison (Haimerl, 1960)

although the Francis turbine attains higher efficiency at 80 percent flow (Haimerl, 1960). The runner or wheel is an assembly of horizontal curved blades formed like a squirrel cage. Two parallel circular disks are joined together at the rim with a series of curved blades usually made from horizontally cut pipes.

The blades are subjected to very severe mechanical loads through centrifugal forces and the periodic impacts of the jet. A large safety margin against fatigue failure must obviously be the first consideration in design. Runners with longer blade length are supported with an extra disk. All runners are to be balanced before assembly. The machine is normally classified as impulse or free-jet, radial-type turbine (Mockmore & Merryfield, 1949; Durali, 1976). This classification is not strictly correct because as has been previously observed by others, there is a slight static pressure at the nozzle exit when the nozzle is shaped to follow the runner periphery especially closely (Haimerl, 1960; Nakase et al., 1982). This reaction effect, however, is true only to the first stage because water piles up during operation. The second stage operates at constant pressure since the pressures are balanced through these blade passages that are not running full. The same applies to the first stage at low flow; reaction effect becomes zero. However a sufficiently large gap between the nozzle and the runner ensures that the jet entering the turbine runner has no static pressure (Haimerl, 1960).



## Theory

The shaft power developed by a turbine (Equation (2.2)) can be determined from a Prony brake or dynamometer and a rotative speed indicator or a tachometer. Output power can be determined also through a generator connected to a turbine. On the other hand, output power can be theoretically predicted from velocity diagrams of the water jet entering the blades.

The water jet enters the runner at an angle with the tangent to the periphery (Figure 2.5). Since the water jet impinges the blades twice, the crossflow turbine consists of two velocity stages as shown in Figure 2.6. Each velocity stage consists of an inlet and an exit stage. The exit of the first stage is approximately equal to the inlet of the second stage. The inner velocity diagrams shown in Figure 2.6, however, take into account the incidence losses on the blades (Balje, 1981).

The Euler energy equation for the crossflow turbine consists of the sum of the energy developed from each stage, which is written as follows (Haimerl, 1960).

$$\frac{P}{(\gamma/g)Q_t} = (U_1 v_{u1} - U_2 v_{u2}) + (U_3 v_{u3} - U_4 v_{u4}) \quad (2.4)$$

where  $U$  and  $v_u$  are peripheral and tangential velocities, respectively. The subscripts represent the number of velocity diagram. Since outer peripheral velocities are

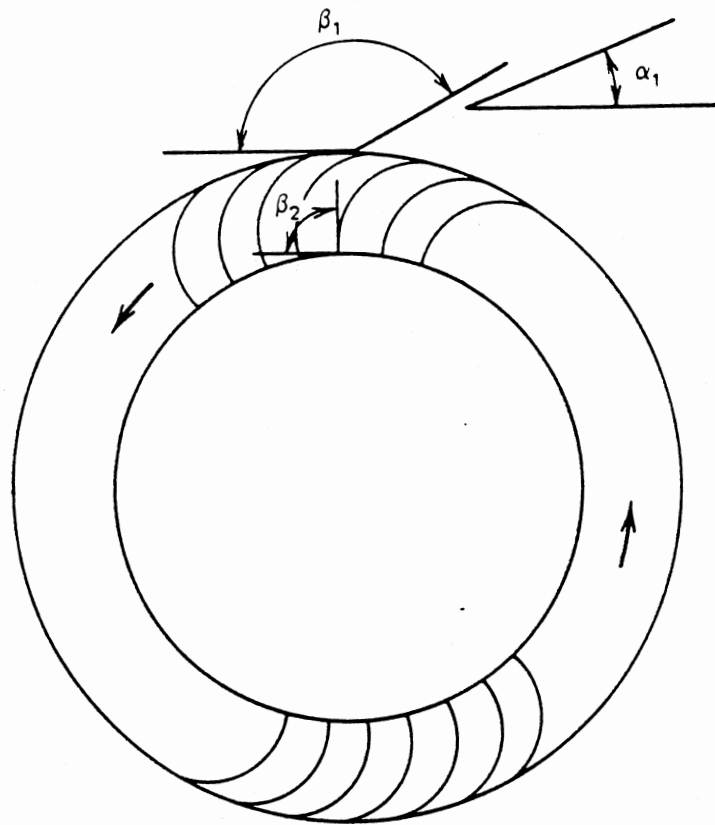


Figure 2.5. Inclination of Water Jet  
Entering the Runner  
(Balje, 1981)

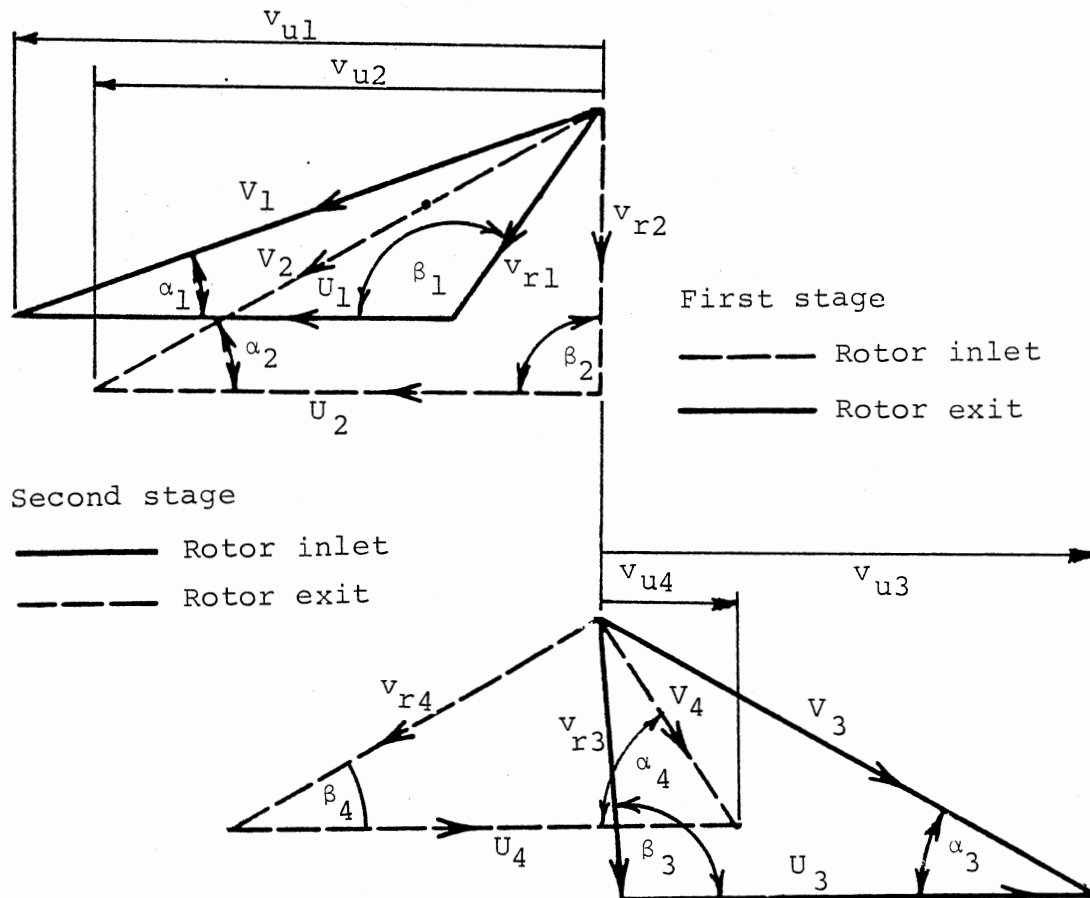


Figure 2.6. The Two Velocity Stages of a Crossflow Turbine

equal ( $U_1 = U_4$ ) and inner peripheral velocities are equal ( $U_2 = U_3$ ), the theoretical power developed in the turbine becomes

$$P_o = (\gamma/g)Q_t [U_1(v_{u1} - v_{u4}) + U_2(v_{u3} - v_{u2})] \quad (2.5)$$

The overall efficiency for the crossflow turbine is normally defined as

$$E = E_h E_m E_q \quad (2.6)$$

where  $E_h$  is the hydraulic efficiency,  $E_m$  is the mechanical efficiency, and  $E_q$  is the volumetric efficiency (Durali, 1976).

Hydraulic efficiency includes all hydraulic head losses across the blades. This is sensitive to the blade profile and flow angles. Hydraulic efficiency is defined as

$$E_h = \frac{\Delta H - H_{\text{loss}}}{\Delta H} \quad (2.7)$$

where  $\Delta H$  is the difference between hydraulic head of the turbine inlet and exit.

Mechanical efficiency  $E_m$  includes friction losses in the brake and in the bearings. It is defined as

$$E_m = \frac{T - T_{\text{loss}}}{T} \quad (2.8)$$

where  $T$  is the shaft torque.

Volumetric efficiency  $E_q$  includes leaks and flow that passes through the turbine without giving any work. It is defined as

$$E_q = \frac{Q_s - Q_{leak}}{Q_s} \quad (2.9)$$

where  $Q_s$  is the supply flow rate.

### Previous Studies

Haimerl (1960) analyzed the theoretical power developed in the Ossberger crossflow turbine. He assumed that the inner velocity diagrams shown in Figure 2.6 are identical. That is, the term  $U_2(v_{u3} - v_{u2})$  of Equation (2.5) equals zero. With this assumption, the Euler equation is simplified as

$$\frac{P}{(\gamma/g)Q_t} = U_1(v_{u1} - v_{u4}) \quad (2.10)$$

The resulting inlet and exit diagrams are shown in Figure 2.7. Using the following geometrical relationships shown in Figure 2.7,

$$v_{u1} = U_1 - v_{r1} \cos \beta_1 \quad (2.11)$$

$$v_{u4} = U_4 - v_{r4} \cos \beta_4 \quad (2.12)$$

$$\beta_4 = 180^\circ - \beta_1 \quad (2.13)$$

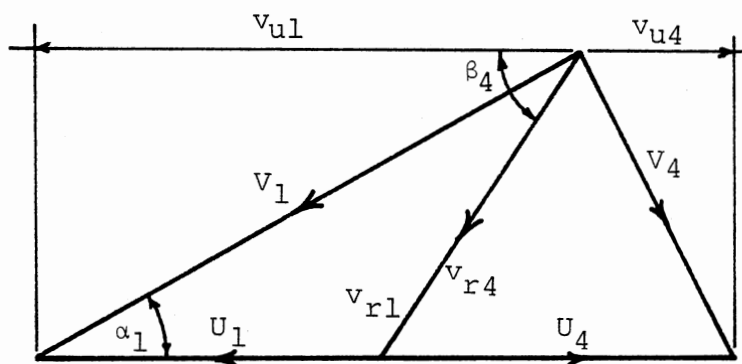


Figure 2.7. Outer Velocity Diagrams  
of a Crossflow Turbine  
Neglecting Shock  
Losses (Haimerl, 1960).

where  $v_r$  is the relative velocity and  $\beta$  is the relative velocity angle. Assuming further that

$$v_{r1} = v_{r4} = U_1 \quad (2.13)$$

The Euler equation becomes

$$\frac{P_o}{(\gamma/g)Q_t} = 2U_1^2 \cos(180-\beta_1) \quad (2.15)$$

Thus, the theoretical power developed can be written as

$$P_o = 2 (\gamma/g) Q_t V_1^2 (U_1/V_1)^2 \cos(180-\beta_1) \quad (2.16)$$

where  $\gamma$  is the specific weight of water,  $g$  is the acceleration due to gravity,  $Q_t$  is volume flow rate through the turbine,  $V_1$  is the absolute velocity or spouting velocity of water jet entering the runner,  $U_1$  is the peripheral velocity, and  $\beta_1$  is the angle between the relative velocity  $v_{r1}$  and the peripheral velocity  $U_1$  of the exit velocity triangle. The ratio  $U_1/V_1$  is known as the velocity coefficient. Turbine efficiency can be calculated using Equations (2.1), (2.16), and (2.3). Maximum efficiency was achieved at 86 percent with an average of about 82 percent. This was achieved at approximately 70 percent gate opening. The basis of these figures is the Ossberger crossflow turbine with runners having 26 to 30 blades (Stapenhorst, 1980).

Haimerl (1960) also predicted the flow rate  $Q_t$  through the turbine to be

$$Q_t = (1/2) U_1 \sin(\beta_1) (L/D_1) D_1^2 \delta \quad (2.17)$$

where  $L$  is the length of the runner and nozzle opening (Figure 2.1),  $D_1$  is the outside diameter of the runner, and  $\delta$  is the entry angle of the nozzle or angle covered by the nozzle curvature.

The theoretical power developed in each stage can be derived from Equation (2.4) where

$$P_o = P_{1-2} + P_{3-4} \quad (2.18)$$

$$P_{1-2} = (\gamma/g) Q_t (U_1 v_{u1} - U_2 v_{u2}) \quad (2.19)$$

$$P_{2-3} = (\gamma/g) Q_t (U_3 v_{u3} - U_4 v_{u4}) \quad (2.20)$$

Since  $U_1 = U_4$  and  $U_2 = U_3$ , and using Haimmerl's velocity diagrams (Figure 2.7),

$$v_{u1} = U_1 - U_1 \cos \beta_1 \quad (2.11)$$

$$v_{u4} = U_1 + U_1 \cos \beta_1 \quad (2.12)$$

$$v_{u2} = U_2$$

$$v_{u3} = U_3$$

Further, with  $U_2 = (D_2/D_1)U_1$ ,

$$P_{1-2} = (\gamma/g) Q_t U_1^2 [(1 - \cos \beta_1) - (D_2/D_1)^2] \quad (2.21)$$

$$P_{3-4} = (\gamma/g) Q_t U_1^2 [(D_2/D_1)^2 - (1 + \cos \beta_1)] \quad (2.22)$$

Adding Equations (2.21) and (2.22) yields Equation (2.16).



The power ratio of the two stages, therefore, is

$$\frac{P_{1-2}}{P_{3-4}} = \frac{(1 - \cos \beta_1) - (D_2/D_1)^2}{(D_2/D_1)^2 - (1 + \cos \beta_1)} \quad (2.23)$$

where  $D_2/D_1$  is the ratio of the inside rotor diameter to the outside rotor diameter and  $\beta_1$  is entrance relative velocity angle of the water jet.

Assuming values  $D_2/D_1 = 2/3$  and  $\beta_1 = 150$  degrees

$$\begin{aligned} \frac{P_{1-2}}{P_{3-4}} &= \frac{(1 - \cos 150^\circ) - (2/3)^2}{(2/3)^2 - (1 + \cos 150^\circ)} \\ &= 4.58 \end{aligned}$$

which means that the theoretical power developed in the first stage is 4.58 times that of the second stage. In terms of proportion of the total power

$$P_{1-2} + \frac{P_{1-2}}{4.58} = P_o$$

$$P_{1-2} = 0.82 P_o$$

$$P_{3-4} = 0.18 P_o$$

In a rerun of Banki's experiment, Mockmore and Merryfield (1949) determined the power output of the crossflow turbine taking into account head losses in the blades. The modified velocity diagrams are shown in Figure 2.8. Like Haimerl (1960), they assumed that the inner velocity

diagrams of Figure 2.8 are identical. The resulting power equation, assuming  $v_{r4} = \psi v_{r1}$ , is

$$P_o = (\gamma/g) Q_t (U_1 V_1 \cos \alpha_1 - U_1^2) (1 + \psi) \quad (2.24)$$

Input water power through the runner assuming total head equals velocity head

$$P_i = \gamma Q_s H \quad (2.1)$$

$$= 0.5 (\gamma/g) \frac{Q_s V_1^2}{C^2} \quad (2.25)$$

$$\text{where } V_1 = C (2gH)^{0.5} \quad (2.26)$$

$\alpha_1$  is the angle between absolute velocity  $V_1$  and peripheral velocity  $U_1$ ;  $C$  is the nozzle coefficient;  $Q_s$  is the supply flow rate coming out of nozzle;  $Q_t$  is the flow rate entering the runner;  $H$  is the total available head; and  $\psi$  is an empirical coefficient less than unity which accounts for shock losses on the blades.

The efficiency of the turbine becomes

$$E = 2C^2 (Q_t/Q_s) [(U_1/V_1) \cos \alpha_1 - (U_1/V_1)^2] (1 + \psi) \quad (2.27)$$

Differentiating

$$\frac{dE}{d(U_1/V_1)} = 0$$

the velocity coefficient at maximum efficiency

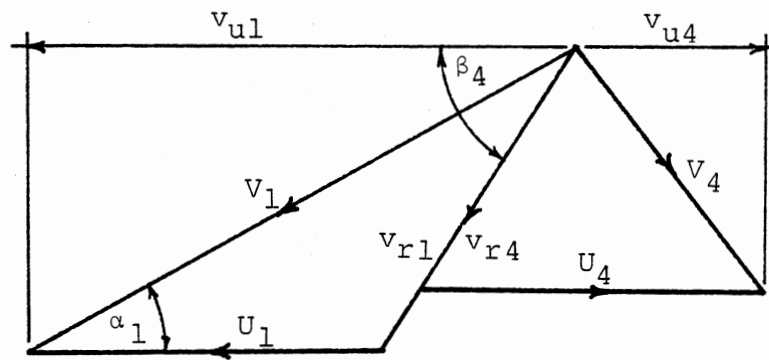


Figure 2.8. Outer Velocity Diagrams of a Crossflow Turbine Taking into Account Head Loss Due to Friction on the Blades (Mockmore & Merryfield, 1949).

$$U_1/V_1 = 1/2 \cos \alpha_1 \quad (2.28)$$

Therefore maximum theoretical power output becomes

$$P_{O(\max)} = (\gamma/g) Q_t V_1^2 (U_1/V_1)^2 (1 + \psi) \quad (2.29)$$

and maximum theoretical turbine efficiency is

$$E_{\max} = 2C^2 (Q_t/Q_s) (U_1/V_1)^2 (1 + \psi) \quad (2.30)$$

The studies of Mockmore and Merryfield (1949) reported an actual maximum efficiency of 68 percent which is much less compared to Banki's 80 percent for a 20-blade runner. Predicted efficiency however can reach as high as 87.8 percent based on  $\alpha_1 = 16$  degrees,  $C = 0.98$  and  $\psi = 0.98$ .

The Mockmore and Merryfield (1949) experiment on the 13.1-inch, 20-blade crossflow turbine with adjustable gate opening gave the following results:

1. The crossflow turbine can be operated efficiently on a wider range of openings than most turbines.
2. Brake horsepower varies almost directly with the three-halves power of the head.
3. Maximum efficiency occurs at practically a constant speed for all gate openings at constant head.
4. The crossflow turbine characteristic speed occupies a position between those for the tangential and reaction turbines.
5. The effective width of the wheel can be changed at will without changing the angle of admission  $\alpha_1$ .

6. It is estimated that some eight percent of the total water input is lost and never touched the wheel, that is,  $Q_t = 0.92 Q_s$ .
7. One cannot expect to attain close to the maximum efficiency on a turbine of such small horsepower.

In another report, Durali (1976) presented a slightly different design and analysis of the crossflow turbine. The design was aimed primarily to produce 5 kW for the highlands of Columbia. The turbine was largely made of steel and steel parts. The runner has its curved blades bent at the edges and riveted to the side plates. The runner has no drive shaft. Power is transmitted through the bearing housing which rotates the rotor, and the shaft which goes through the rotor bearing supports only the rotor. Durali (1976) assumed an idealized velocity diagrams for the turbine as shown in Figure 2.9. Assuming the absolute velocity of the jet  $V_4$  leaving the second stage as radial (i.e.,  $\alpha_4 = 90$  degrees and hence  $v_{u4} = 0$ ), the predicted theoretical power output equation presented by Haimerl in Equation (2.10) can be shown to be reduced to

$$P_o = (\gamma/g) Q_t U_1 v_{u1} \quad (2.31)$$

$$= 2 (\gamma/g) Q_t V_1^2 (U_1/V_1)^2 \quad (2.32)$$

Using

$$P_i = 2(\gamma/g) Q_s V_1^2 / C^2 \quad (2.25)$$

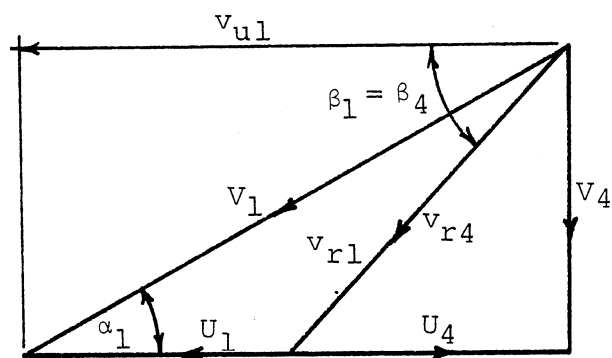


Figure 2.9. Idealized Outer Velocity Diagrams of a Crossflow Turbine (Durali, 1976).

the theoretical turbine efficiency becomes

$$E = 4 c^2 (Q_t/Q_s) (U_1/V_1)^2 \quad (2.33)$$

The calculated turbine efficiency was below 60 percent.

While experimenting on nozzle shapes, a group of Japanese experimenters led by Nakase et al. (1982) came up with an actual velocity diagram shown in Figure 2.10. The diagram was based on the observation that the water crossing the open center space of the runner gives rise to contraction and the flow is accelerated from the first stage to the second stage. It also revealed that the flow at nozzle exit has a higher pressure than atmospheric and therefore the inlet velocity  $V_1$  is lower than the design value. Likewise the flow angle  $\alpha_1$  at the first stage inlet is smaller than its design value. However, the relative inlet flow angle  $\beta_1$  is almost equal to the design value near design rotational speed. Without acceleration, the velocity diagram would be similar to Figure 2.9. From Figure 2.10 the following equations can be deduced

$$P_o = (\gamma/g) Q_t U_1 (V_1 \cos \alpha_1 - 0) \quad (2.34)$$

Since actual  $\alpha_1$  is foreseen to be less than its design value,  $\alpha_1$  may be expressed in measurable terms of  $U_1$ ,  $V_1$ ,  $\beta_1$  or  $\beta_4$ . Hence using geometrical relationships of Figure 2.9

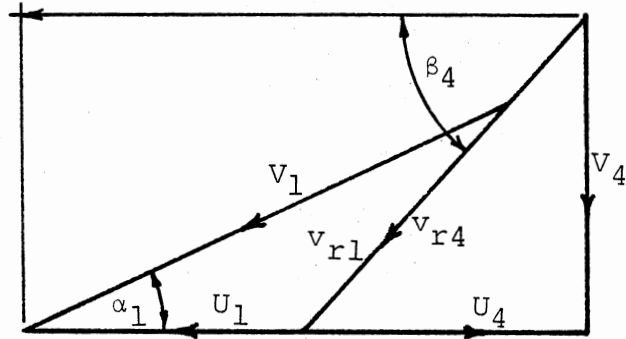


Figure 2.10. Outer Velocity Diagrams of a Cross-flow Turbine in Actual Flow (Nakase et al., 1982).



$$\begin{aligned} \cos \alpha_1 = (U_1/V_1) \{ \sin^2 \beta_1 \\ - \cos \beta_1 [ \frac{1}{(U_1/V_1)} - \sin^2 \beta_1 ]^{1/2} \} \end{aligned} \quad (2.35)$$

$$\begin{aligned} P_o = (\gamma/g) Q_t V_1^2 (U_1/V_1)^2 \{ \sin^2 \beta_1 \\ - \cos \beta_1 [ \frac{1}{(U_1/V_1)} - \sin^2 \beta_1 ]^{1/2} \} \end{aligned} \quad (2.36)$$

An actual maximum efficiency of about 82 percent was reported on a 26-blade runner.

It may also be stated that Nakase's velocity diagrams shown in Figure 2.10 are somewhat similar to Mockmore and Merryfield's (1949) Figure 2.8. According to Nakase et al. (1982) the difference lies in that  $v_{r4} > v_{r1}$  due to jet acceleration within the runner and therefore admission angle  $\alpha_1$  is less than its design value. Mockmore and Merryfield (1949), on the other hand, stated that  $V_{r1} > V_{r4}$  or  $v_{r4} = \psi v_{r1}$  with  $\psi$  has some value less than unity.  $\psi$  accounts for shock losses inside the blades (See Figure 2.8). Also the admission angle  $\alpha_1$  remains constant. Another difference is that Nakase's diagrams show that, like Durali's diagrams, the absolute velocity of the jet as it leaves the second stage  $V_4$  is approximately radial which means the exit tangential velocity of the second stage  $v_{u4}$  is almost equal to zero. Deriving a power equation for Nakase et al. using Mockmore and Merryfield's analysis, let

$$v_{r1} = \psi_1 v_{r4} \quad (2.37)$$

$$v_{u4} > 0 \quad (2.38)$$

The resulting velocity diagram is shown in Figure 2.11. Using the geometrical relationship in Figure 2.11, predicted output power

$$P_o = (\gamma/g) Q_t V_1^2 (U_1/V_1)^2 (\psi_1 + 1) \psi_1 \quad (2.34)$$

where  $\psi_1 = v_{r1}/v_{r4}$ , a factor less than unity which takes care of the acceleration of the water jet inside the runner. Equation (2.34) gives a slightly higher value than Mockmore and Merryfield's power equation (Equation (2.29)).

Nakase's experiments on a 12.4-inch, 26-blade turbine yielded the following conclusions:

1. The flow at nozzle exit has some static pressure and therefore the crossflow turbine is not a perfect impulse turbine.
2. Decreasing of pressure at nozzle exit is not always related to increasing of the maximum efficiency.
3. The value of a suitable nozzle throat width factor  $2S_o/(D_1 \delta)$  is near 0.26 but it changes slightly with the nozzle entry arc  $\delta$  (Figure 2.12).
4. Two types of flow shown in Figure 2.12, are present in the turbine. One is cross flow which goes through the stages and the other is non-cross flow which flows through only the first stage.

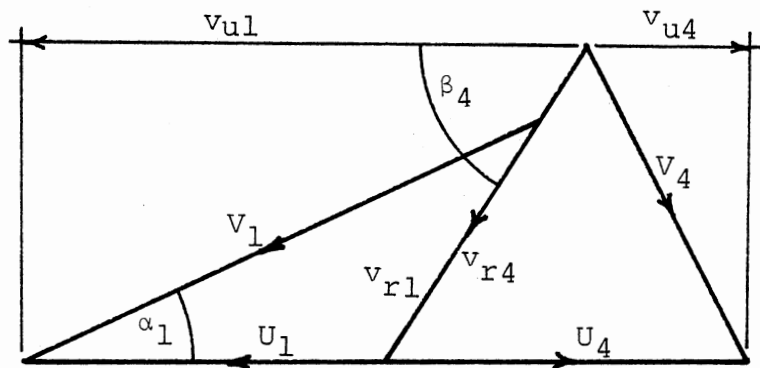


Figure 2.11. A Modification of the Outer Velocity Diagrams of Figure 2.10.

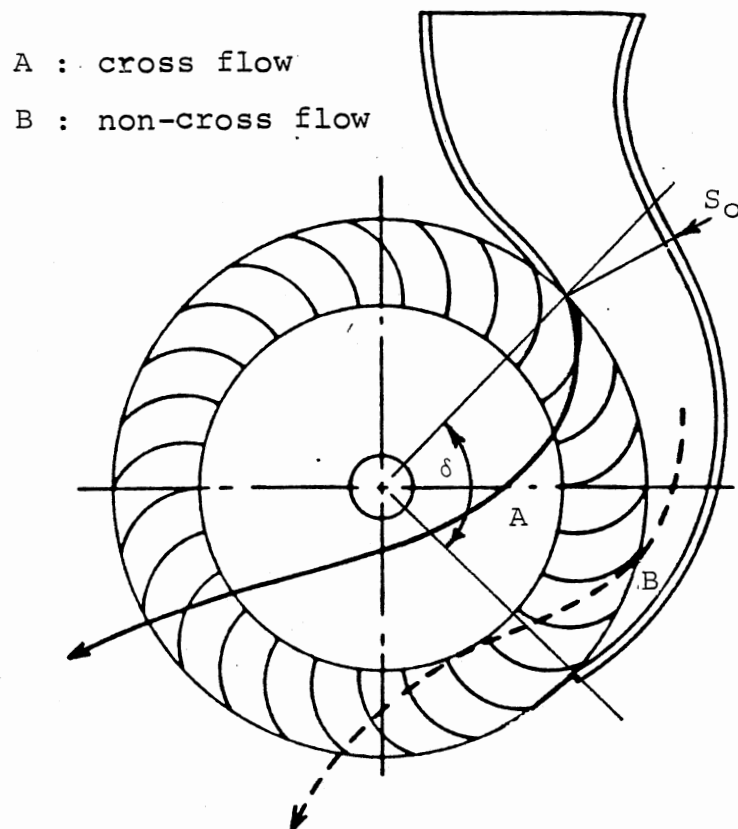


Figure 2.12. Schematic Diagram of the Flow Pattern Inside of the Runner  
(Nakase et al., 1982)

This finding may alter the power ratio of the two stages as presented by Haimerl in Equation (2.23).

5. The flow accelerates from the first stage to the second stage.

Other reports describing the performance of the cross-flow turbine also give varied values of efficiency. For example, the Ossberger Turbine Company claims efficiencies of up to 84 percent (Haimerl, 1960). Tests conducted by Johnson, Ely, and White (1982) yielded efficiencies of 60 to 80 percent over a wide range of flow rates, heads, and runner speeds on an 18-blade runner. The runner was constructed out of PVC plastic and the double entry nozzle and guide vanes are of wood coated with ultra-high-molecular-weight polyethylene. The casing is of wood construction and the turbine had a draft tube. The best efficiency was achieved with a nozzle entry angle of  $16^{\circ}$  with a total entry arc of  $120^{\circ}$ . Also, Mother Earth News, Inc. through its own-built crossflow turbine achieved a 70 percent efficiency excluding generator efficiency on a 20-blade runner (Mother Earth News, 1985). On the other hand, Balje's (1981) analysis showed a calculated efficiency of about 73 percent.

From the foregoing reports, the efficiency of small crossflow turbines is not clearly established. Actual turbine efficiencies still lagged behind the theoretical values. Maximum theoretical efficiencies are around 85 percent while the actual efficiencies of experimental

models are around seventy percent or less. This could go down even more on small turbine prototypes. The variations are affected by many factors, some of which are turbine size, blade design, nozzle design, blade surface quality, and construction quality.

On the other hand, the theoretical formulas for power and efficiency presented do not include blade number or blade spacing. Indeed more tests are still needed to add insight into the little known world of crossflow turbines.

## CHAPTER III

### DESIGN AND CONSTRUCTION

One of the objectives of this study is the design and construction of a small crossflow turbine prototype with 6-inch-diameter runners. The turbine was constructed so that runners of the same size, but with different number of blades, can be interchanged.

The formulas presented by Haimerl (1960), Mockmore and Merryfield (1949), and Durali (1976) were adapted in sizing the runner and its blades. Some results of the experiment led by Nakase (1982) were also used particularly in the design of the nozzle.

#### Design of the Crossflow

#### Turbine Prototype

The following assumptions were made as initial values in the determination of other turbine parameters:

1. Output or shaft power,  $P_o = 0.50$  hp
2. Length of runner,  $L = 8$  inches
3. Outside diameter of runner,  $D_1 = 6$  inches
4. Entry angle of the nozzle,  $\delta = 90$  degrees
5. Angle between relative velocity and peripheral velocity of first stage

inlet (a function of blade geometry),  $\beta_1 = 150$  degrees  
 6. Hydraulic efficiency,  $E_h = 60$  percent

A very small crossflow turbine, simple in design, was constructed for the tests to minimize the effects of the many constraints placed upon the entire project.

The turbine has a very small horsepower output rating suitable for a small homeowner in a remote rural location, which called for a small turbine runner as well. The hydraulic efficiency goal was conservatively set at a low value to offset the expertise level of the construction crew who were manufacturing the turbine for the first time. Overall, turbine efficiency is expected to be much lower.

The following parameters were calculated based on the above assumptions:

1. Runner peripheral velocity,  $U_1$
2. Runner rotative speed,  $N$
3. Flow rate through the turbine,  $Q_t$
4. Spouting or absolute velocity of water entering the runner,  $V_1$
5. Total head,  $H$
6. Width of throat of nozzle,  $S_o$
7. Supply flow rate (after nozzle),  $Q_s$
8. Input water power (at nozzle),  $P_i$
9. Blade radius of curvature,  $r$
10. Angle covered by blade curvature,  $\theta$
11. Chord length of blade,  $c$
12. Number of blades,  $Z$



The calculations for the unknown parameters are presented as follows:

1. Peripheral velocity of the runner,  $U_1$ :

Haimeri's predicted power and flow rate equation are used; that is,

$$P_o = 2 (\gamma/g) Q_t U_1^2 \cos(180^\circ - \beta_1) \quad (2.16)$$

$$Q_t = (1/2) U_1 \sin(\beta_1) (L/D_1) D_1^2 \delta \quad (2.17)$$

Substituting the given values in Equation (2.17)

$$Q_t = (1/2) U_1 \sin 150^\circ (8/6) (6^2) \\ (90)(\pi/180)(1/144) \quad (3.1)$$

$$= 0.1309 U_1 \text{ cfs}$$

where  $U_1$  is in fps. Substituting  $Q_t$  in Equation (2.16) and solving for  $U_1$ ,

$$U_1 = \left\{ \frac{P_o}{2(\gamma/g) (0.1309) \cos(180^\circ - \beta_1)} \right\}^{1/3} \quad (3.2)$$

$$= \left\{ \frac{(0.5)(550)}{2(62.4/32.2)(0.1309) \cos 30^\circ} \right\}^{1/3}$$

$$U_1 = 8.55 \text{ fps}$$

2. Runner rotative speed,  $N$ :

$$U_1 = \pi D_1 N \quad (3.3)$$

$$N = \frac{(8.55)(60)}{(6/12)\pi}$$

$$= 326.58 \text{ rpm}$$

3. Volume flow rate through the turbine,  $Q_t$

From item 1:

$$Q_t = 0.1309 U_1$$

$$= 0.1309 (8.55)$$

$$= 1.12 \text{ cfs}$$

4. Spouting velocity or absolute velocity of the jet entering the runner,  $V_1$  Equation (2.15), which is:

$$\frac{P}{(\gamma/g) Q_t} = 2 U_1^2 \cos(180^\circ - \beta_1) \quad (2.15)$$

can also be written as

$$E_h g H = 2U_1^2 \cos(180^\circ - \beta_1) \quad (3.4)$$

Also

$$H = (V_1^2/2g) + (P_n/\gamma) + h \quad (3.5)$$

where  $H$  is the total available head, which is the sum of the velocity head,  $V_1^2/2g$ ; a small nozzle pressure head,  $p_n/\gamma$ , at the nozzle exit; and the fall,  $h$ , from the nozzle tip to the center axis of the runner which is approximately equal to the radius of the runner. Assuming  $p_n/\gamma = 0.063H$  (Haimerl, 1960) and since  $h = (D_1/2)/12 = 0.25 \text{ ft}$ ,

$$H = \frac{V_1^2}{2g} + 0.063H + 0.25$$

$$H = \left( \frac{V_1^2}{2g} + 0.025 \right) \frac{1}{0.937} \quad (3.6)$$

Substituting H in Equation (3.4) and solving for  $V_1$ ,

$$E_h g \left( \frac{V_1^2}{2g} + 0.025 \right) \frac{1}{0.937} = 2 U_1^2 \cos(180^\circ - \beta_1)$$

$$V_1 = \left\{ \frac{4 U_1^2 \cos(180 - \beta_1)}{E_h} - 0.25 (2g) \right\}^{1/2} \quad (3.7)$$

$$= \left\{ \frac{4 (8.5)^2 \cos(180 - 150)}{0.60} - 0.25 (2)(32.2) \right\}^{1/2}$$

$$= 20.15 \text{ fps}$$

5. Total head, H:

Using Equation (3.6)

$$H = \left( \frac{V_1^2}{2g} + 0.025 \right) \frac{1}{0.937}$$

$$= \left\{ \frac{(20.15)^2}{2(32.2)} + 0.025 \right\} \frac{1}{0.937} \quad (3.6)$$

$$= 6.99 \text{ ft}$$

6. Width of nozzle throat,  $S_o$ :

Nakase et al. (1982) showed that the optimum efficiency of a crossflow turbine occurred when the nozzle shape as described by the ratio  $2 S_o/D_1 \delta = 0.257$ . Using this value to calculate  $S_o$  for a nozzle entry arc  $\delta$  of  $90^\circ$ ,

$$\begin{aligned} S_o &= 0.257 (D_1/2) \delta & (3.8) \\ &= 0.257 (6/12) (90) (\pi/180) \\ &= 1.211 \text{ inches} \end{aligned}$$

Throat width of 1.25 inches was used.

7. Supply flow rate  $Q_s$ :

Supply flow rate can also be calculated from

$$Q_s = A V_1 \quad (3.9)$$

where A is the cross-sectional area of the nozzle end and  $V_1$  is the water velocity at the nozzle tip. Further,

$$\begin{aligned} Q_s &= (L S_o) V_1 & (3.10) \\ &= \frac{(8) (1.25)}{144} 20.15 \\ &= 1.40 \text{ cfs} \end{aligned}$$

8. Input water power at nozzle end,  $P_i$ :

From Equation (2.1)

$$P_i = \gamma Q_s H \quad (2.1)$$

where H is the available head at the nozzle end.

Therefore,

$$P_i = \frac{(62.4) (1.40) (6.99)}{550}$$

$$= 1.11 \text{ hp}$$

The input water power value does not include mechanical efficiency. It should be higher than 1.11 hp to compensate for power loss due to friction in bearings and in the brake.

9. Blade radius of curvature, r:

Mockmore and Merryfield (1949) gave the formula for the radius of curvature of the runner blade as

$$r = \frac{D_1 [ 1 - (D_2/D_1)^2 ]}{4 \cos(180^\circ - \beta_1)} \quad (3.11)$$

Using  $D_2/D_1 = 2/3$

$$r = \frac{6 [ 1 - (2/3)^2 ]}{4 \cos (180^\circ - \beta_1)}$$

$$r = 0.962 \text{ inch}$$

10. Angle covered by blade curvature,  $\theta$ :

Mockmore and Merryfield (1949) also presented the angle covered by blade curvature to be

$$\theta = 2 \tan^{-1} \frac{\cos (180-\beta_1)}{\sin \beta_1 + (D_2/D_1)} \quad (3.12)$$

$$= 2 \tan^{-1} \frac{\cos (180-150)}{\sin 150^\circ + (2/3)}$$

$$\theta = 73.17^\circ$$

An angle of 74 degrees was used.

11. Chord length of blade, c:

Durali (1976) reported the length of the blade chord to be

$$c = \frac{r \sin}{\sin(\beta_1-90^\circ)} \quad (3.13)$$

$$= \frac{(0.96225) \sin 74^\circ}{\sin(150^\circ-90^\circ)}$$

$$c = 1.0680 \text{ inches or } 1-1/16 \text{ inches}$$

12. Number of blades, Z

The number of blades was given by Morkmore and Merryfield (1949) as

$$Z = (\pi/K) \sin \beta_1 \quad (3.14)$$

where K is a blade constant ranging from 0.075 to 0.1.

At K = 0.075,

$$Z = 20.94 \text{ blades}$$

At  $K = 0.10$ ,

$$Z = 15.70 \text{ blades}$$

14. Blade plate size required

$$\begin{aligned} \text{Length of the blade arc} &= \theta r && (3.15) \\ &= 74^\circ (\pi/180^\circ) 0.96225 \\ &\doteq 1.24 \text{ inches} \end{aligned}$$

Unpressed blade strips were sized at 1.25 inches by 8.50 inches; the 0.50-inch extra length was for hinging purposes on the side disks' slots.

Plans were drawn for four runners with 10, 15, 20, and 30 blades respectively. These numbers were chosen as calculated and because these are along the range of the number of blades suggested by Mockmore and Merryfield (1949). First, plans for side disks were drawn, each having a different number of blade slots (Figures 3.1, 3.2, 3.3, and 3.4). Next the nozzle, nozzle flange, and nozzle adapter were drawn (Figures 3.5, and 3.6, respectively).

#### Construction of the Turbine

The crossflow turbine system was constructed at InEn Corporation in Stillwater, Oklahoma with the help of two shop personnel, under the author's direction. Later the turbine housing was replaced and improved at the shop of OSU's Fire Service Training, Storage, and Maintenance Facility. The design and construction, choice of construction materials, and the choice of testing equipment and experimental setup for the turbine were greatly in-

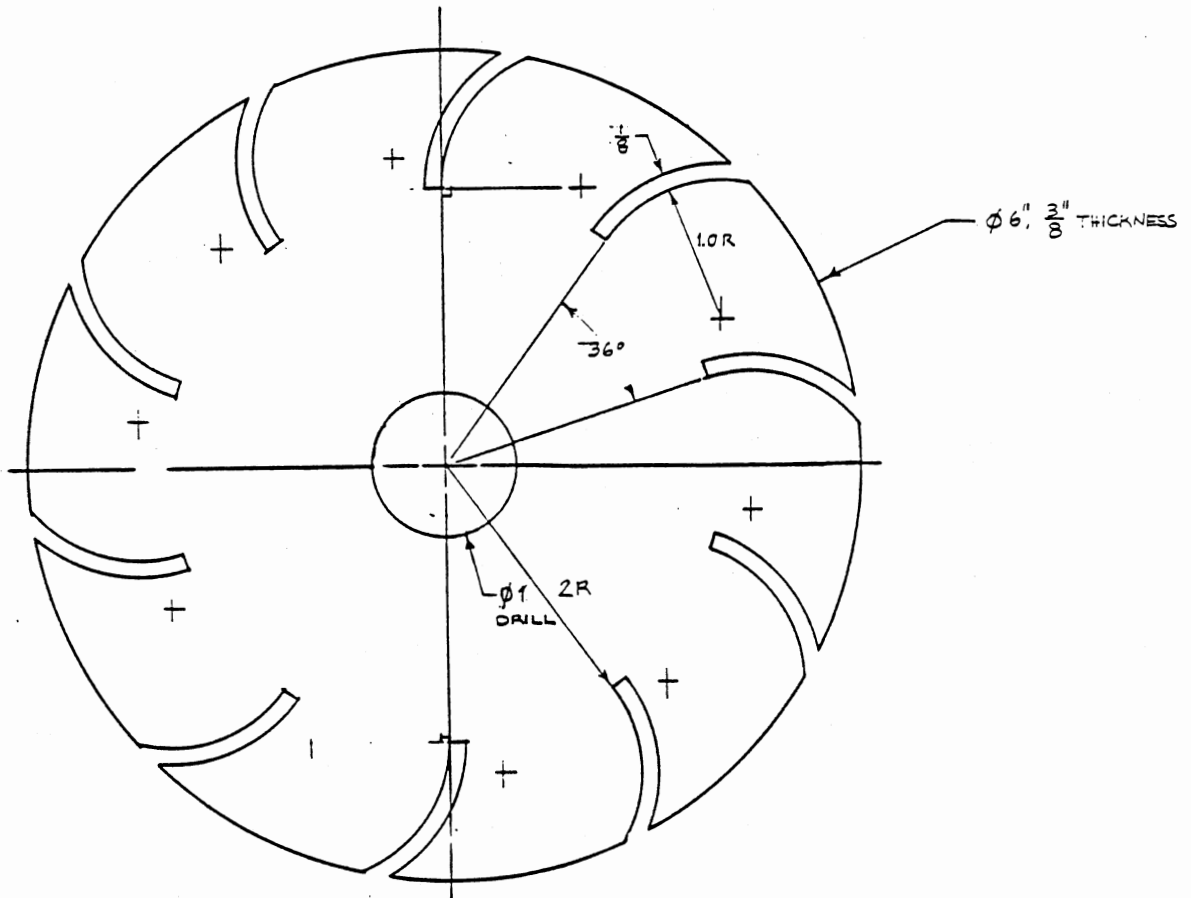


Figure 3.1. Plan for the Side Disk of the 10-Blade Runner



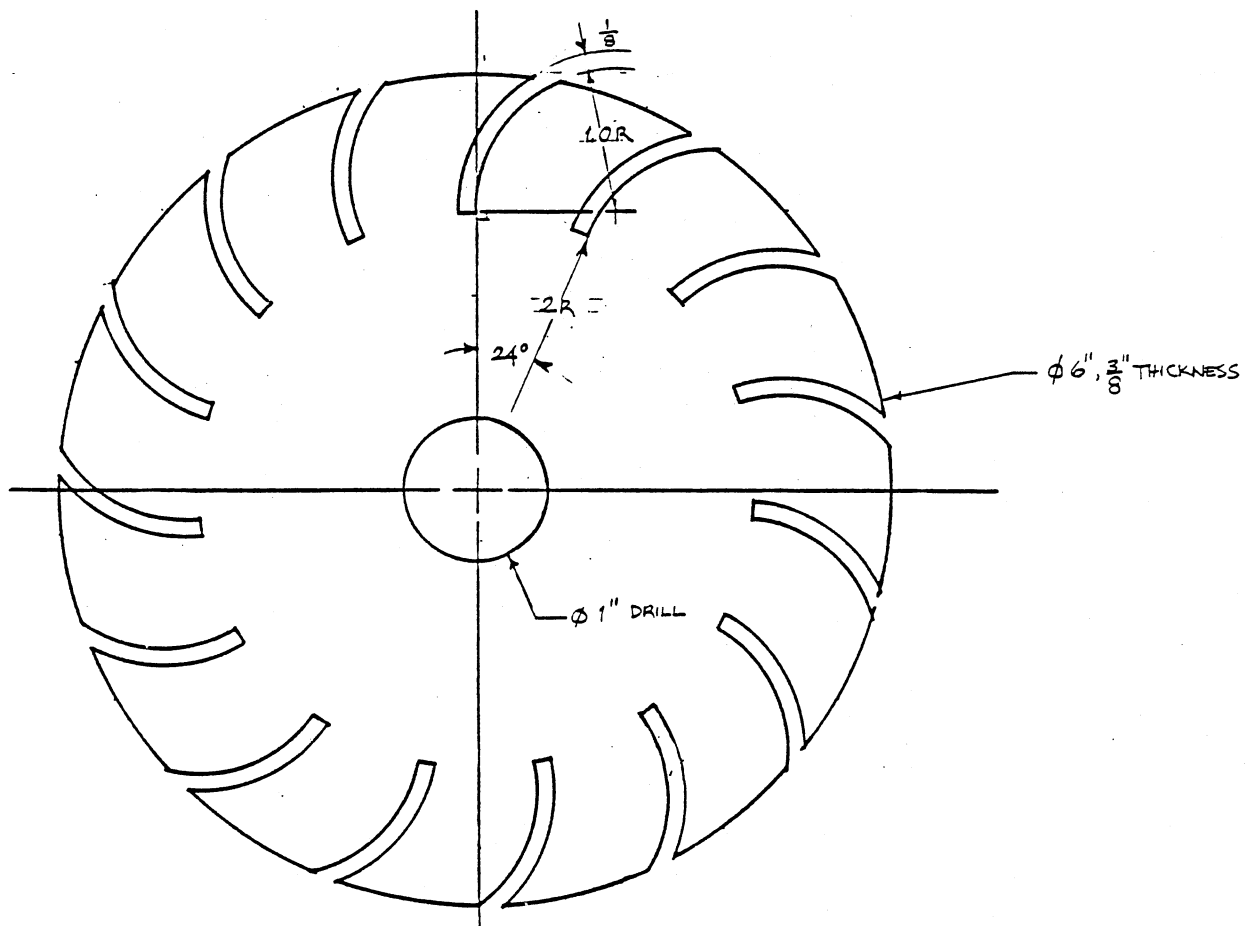


Figure 3.2. Plan for the Side Disk of the 15-Blade Runner

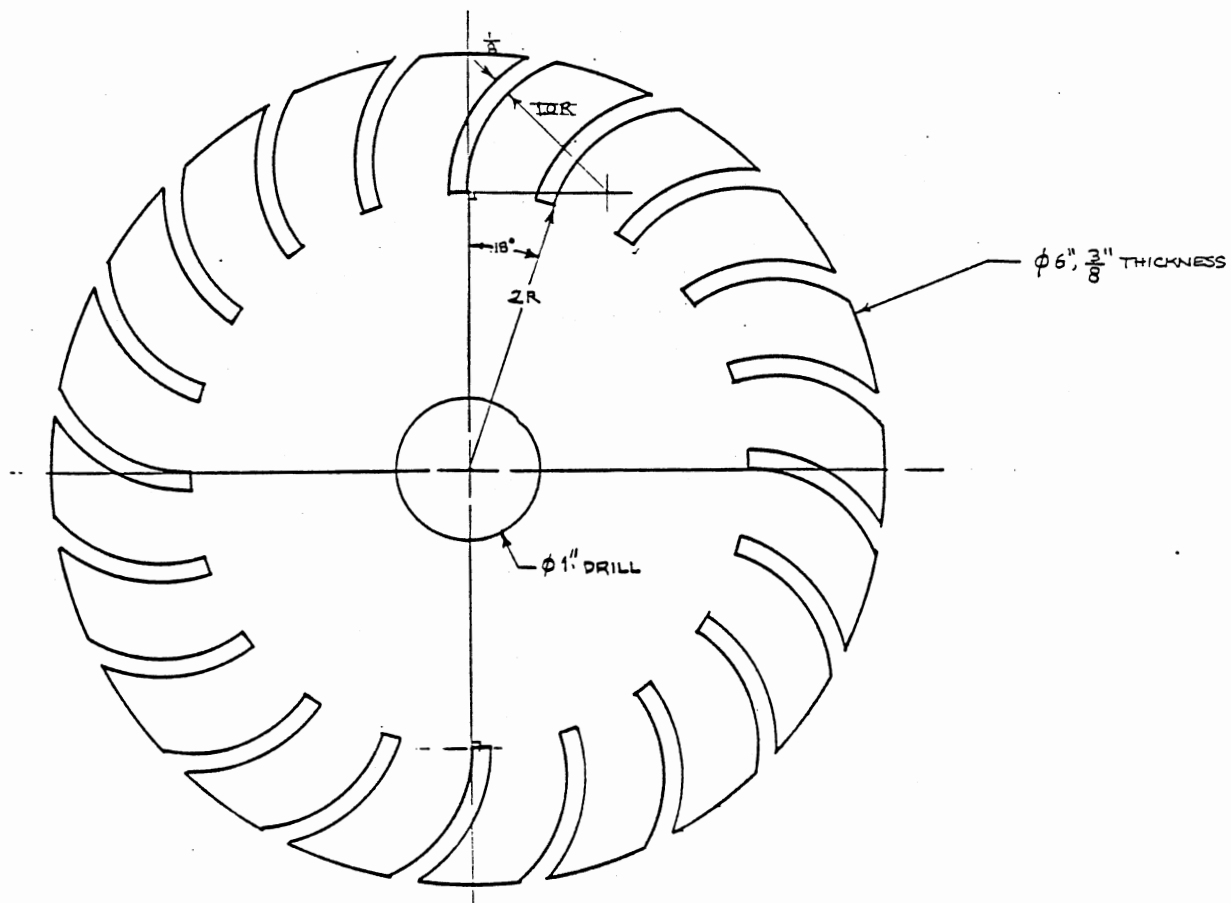


Figure 3.3. Plan for the Side Disk of the 20-Blade Runner

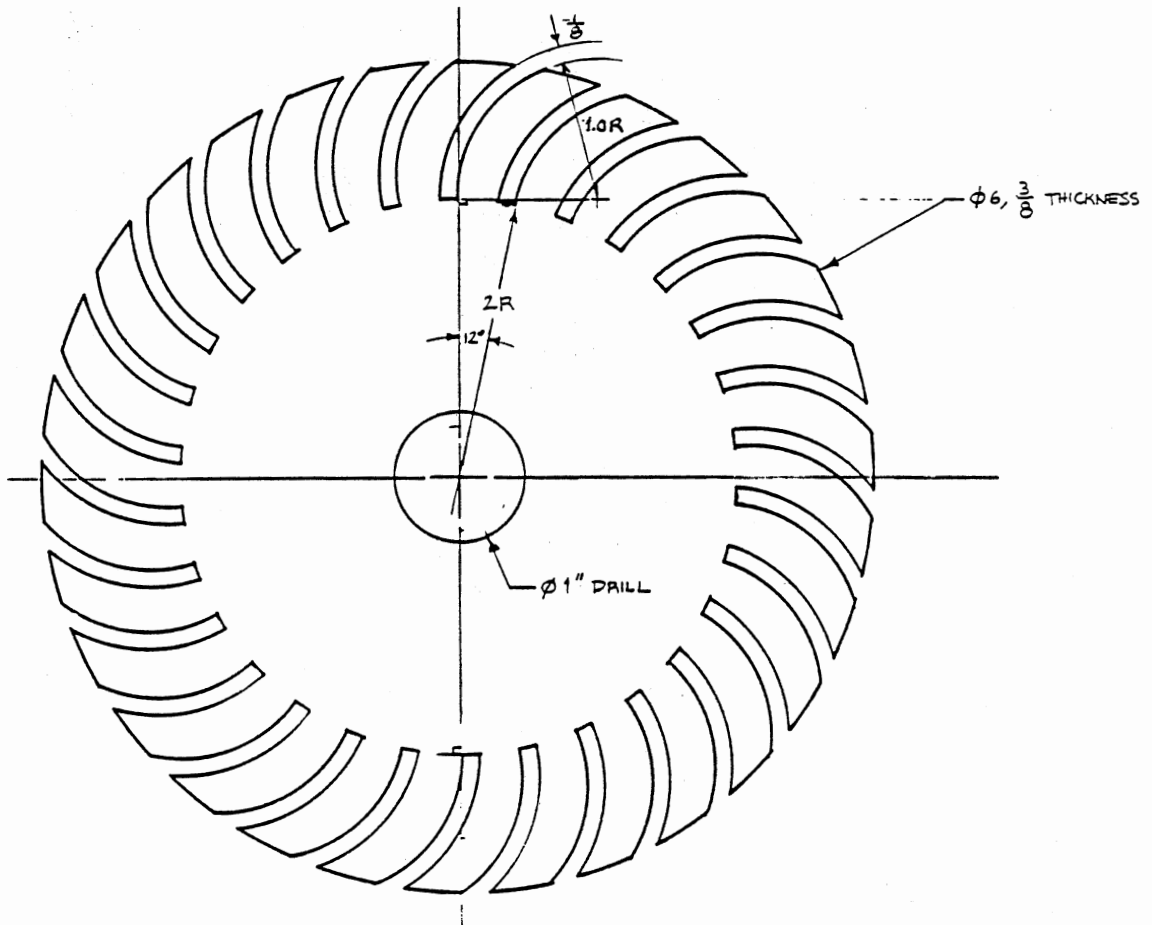


Figure 3.4. Plan for the Side Disk of the 30-Blade Runner

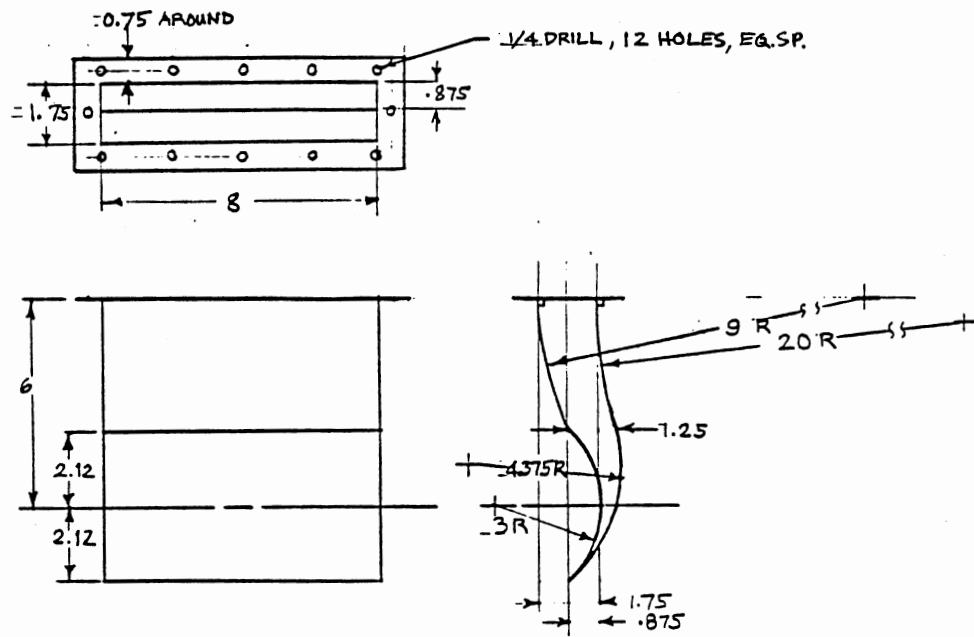


Figure 3.5. Plan for the Nozzle

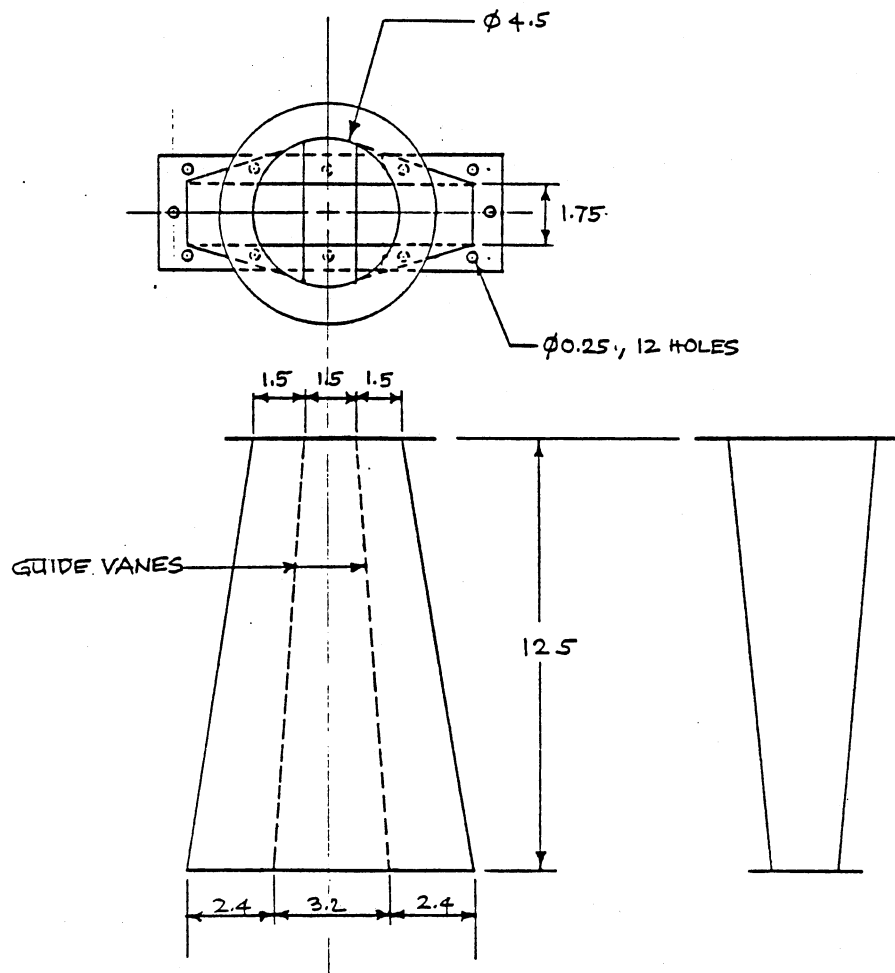


Figure 3.6. Plan for the Nozzle Adaptor

fluenced by the financial constraints placed upon the research project and the availability of a test facility.

The turbine system and the Prony brake were constructed mostly from either discarded or unusable materials in the shop or shop's junkyard. Because the company uses aluminum extensively for its products, it became appropriate that the turbine system was to be constructed out of aluminum.

First, the side disks or side plates of the various turbine runners were constructed. The side disks were cut out of 3/8 inch aluminum plate using an aluminum torch cutting machine. Half-inch centerholes were drilled and its edges smoothed to attain a 6-inch diameter. Next, slots for the blades were cut out. This was carefully done so that the slots were all identical. To maintain uniformity in the cutting of slots for both disks, a pair was bolted through the center together with a dummy disk. The dummy disk was made of plywood. It is thicker but with the same diameter as the aluminum disks. The wooden disk's centerhole was formed with a countersink to prevent the bolt head from protruding. A full scale copy of the disk drawing was pasted on top of one of the disks to serve as pattern. The foregoing preparation eased up the positioning of the bolted piece and insured uniformity in cutting the slots and hence in parallelism of the blades to be installed later.

The cutting process of the slots consisted of drilling and sawing. With the pair of disks and the plywood disk

bolted together, 1/8 inch holes were drilled at the base of the slots. Then the slots were cut using a thin bandsaw. The drilling facilitated the slot-making process because the cut-outs just fell off after sawing. The number of slots cut depended on the number of blades for a particular runner. The pair and its twin slots were marked before disassembly. This was to insure that the twin slots lie on the same horizontal line during insertion of the blades. The whole cutting process was repeated for three other pairs of disks.

The blades were cut from discarded 1/8-inch aluminum edgings. They were cut into 1.25- by 8.50-inch strips and curved to a 1-1/16-inch chord length using a hydraulic press and a piece of solid shaft and an angle bar as molds. More than 75 strips were prepared. One side of the strips' long edges was filed and tapered after pressing. This makes insertion easier. Also, it gave a hydraulic shape to the blades for the second stage entrance.

The disk centerholes were first sized with a 3/4-inch diameter steel shaft in mind but since a 1-inch solid aluminum shaft was available the hole size was increased to fit the shaft with the larger diameter. During assembly of the blades, the shaft was mounted on a lathe with a pair of disks in place. The blades were inserted in the slots around the disks' periphery making sure that the twin slots were opposite each other. The assembly was adjusted accordingly to ensure that the disks were parallel with

each other and were perpendicular to the shaft. The runner assembly was tightly bound and released from the lathe to be ready for the welding phase. The entire procedure was repeated on three other runner assemblies. The same shaft was used because the turbine system was designed to have an interchangeable runner.

The blade strips' length (8.50 inches) was intentionally cut shorter than the total length of the runner which is 8.75 inches including the thickness of the two 3/8-inch thick side disks. Hence a 1/8-inch deep vacant space was available on both ends of the blade for weld fill-up. Welding of the blades to the side disks was accomplished using special aluminum welding equipment.

A pair of hubs was then constructed also out of aluminum. The purpose of the hubs was to hold the runner and shaft together. The hubs are attached to the disks by a pair of flat head machine screws and to the shaft by a pair of hex socket screws, at each end of the runner. The disks, hubs, and shaft were drilled and threaded to accomplish this task. The assembly was then mounted on a lathe. Uneven edges or joints, sharp corners, and extra weld were ground carefully. The blades' outer edges were further filed manually to give a hydraulic appearance thus open up more space for water inflow. The entire process was done on three other runners as well. The finished runners are shown in Figures 3.7 and 3.8. The finished shaft and hubs are shown in Figure 3.9; the pair of self-aligning



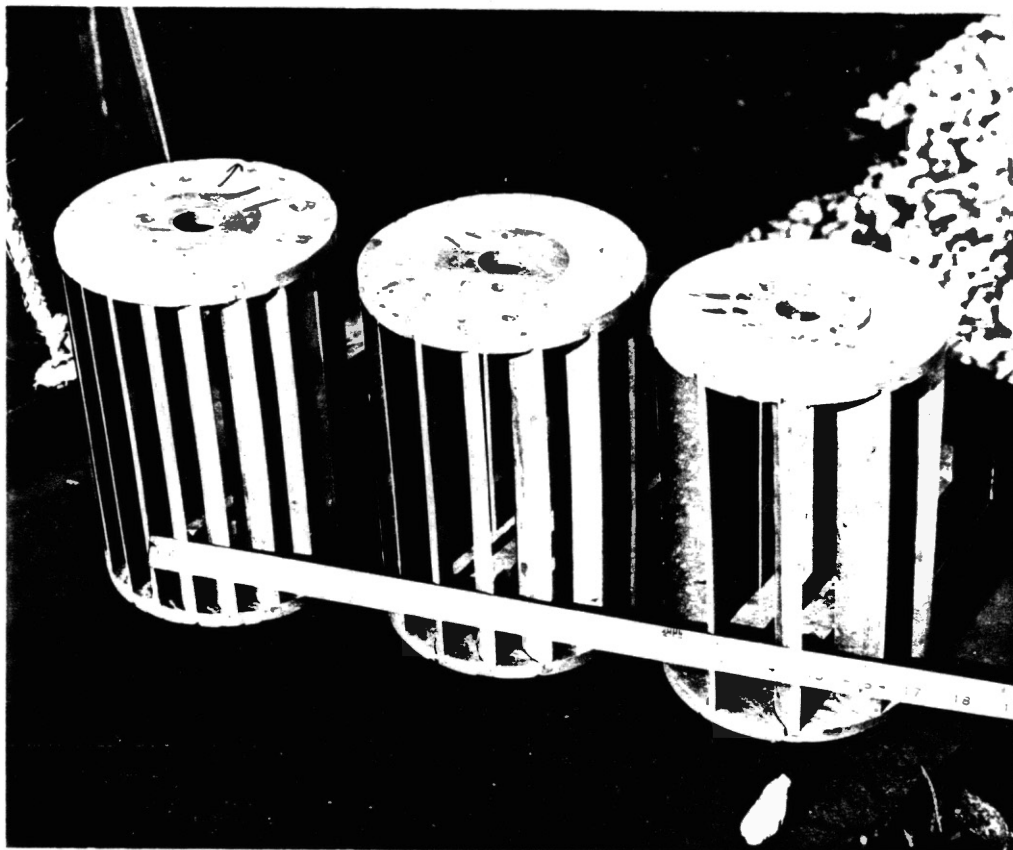


Figure 3.7. The Finished Runners (10, 15, and 20 Blades)

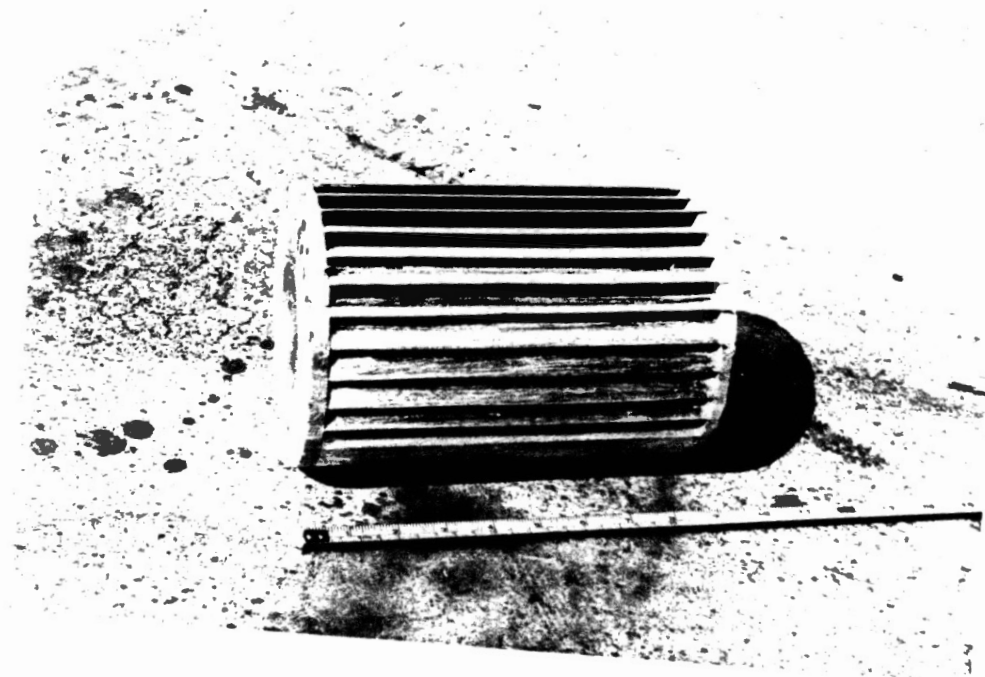


Figure 3.8. The 30-Blade Runner

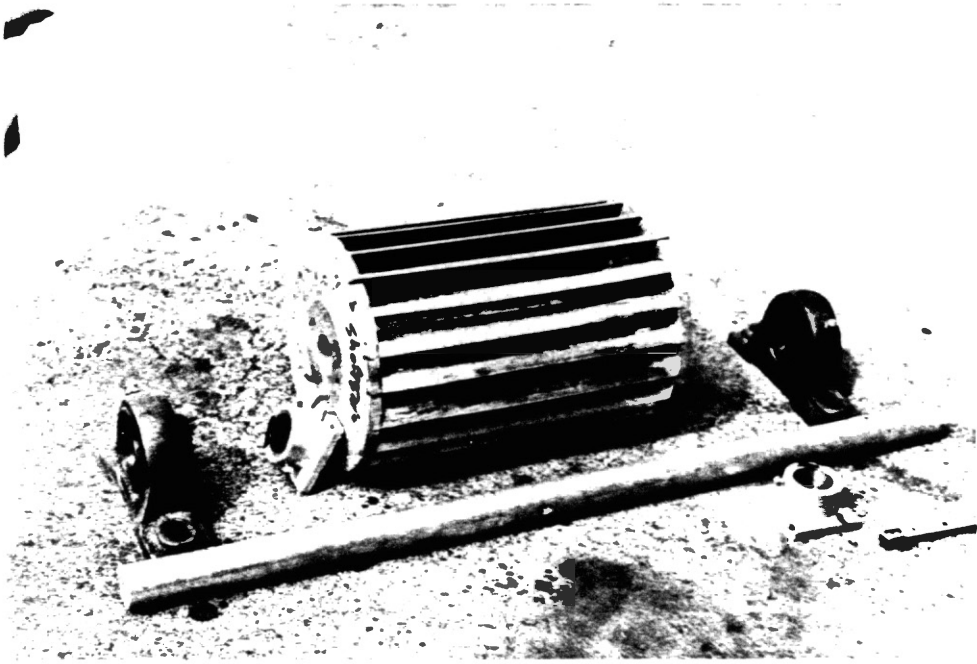


Figure 3.9. The Finished Shaft and Hubs

bearings shown was cannibalized from other equipment.

### Construction of the Turbine

#### Nozzle and Adapter

The nozzle parts were cut out 1/16-inch sheet aluminum. Lack of jigs and molds and equipment made the shaping of the nozzle parts to exact specifications rather difficult. The problem was aggravated by the warping of sheet aluminum when subjected to welding. The same problem was encountered with the construction of the nozzle adapter and the welding of vertical guide plates inside the adapter. The nozzle is bolted to the nozzle adapter which in turn is bolted to the fire hose adapter (Figures 3.10 and 3.11). The 3.5-inch canvas fire hose was used as the penstock in this experiment.

The turbine housing was constructed out of 3/4-inch plywood from used crates but was later replaced due to vibration problems during trial runs. A steel box picked up from the junkyard of the Fire Service Training, Storage, and Maintenance Facility proved to be just the right replacement. The 25- by 18- by 14-inch box was already open on the top side but windows had to be cut at the front and rear and an opening at the bottom for the water from the blades to drain. Vertical slots were also cut on both sides of the box for the shaft to slide through. The nozzle assembly was installed with the nozzle face down and parallel to the ground. Slotted short angle bars were

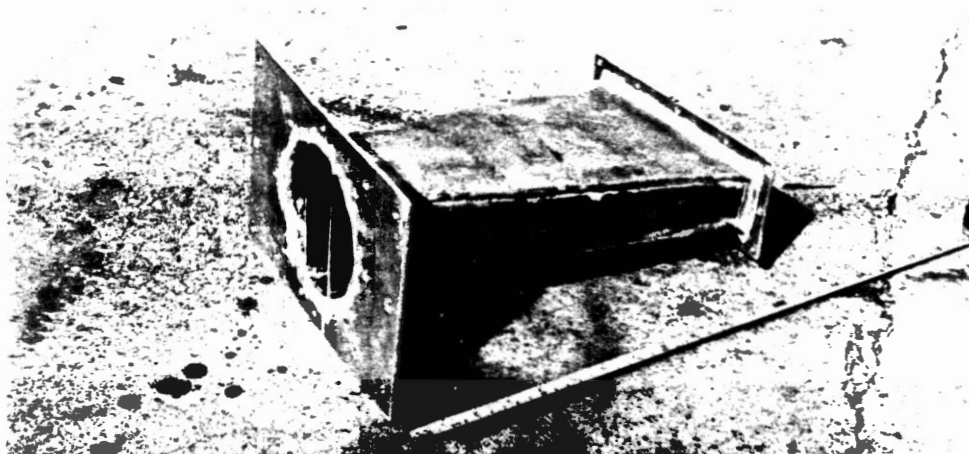
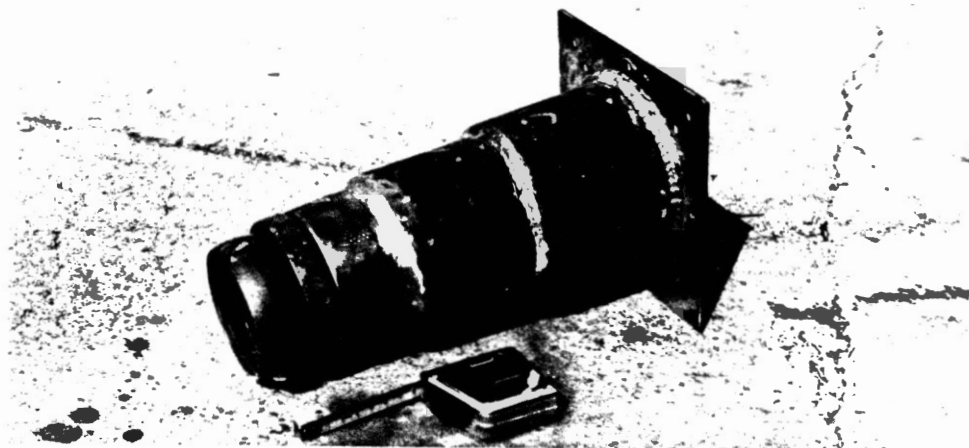


Figure 3.10. The Finished Fire Hose Adaptor,  
Nozzle Adaptor and Nozzle

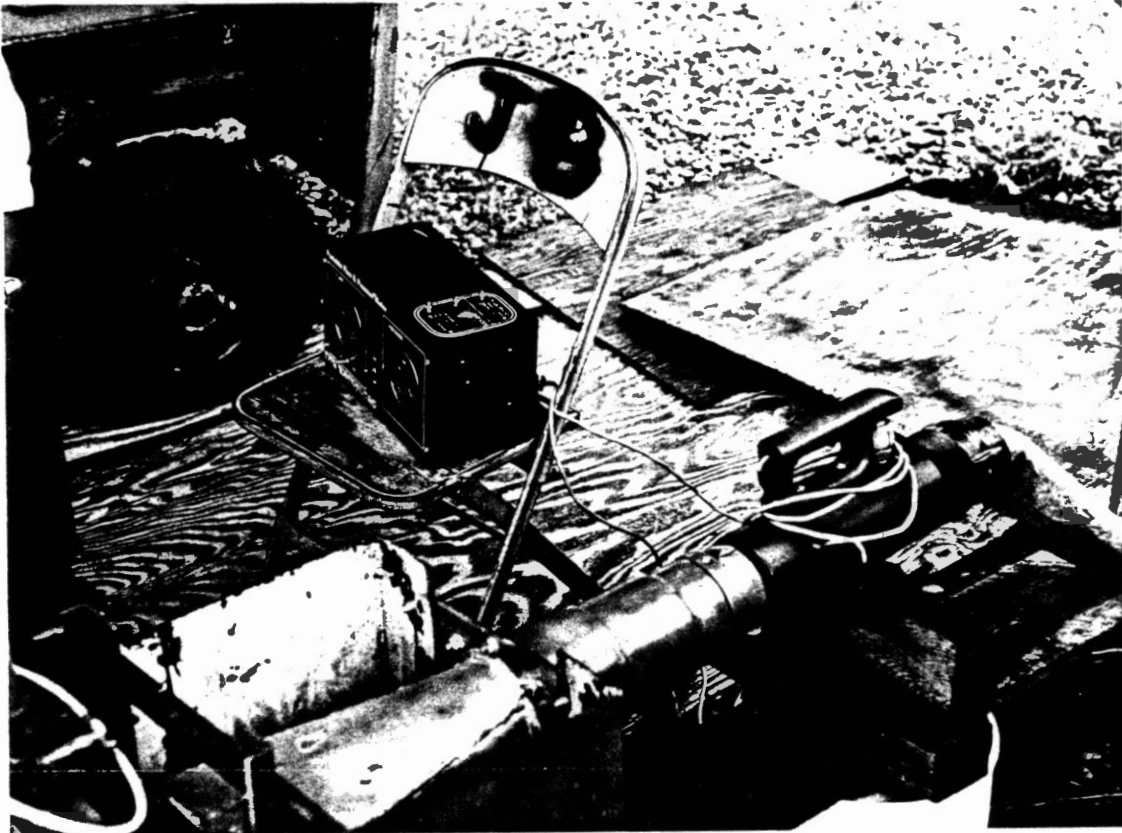


Figure 3.11. The Assembled Fire Hose Adaptor,  
Nozzle Adaptor and Nozzle

welded at the base of the slots for a pair of self-aligning bearings to sit upon. The angle bars and bearings were at such height that the runner assembly was close enough against, but not touching, the nozzle curvature. Replacement of the runner was accomplished by loosening the hub screws and pulling out the shaft. The detached runner had to be passed through the front window because the top part is occupied by the nozzle assembly. Assembly was done on a reverse sequence. In addition to the parts mentioned, a discarded 12-inch gear pulley was used as a flywheel. The assembled turbine system is shown in Figure 3.12.

#### Construction of the Prony Brake

In the absence of a factory-made dynamometer to obtain power output, a Prony brake was constructed out of discarded 1-inch thick canvas blocks, an insulator used in electrical assemblies. A steel bushing was also made for the brake. The bushing was attached tightly to the shaft's end. Brake force against the bushing or shaft can be varied by adjusting a pair of bolts clamping the brake. A leather strip permanently soaked in engine oil through a makeshift lubrication system was used as a friction heat absorber between the brake and the steel bushing. The brake had an adjustable length lever arm hinged at one end by a weighing scale. Several Prony brakes were previously constructed and tested but failed to do the job. Figure 3.13 shows the Prony brake assembly attached to the turbine.

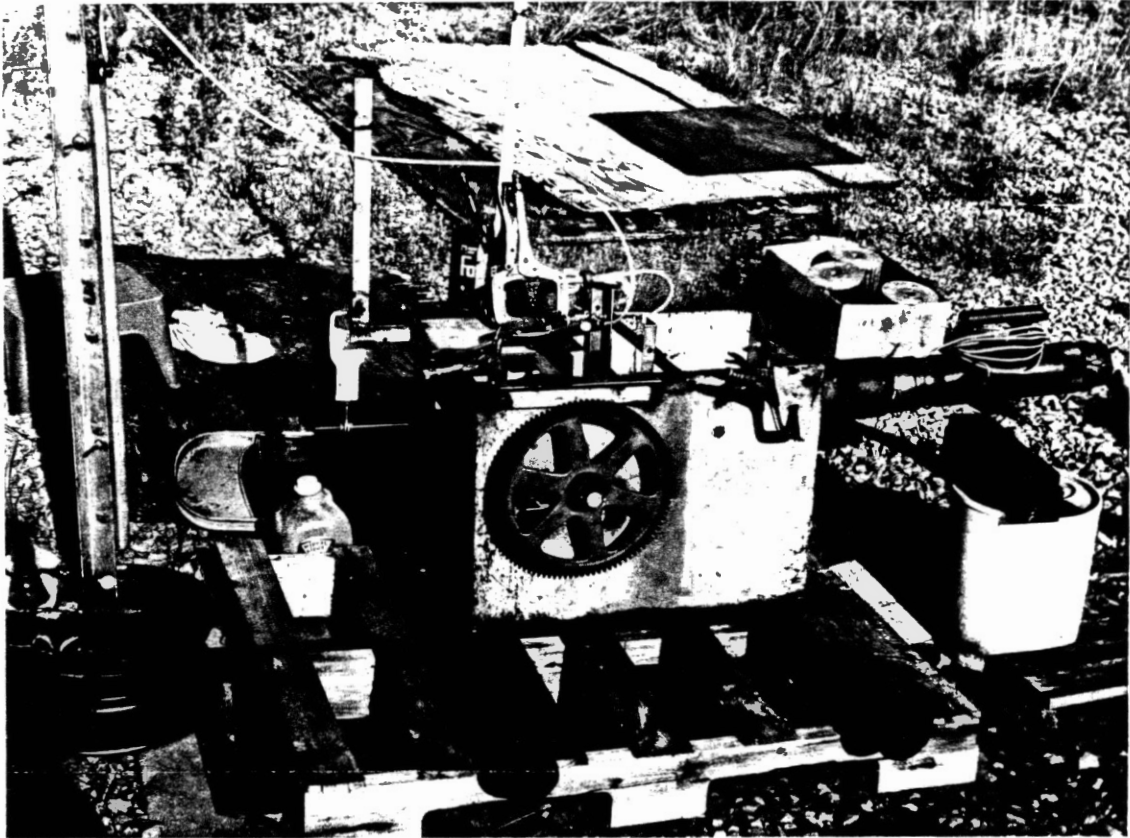


Figure 3.12. The Crossflow Turbine Prototype



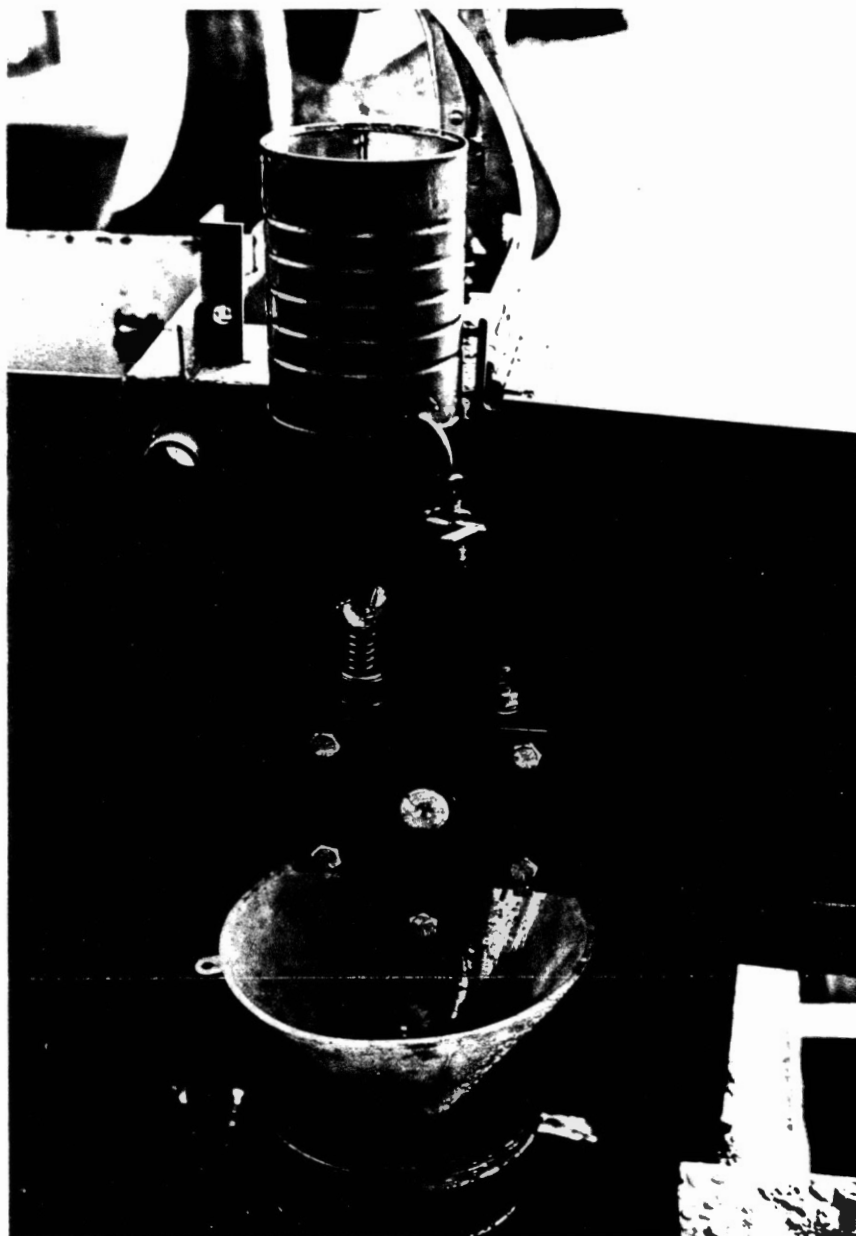


Figure 3.13. Prony Brake Assembly

Construction of the foregoing turbine system indeed simulated developing country situations in which only available and cheap (discarded) materials were utilized. The construction and materials may not be of excellent quality but it established a pioneering spirit and opened many challenges for the improvement of the design and adaptation to developing country conditions.

## CHAPTER IV

### INSTRUMENTATION AND TEST PROCEDURE

#### Instrumentation

The test run was conducted at the 10-acre grounds of the OSU Fire Training, Storage, and Maintenance Facility. The facility is mainly used to train firefighters in fire prevention techniques involving various types of fires. It was chosen as the experimental area because it already contains a good water supply network complete with a pond, a sump, and a series of hydrants and water supply lines. A firetruck was standing by to pump water from the pond to the receiving hydrant (Figure 4.1). Water was fed to the receiving hydrant using firehoses. Water supply to the turbine came from one of the other hydrants connected to the underground pipe network. Water supplied to the turbine drained through the sump and back to the pond. Supply flow rate  $Q_s$  was regulated from the firetruck as well as from the supply hydrant although not simultaneously.

The experiment called for the measurement of the independent variables, namely; supply volume flow rate  $Q_s$ , shaft brake force  $F$  and shaft or runner rotative speed  $N$ . Blade number,  $Z$ , is also one of the variables but obviously a



Figure 4.1. Firetruck as Pump in the Water Supply Network

measuring instrument is not necessary to know this. Water supply to the turbine,  $Q_s$ , was measured by a battery-powered paddle-type electronic flowmeter with an analog readout shown in Figure 4.2. The flowmeter was situated about five feet before the entrance to the nozzle adapter. Dynamic and static pressures were picked up by a pitot-static tube hooked to a graduated vertical U-tube mercury manometer. The pitot-static tube was positioned at the exit of the nozzle where its tip is parallel to and against the direction of flow. Because of highly distorted pressure readings, water pressure and hence available head was calibrated against the supply flow rate (See Chapter V, Results and Discussion). A weighing scale shown in Figure 4.3 was used to quantify brake force from the Prony brake. Brake force was varied by tightening or loosening one or two bolts that held down the Prony brake against the rotating shaft. The brake was continuously lubricated with engine oil through a makeshift lubrication system to prevent the leather brake pads from burning and to minimize the jerking of the moment arm so the reading of a precise brake force could be as accurate as possible. A stopwatch-type hand-held dial tachometer was used to measure rotative speed during various levels of brake applications (Figure 4.4). In all cases, recording was manual.

#### Test Procedure

Before final data acquisition was done, everything was

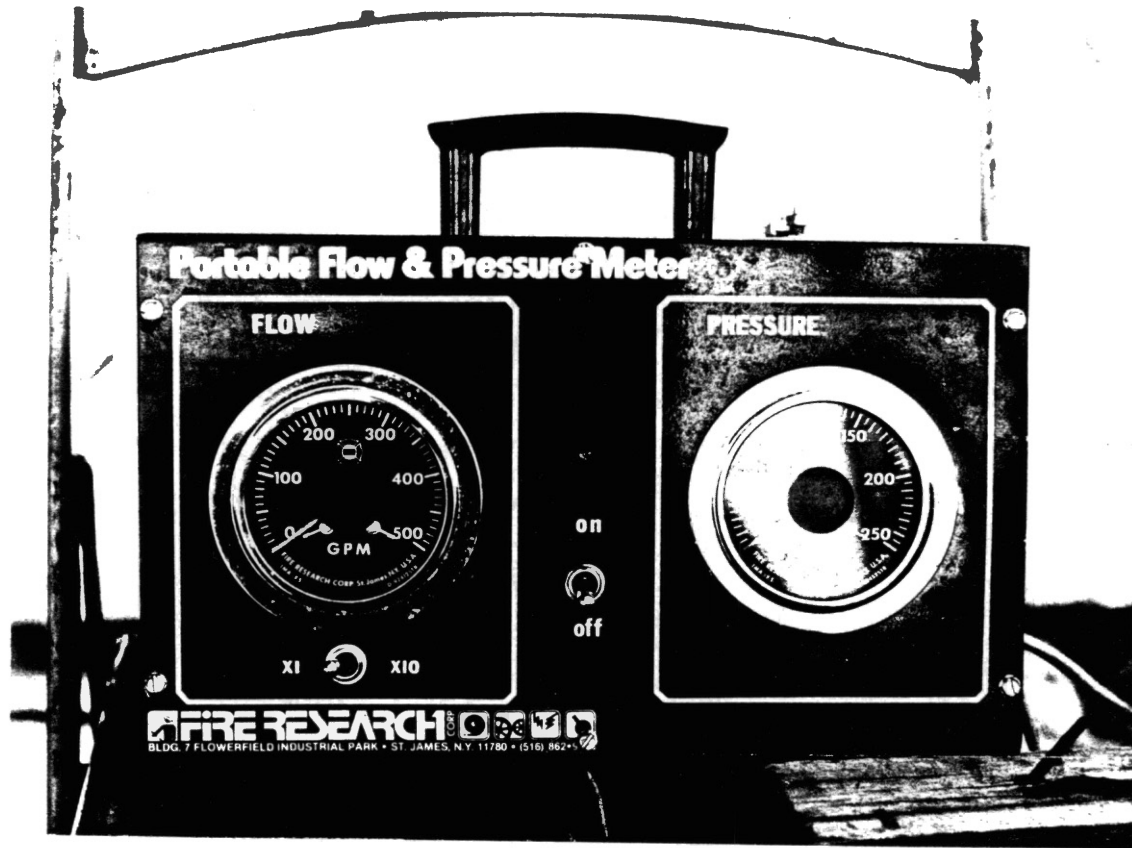


Figure 4.2. Flowmeter Readout



Figure 4.3. Weighing Scale

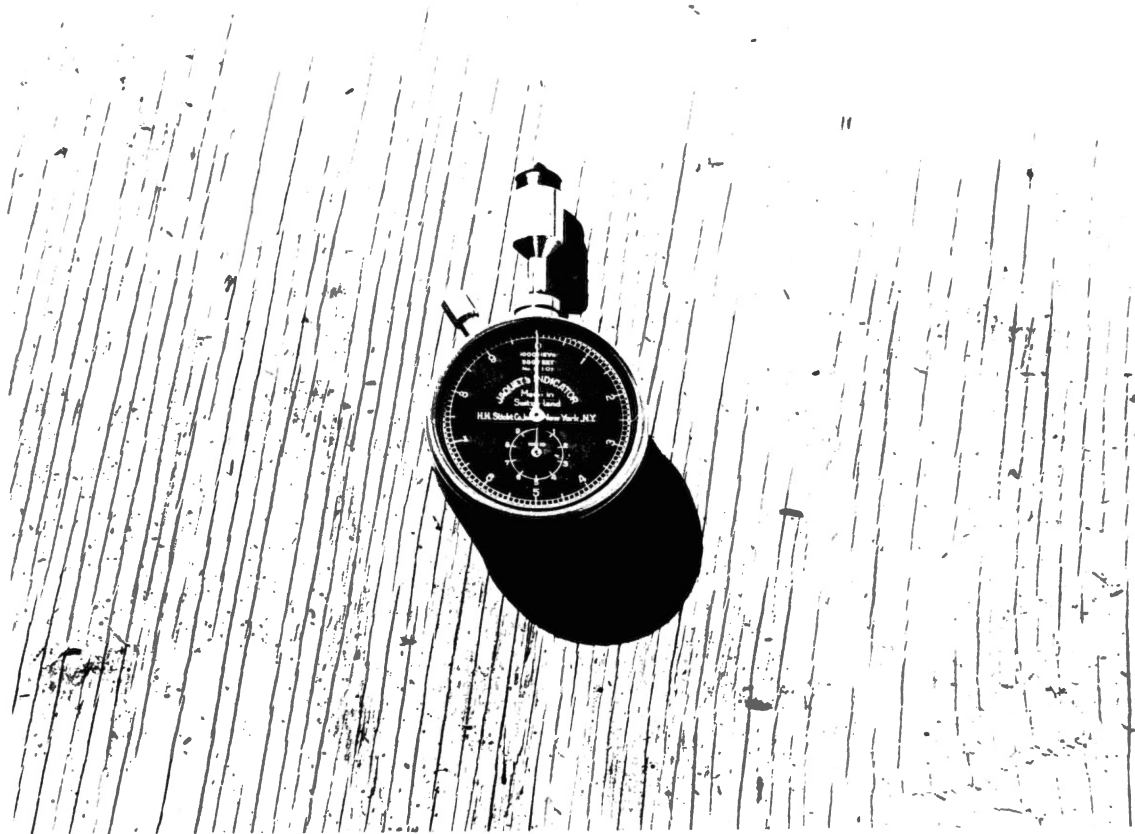


Figure 4.4. Tachometer



checked to insure that all system components, that is, turbine, water supply, and measurement systems, worked properly. Pressure readings, however, were observed to be distorted during applications especially at low rotative speeds. Apparently the distortion was caused by high turbulent characteristics of flow and the build-up of water volume at the nozzle exit when the runner shaft was held down to low rotative speeds. Due to this distortion, water pressure at nozzle exit was derived as a function of supply flow rate. These pressure values were used in the calculation of available head and subsequently in calculation of input power (See Figure 4.5).

The main purpose of this experiment was to test the performance of the turbine runners, each having a different number of blades. For each runner at a particular supply flow rate  $Q_s$ , the Prony brake was slowly tightened at arbitrary increments of rotative speeds,  $N$ . At each increment, torque or brake force,  $F$ , was recorded from the weighing scale and runner rotative speed,  $N$ , was recorded from the hand-held tachometer. Brake was applied until the runner stopped turning or until the brake could no longer clamp the rotating shaft to a halt. For the same runner, a new flow rate,  $Q_s$ , value was used and the brake application steps were repeated. All in all the four runners were subjected to three levels of flow rates  $Q_s$ ; each level was subjected to a range of brake force,  $F$ , and rotative speed,  $N$ , values. All recordings were done manually.

Figures 4.5 and 4.6 illustrate how power and efficiency are attained. Figures 4.7 and 4.8 show the turbine in operation.

Independent variables

Dependent variables

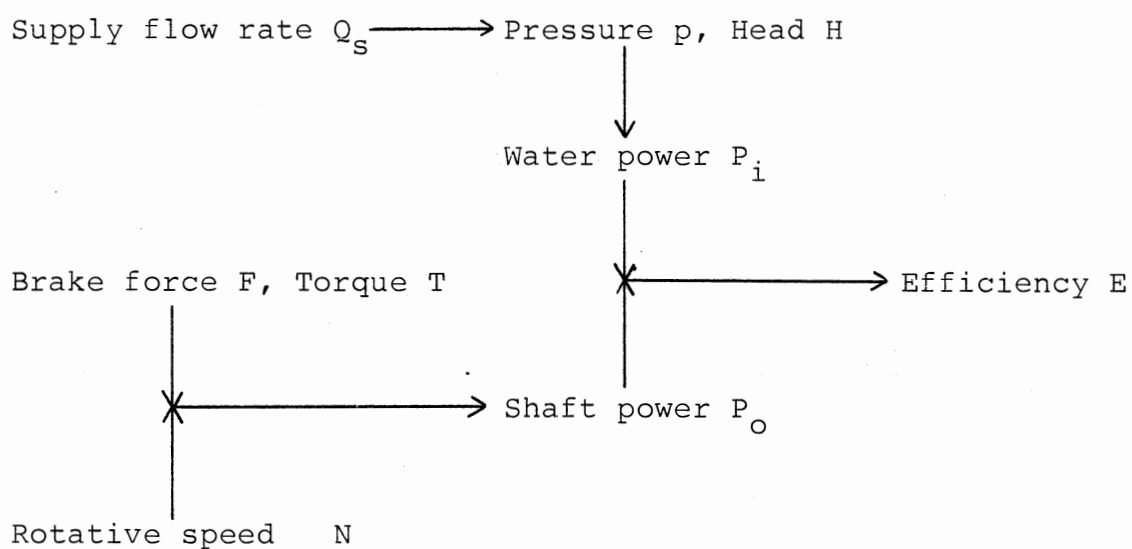


Figure 4.5. Schematics for power and efficiency determination for a particular runner with  $Z$  blades and at a particular supply flow rate  $Q_s$ .

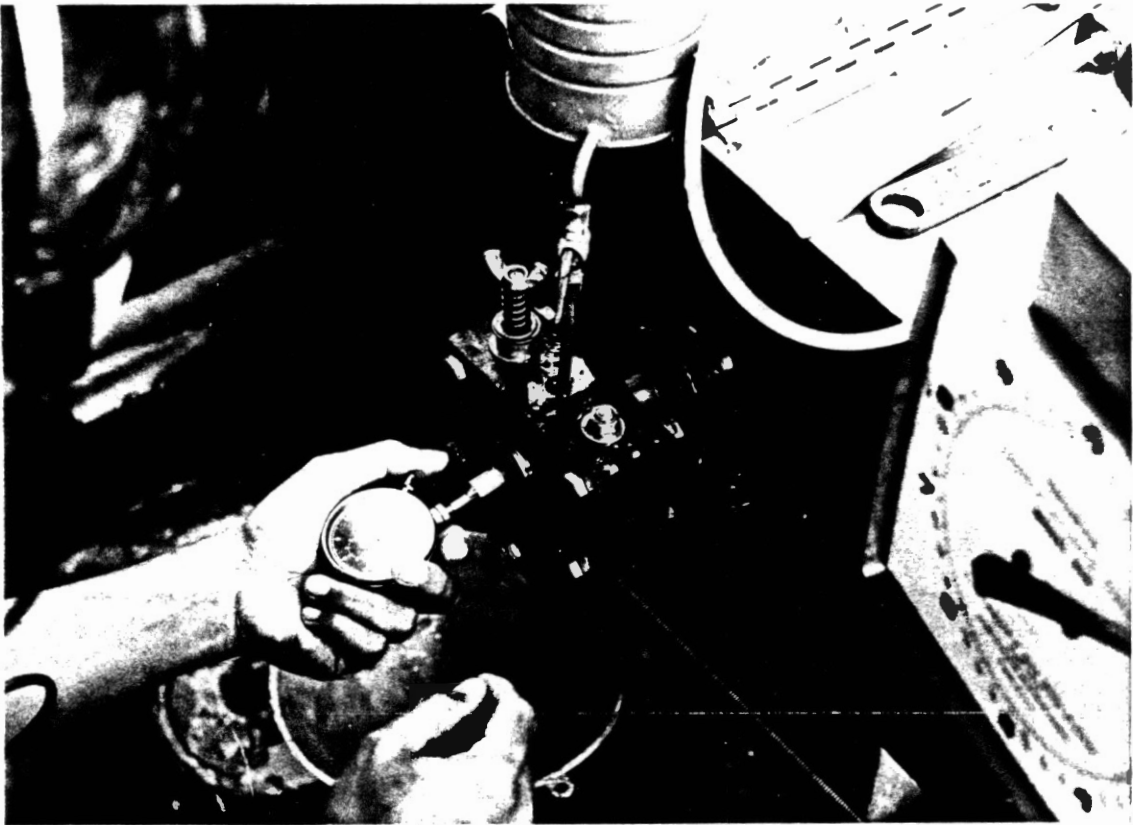


Figure 4.6. Measurement of Rotative Speed and Torque

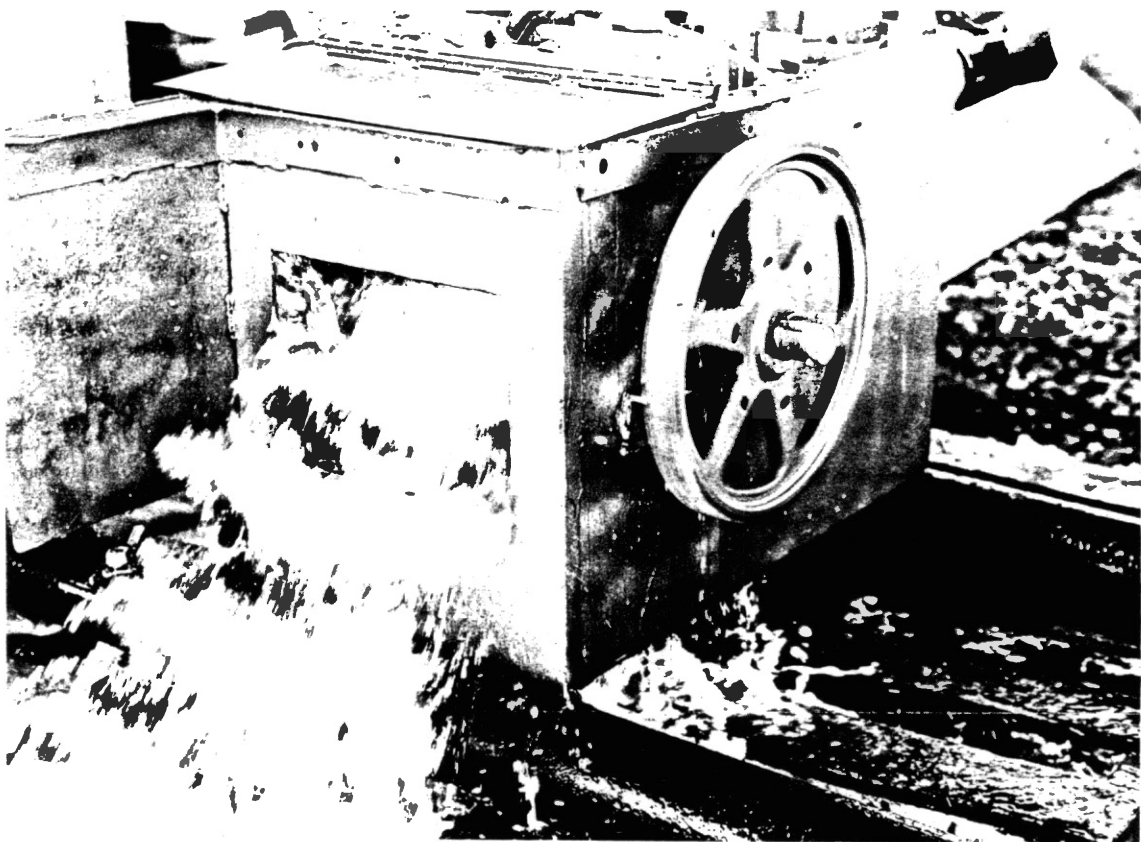


Figure 4.7. The Crossflow Turbine  
in Operation

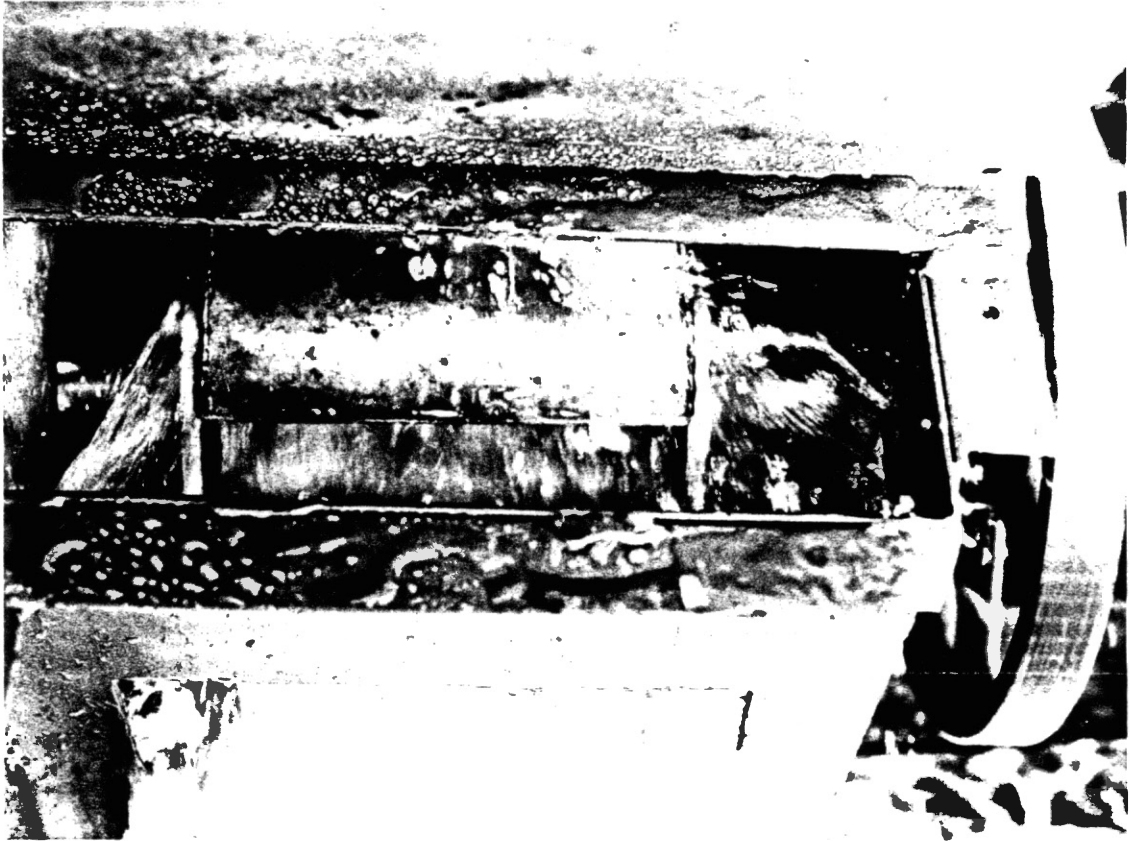


Figure 4.8. An Inside View of the  
Operating Turbine

## CHAPTER V

### RESULTS AND DISCUSSION

Performance data of the four runners at various levels of supply flow rates  $Q_s$  and rotative speeds  $N$  are shown in the following pages. Number of blades  $Z$ , supply flow rate  $Q_s$ , rotative speed  $N$ , and brake force  $F$  or torque  $T$  are the input variables. Another input variable, average nozzle dynamic head  $H_{nd}$ , was derived as a function of supply flow rate  $Q_s$ .

#### Calculation of Total Available Head, H

Because of the highly turbulent behavior of flow during brake applications which resulted in wide-ranging readings of nozzle pressure, a mathematical relationship was established to determine the nozzle pressure or head based on a specific supply flow rate. This calibration of the nozzle pressure relative to the supply flow rate was done without the runner in the turbine. Pressure readings were taken from various points within the nozzle outlet cross-section for each specified flow rate. Pressure readings were also taken for other levels of flow rates.

The location of the points are shown in Figure 5.1, fifteen points along the horizontal axis and seven points

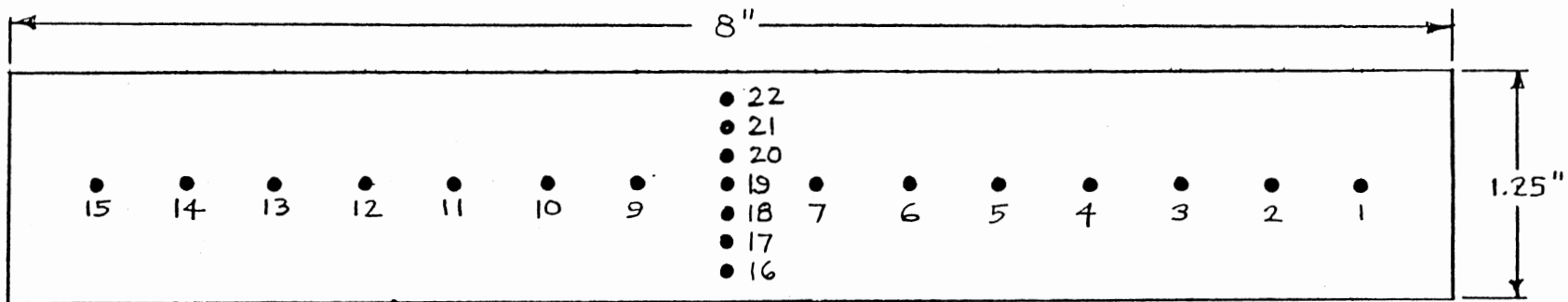


Figure 5.1. Point Location of Pitot-Static Tube at Nozzle Cross-Section (Direction of Flow is Toward the Reader)

along the vertical axis. The set-up of the nozzle calibration is shown in Figure 5.2. A 0.5 mm Pitot-static tube connected to a U-tube mercury manometer was used to pick up nozzle pressure at each point. The Pitot-static tube was positioned in such a way that its tip faced the direction of flow and gave the maximum reading for that point location. A system of gate valves was assembled to get both dynamic and static pressures, although not simultaneously because there was only one manometer available. The pressure data are shown in Table I. The average nozzle dynamic head  $H_{nd}$  of a particular flow rate was calculated based on the average of the 22 readings. The average nozzle dynamic head  $H_{nd}$  was plotted against the supply flow rate  $Q_s$  shown in Figure 5.3, which gives the regression equation.

$$H_{nd} = 0.0105 Q_s - 0.8031 \text{ ft} \quad (5.1)$$

where  $H_{nd}$  is in ft of water and  $Q_s$  is in gpm. R-square (coefficient of determination) is 0.98.

Equation (5.1) was used to calculate total head available in the turbine, which is,

$$H = H_{nd} + h \quad (5.2)$$

where  $H$  is the total available head in ft of water and  $h$  is the drop of the water jet within the runner, which is the vertical distance from the nozzle tip to the center axis of the runner. This distance is approximately equal to 0.25



TABLE I  
NOZZLE PRESSURE DATA AT  
VARIOUS FLOW RATES

Outlet Point	Hg Manometer Pressure (1/2 X reading)							
	305 gpm		355 gpm		400 gpm		465 gpm	
	dyn	stat	dyn	stat	dyn	stat	dyn	stat
1	1.05	0.36	1.35	0.40	1.60	0.75	1.85	0.92
2	1.10	0.38	1.45	0.65	1.85	0.75	2.00	0.90
3	1.10	0.40	1.40	0.65	1.80	0.68	1.85	0.95
4	1.10	0.38	1.30	0.55	1.60	0.65	2.00	0.90
5	1.10	0.36	1.30	0.50	1.55	0.68	1.80	0.85
6	1.15	0.35	1.35	0.50	1.55	0.65	1.70	0.75
7	1.20	0.35	1.32	0.50	1.54	0.68	1.60	0.70
8	1.23	0.35	1.40	0.45	1.60	0.65	1.70	0.80
9	1.20	0.37	1.30	0.50	1.50	0.65	1.65	0.75
10	1.20	0.40	1.30	0.50	1.50	0.65	1.70	0.70
11	1.10	0.34	1.20	0.45	1.36	0.65	1.75	0.70
12	0.90	0.32	1.00	0.45	1.10	0.60	1.80	0.65
13	0.85	0.30	0.95	0.50	1.08	0.60	1.96	0.66
14	0.85	0.31	0.94	0.50	1.05	0.60	2.30	0.67
15	0.85	0.33	0.95	0.55	1.08	0.60	2.80	0.75
16	1.20	0.34	1.30	0.45	1.50	0.60	1.60	0.65
17	1.20	0.35	1.35	0.45	1.50	0.60	1.65	0.60
18	1.20	0.38	1.40	0.45	1.55	0.60	1.75	0.75
19	1.27	0.40	1.35	0.45	1.55	0.61	1.80	0.75
20	1.20	0.45	1.30	0.50	1.54	0.62	1.90	0.75
21	1.15	0.50	1.35	0.52	1.50	0.60	1.75	0.75
22	1.05	0.50	1.20	0.55	1.37	0.65	1.65	0.80
Total	24.250	8.220	27.760	11.020	32.270	14.200	40.560	16.800
Ave	1.102	0.373	1.261	0.501	1.467	0.641	1.840	0.760
$H_n$ (in-Hg)	2.204	0.747	2.523	1.000	2.934	1.283	3.680	1.527
$H_n$ (ft-H <sub>2</sub> O)	2.497	0.846	2.858	1.133	3.324	1.453	4.169	1.730

$H_n$  - average head  
at nozzle

$H_{ns}$  - static average  
head at nozzle

$H_{nd}$  - average dynamic  
head at nozzle

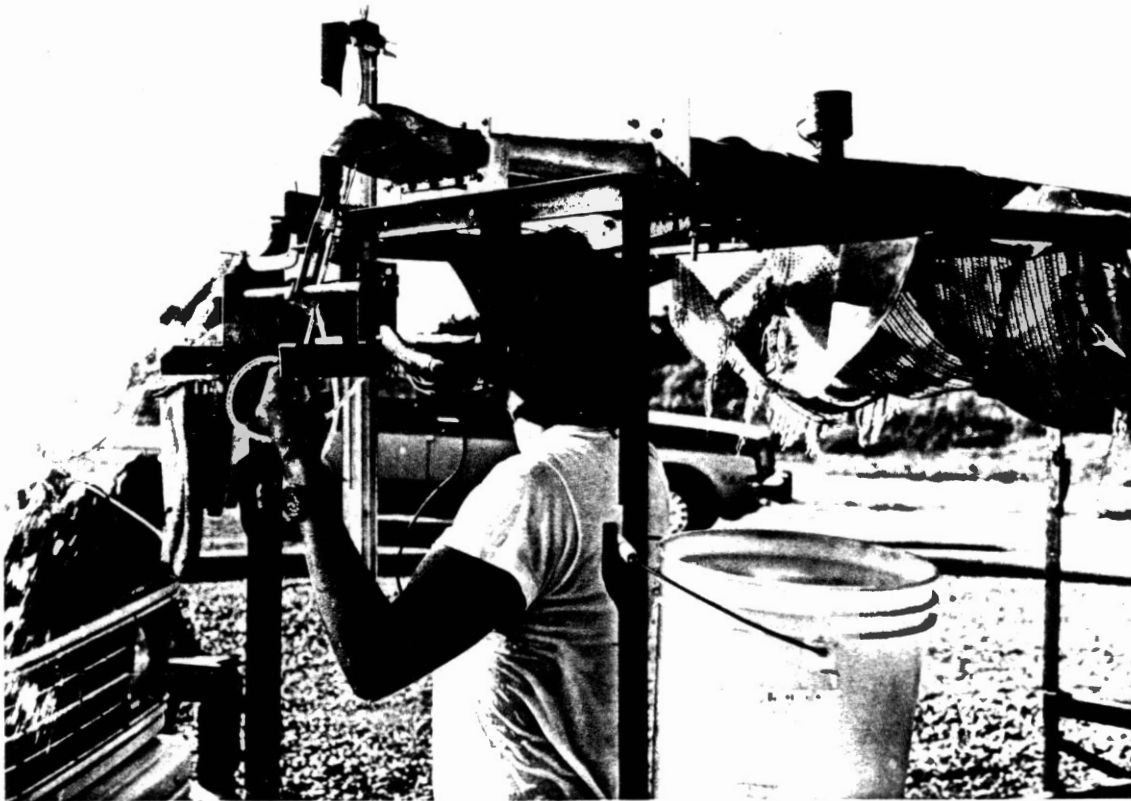


Figure 5.2. Measurement of Nozzle Cross-  
Section Pressures

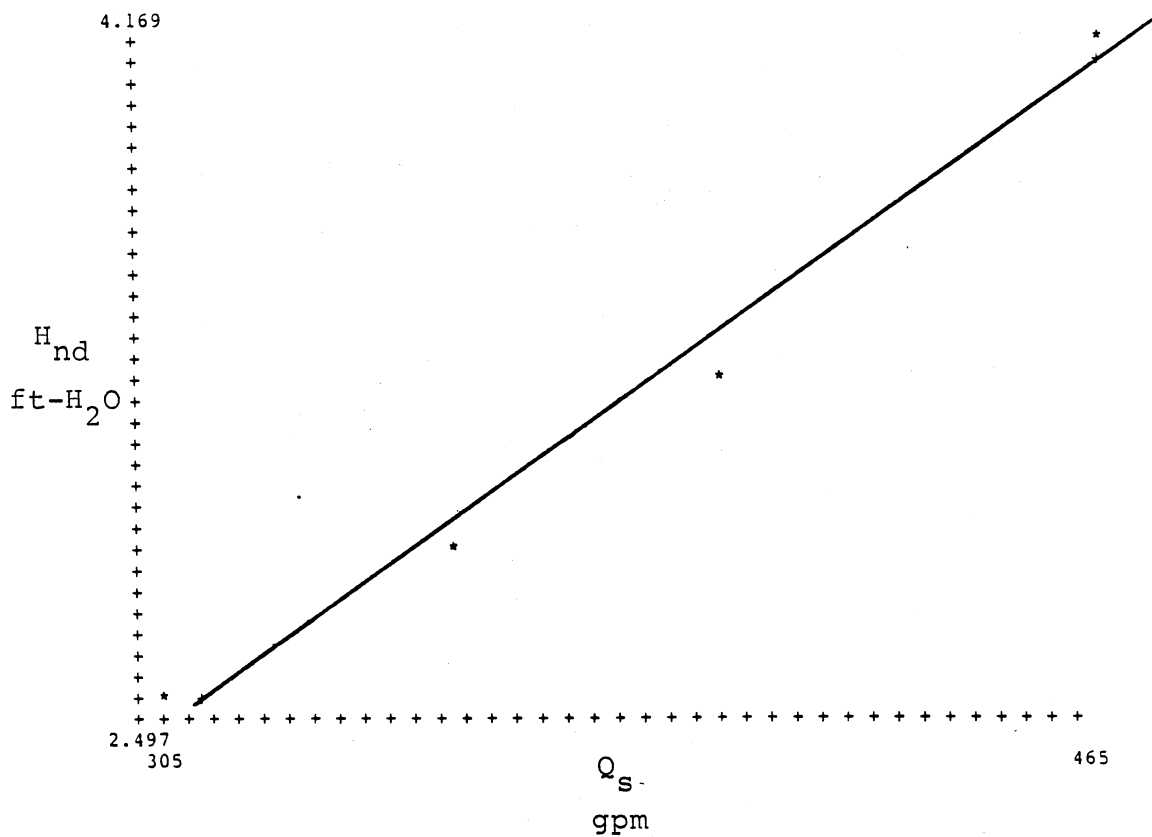


Figure 5.3. Nozzle Dynamic Head as a Function of Supply Flow Rate

feet which is the radius of the runner.

### Runner Performance

Subsequently, total available head  $H$  is used in the calculation of input water power  $P_i$ , water jet velocity entering the runner  $V_1$ , turbine efficiency  $E$ , and velocity coefficient  $U_1/V_1$ . Using Equation (2.1), input power becomes

$$P_i = 2.5277 \times 10^{-4} Q_s H \text{ hp} \quad (5.3)$$

where  $Q_s$  is in gpm and  $H$  is in ft. Spouting velocity entering the runner was calculated from

$$V_1 = (2g H)^{1/2} \quad (5.4)$$

$$\text{or } V_1 = 8.0249 H^{1/2} \text{ fps} \quad (5.5)$$

where  $g$  = acceleration due to gravity =  $32.2 \text{ ft/sec}^2$ .

On the other hand, torque was derived from

$$T = F\ell \text{ in-lb} \quad (5.6)$$

where  $F$  is the brake force in pounds and  $\ell$  is the length of the moment arm in inches. Likewise, output power was calculated using Equation (2.2), as

$$P_o = 1.5866 \times 10^{-5} TN \text{ hp} \quad (5.7)$$

where  $T$  is in in-lb and  $N$  is in rpm.

Turbine efficiency was derived from

$$E = (P_i/P_o) \times 100 \text{ percent} \quad (2.3)$$

Other relevant variables, such as runner peripheral velocity  $U_1$  was calculated from

$$U_1 = \pi D_1 N \quad (3.3)$$

or, for runner diameter  $D_1 = 6$  inches,

$$U_1 = .0262 N \quad \text{fps} \quad (5.8)$$

Also, the velocity coefficient  $U_1/V_1$  is simply the quotient of Equations (5.8) and (5.5). Further, runner solidity  $\sigma$ , which is the ratio of the blade chord to the spacing of the blades in the runner diameter, is given by

$$\sigma = \frac{c}{(D_2/Z)} \quad (5.9)$$

where  $c$  is the blade chord which is equal to 1-1/16 inches,  $D_2$  is the inside diameter of the runner which is equal to 4 inches, and  $Z$  is the number of blades. Therefore, for this research

$$\sigma = 8.45 \times 10^{-2} Z$$

Except for the variables  $Z$ ,  $N$ ,  $Q_s$ , and  $F$ , the foregoing formulas, namely Equations (5.1) to (5.10) were used in calculating the unknown variables shown in Tables II to XIII.

The  $N$  column was sorted in descending order for purposes of clarity. Original  $N$  data was not strictly in descending sequence because of the highly variable

frictional forces that developed in the brake during the test. Thus, the developed torque  $T$  does not appear to be exactly directly proportional to the decreasing rotative speed  $N$ . This irregularity is carried on to the calculation of output power  $P_o$  and Efficiency  $E$ . Figures 5.4 to 5.15 illustrate the data points of runner performance data in Tables II to XIII. The scattered points were the effects of the uncertainty and unpredictability of frictional forces. Nevertheless, the data points generally show a parabolic curve pattern typical of the performance of crossflow turbines. The curve describes a second degree equation which is of the form

$$f(x) = P(1) + P(2)x + P(3)x^2 \quad (5.10)$$

or, for this study

$$E = P(1) + P(2)N + P(3)N^2 \quad (5.11)$$

where  $P(1)$ ,  $P(2)$ , and  $P(3)$  are coefficients and  $E$  and  $N$  are turbine efficiency and rotative speed, respectively. The method used to curve-fit the points was the Simplex algorithm of a software program called MacMulti. The empirical efficiency equation of each runner running at various flow rates is summarized in Table XIV.

Another peculiar observation made from most of the plots is the concentration of the points or readings on the right side half of the curve, i.e. on the faster half of rotative speeds. This can be explained by the fact that it

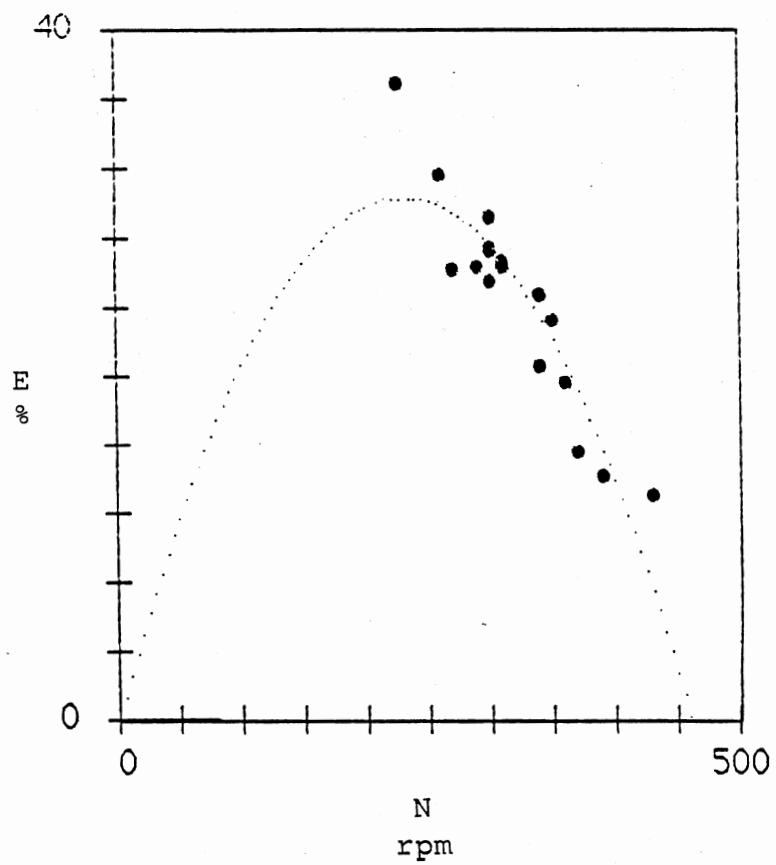


Figure 5.4. Efficiency as a Function of Rotative Speed for the 10-Blade Runner at 300 gpm.

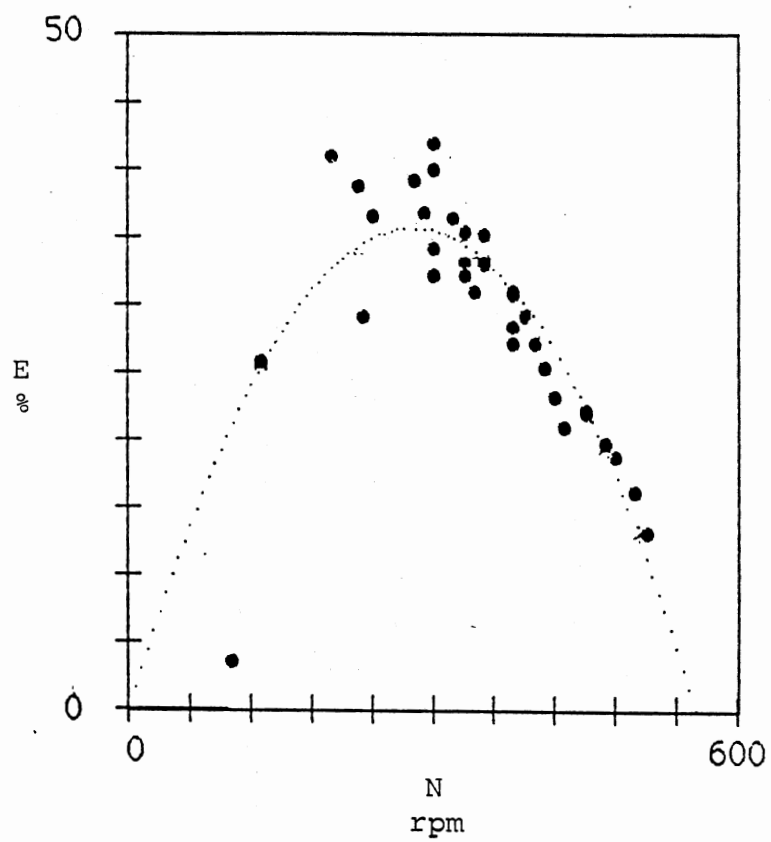


Figure 5.5. Efficiency as a Function of Rotative Speed for the 10-Blade Runner at 400 gpm.



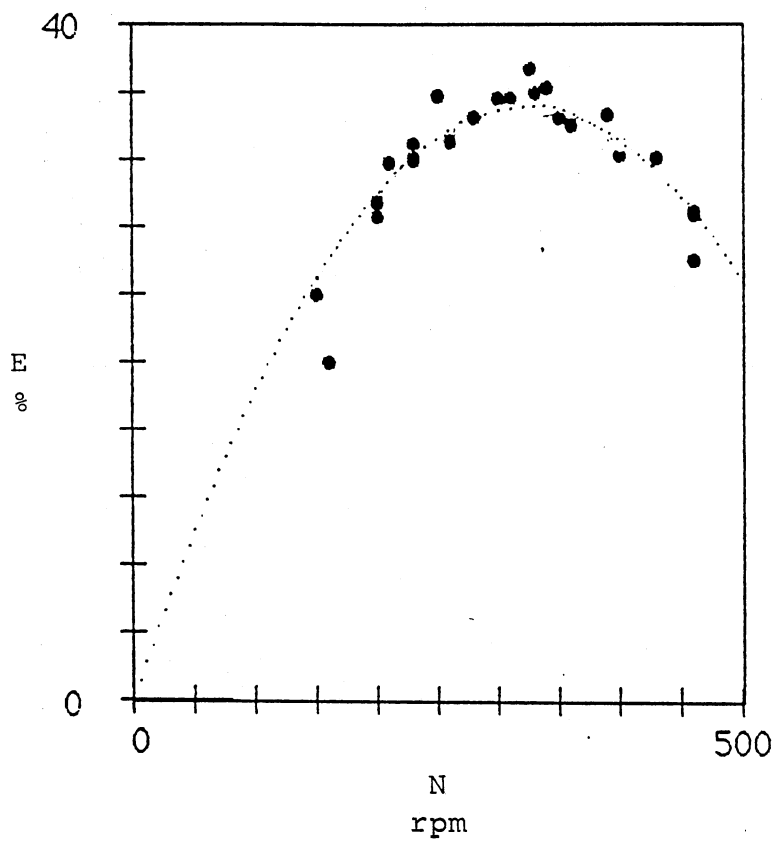


Figure 5.6. Efficiency as a Function of Rotative Speed for the 10-Blade Runner at 500 gpm.

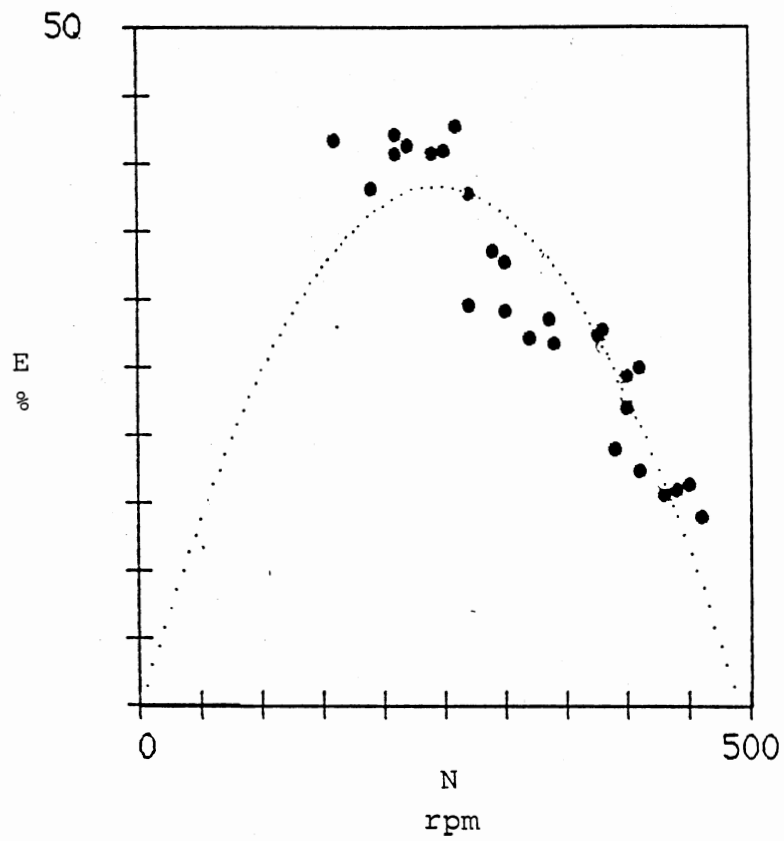


Figure 5.7. Efficiency as a Function of Rotative Speed for the 15-Blade Runner at 300 gpm.

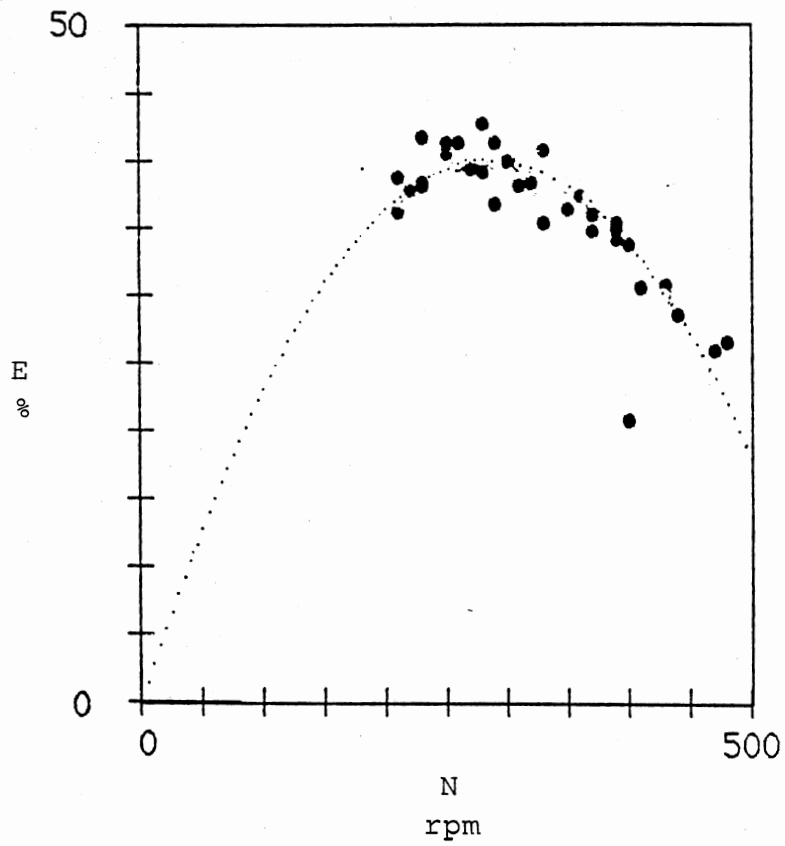


Figure 5.8. Efficiency as a Function of Rotative Speed for the 15-Blade Runner at 400 gpm.

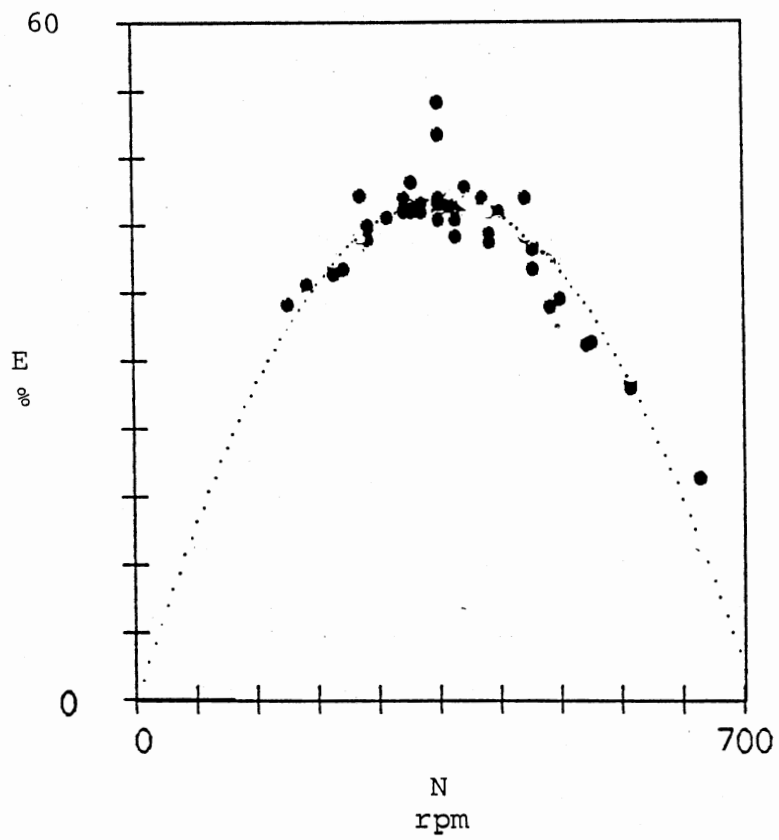


Figure 5.9. Efficiency as a Function of Rotative Speed for the 15-Blade Runner at 500 gpm.

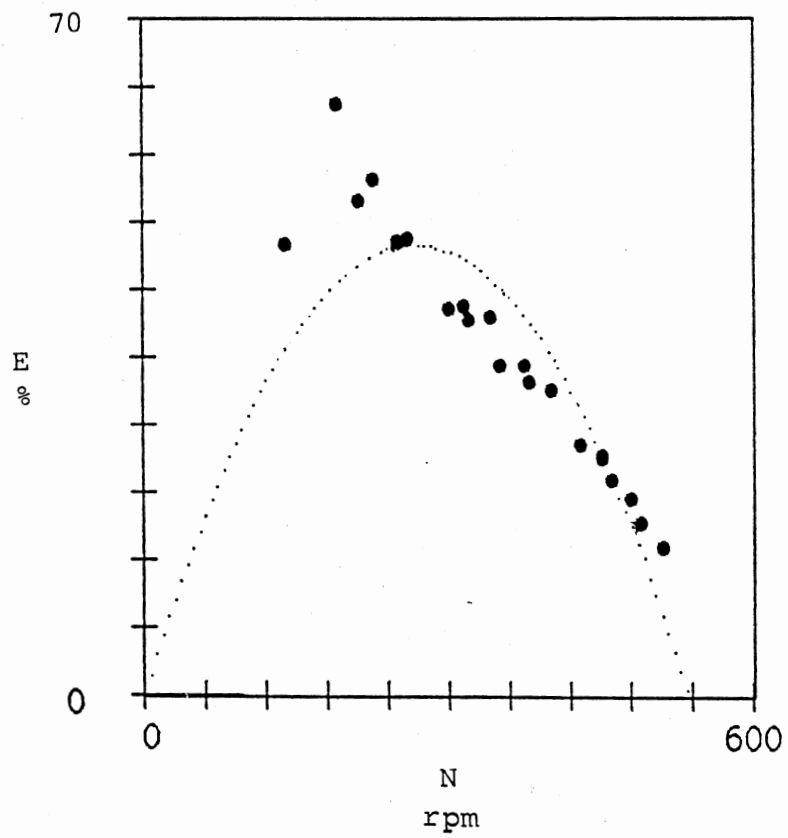


Figure 5.10. Efficiency as a Function of Rotative Speed for the 20-Blade Runner at 300 gpm.

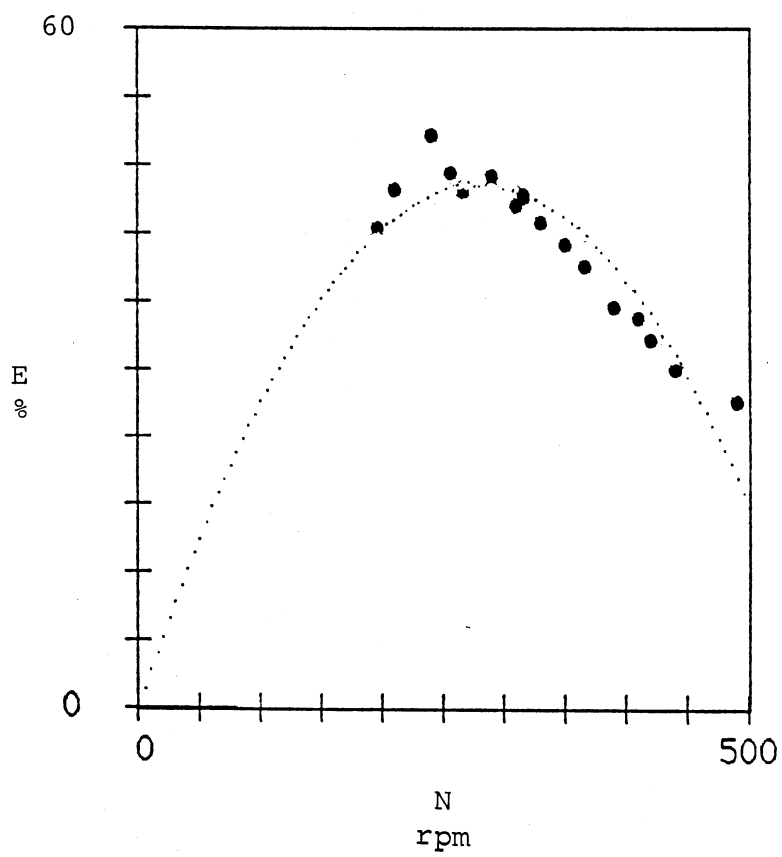


Figure 5.11. Efficiency as a Function of Rotative Speed for the 20-Blade Runner at 400 gpm.

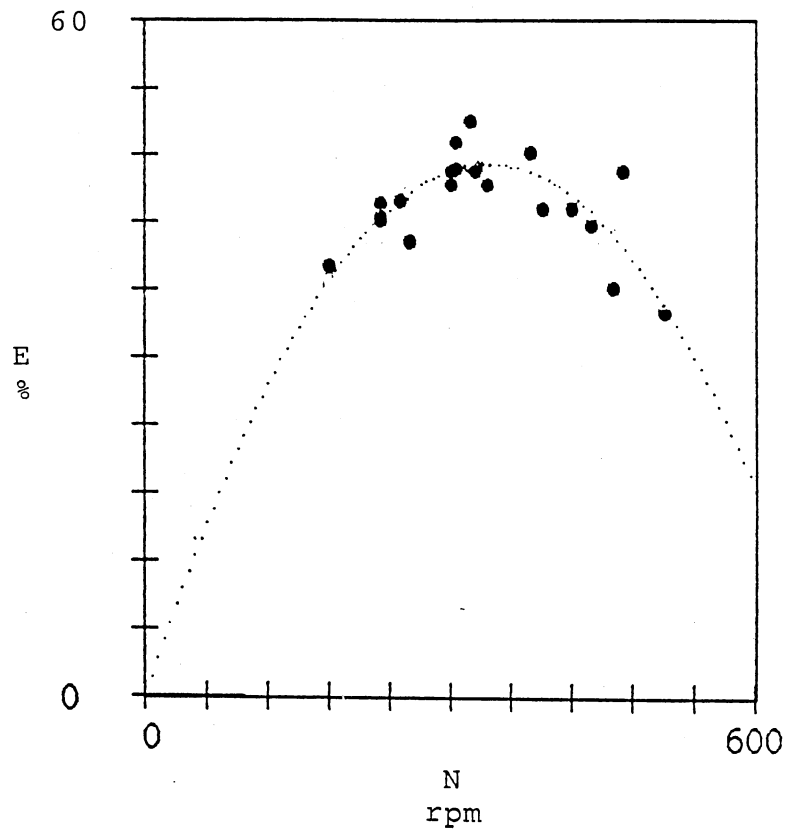


Figure 5.12. Efficiency as a Function of Rotative Speed for the 20-Blade Runner at 500 gpm.

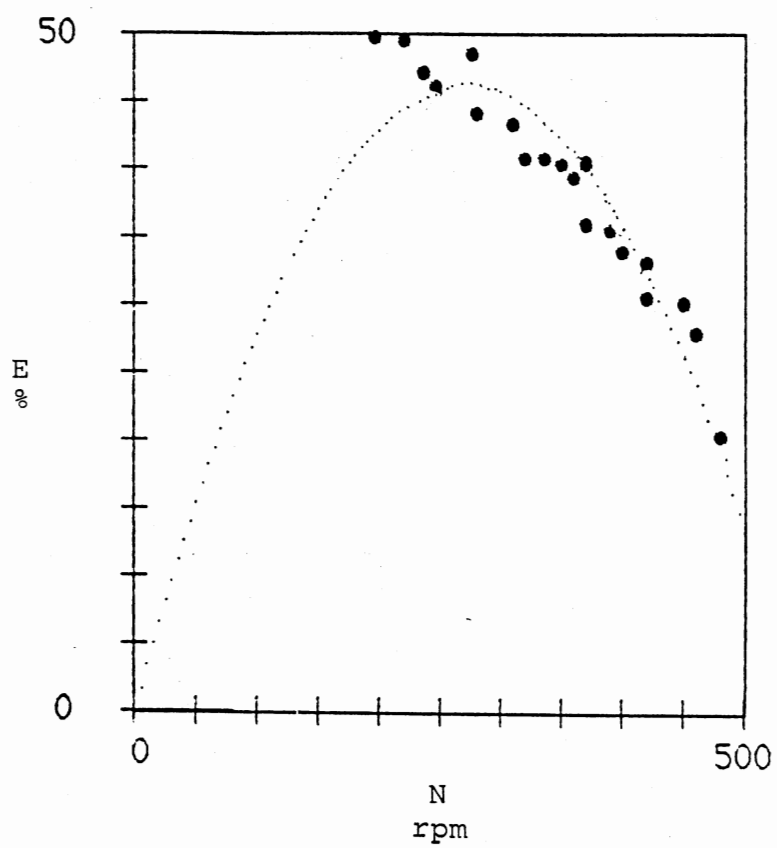


Figure 5.13. Efficiency as a Function of Rotative Speed for the 30-Blade Runner at 300 gpm.



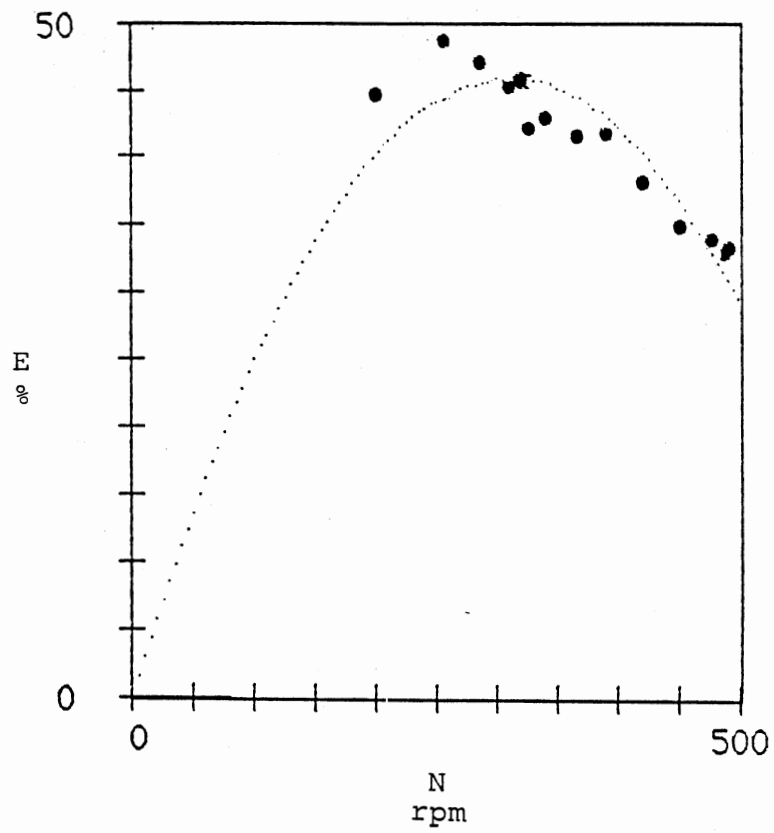


Figure 5.14. Efficiency as a Function of Rotative Speed for the 30-Blade Runner at 400 gpm.

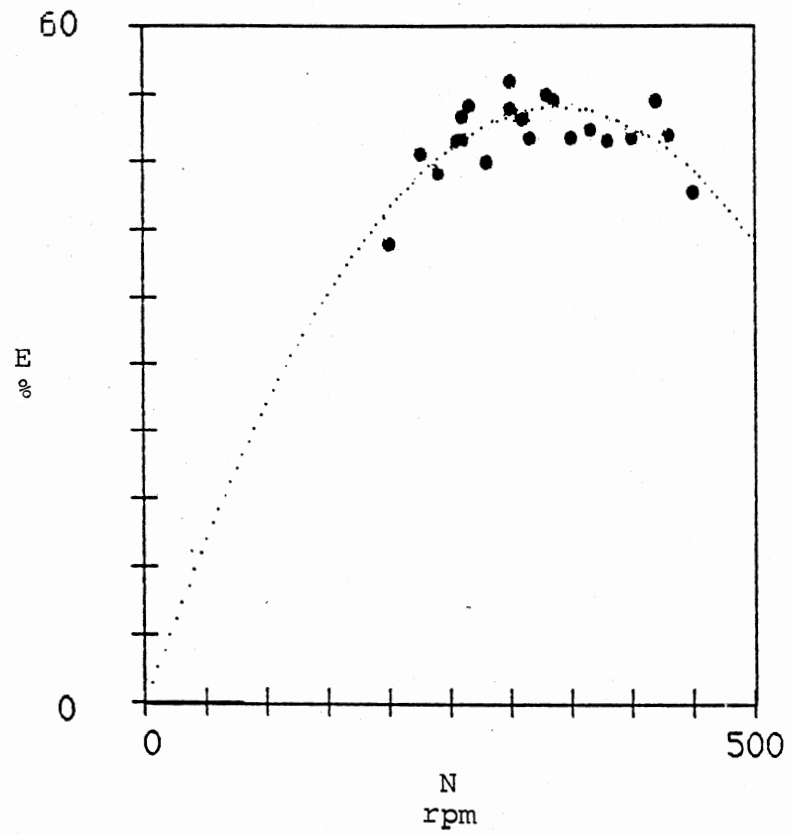


Figure 5.15. Efficiency as a Function of Rotative Speed for the 30-Blade Runner at 500 gpm.

TABLE II  
PERFORMANCE DATA FOR THE 10-BLADE  
RUNNER AT 300 GPM

	N	F	T	P <sub>o</sub>	E	U <sub>1</sub>	U <sub>1</sub> /V <sub>1</sub>
1	430.0000	.3125	3.7891	.0259	13.0801	11.2574	.8689
2	390.0000	.3750	4.5469	.0281	14.2361	10.2102	.7881
3	390.0000	.3750	4.5469	.0281	14.2361	10.2102	.7881
4	370.0000	.4375	5.3047	.0311	15.7570	9.6866	.7477
5	360.0000	.5625	6.8203	.0390	19.7115	9.4248	.7275
6	350.0000	.6875	8.3359	.0463	23.4226	9.1630	.7073
7	340.0000	.6250	7.5781	.0409	20.6849	8.9012	.6871
8	340.0000	.7500	9.0938	.0491	24.8218	8.9012	.6871
9	310.0000	.8750	10.6094	.0522	26.4036	8.1158	.6264
10	300.0000	.9375	11.3672	.0541	27.3770	7.8540	.6062
11	300.0000	.8750	10.6094	.0505	25.5519	7.8540	.6062
12	300.0000	1.0000	12.1250	.0577	29.2022	7.8540	.6062
13	290.0000	.9375	11.3672	.0523	26.4645	7.5922	.5860
14	270.0000	1.0000	12.1250	.0519	26.2820	7.0686	.5456
15	260.0000	1.2500	15.1563	.0625	31.6357	6.8068	.5254
16	225.0000	1.6875	20.4609	.0730	36.9590	5.8905	.4547

Z	= 10 blades	N	in rpm
Q <sub>s</sub>	= 300 gpm	F	in lbs
H <sub>s</sub>	= 2.3563 ft	T	in lb-in
H <sub>nd</sub>	= 2.6063 ft	P <sub>o</sub>	in hp
l	= 12.125 inches	E	in percent
P <sub>i</sub>	= 0.1976 hp	U <sub>1</sub>	in fps
V <sub>1</sub> <sup>i</sup>	= 12.9555 fps	U <sub>1</sub> /V <sub>1</sub>	is dimensionless
σ <sub>1</sub>	= 0.8455		

TABLE III  
PERFORMANCE DATA FOR THE 10-BLADE  
RUNNER AT 400 GPM

	N	F	T	P <sub>o</sub>	E	U <sub>1</sub>	U <sub>1</sub> /V <sub>1</sub>
1	510.0000	.5000	6.0625	.0491	13.2588	13.3518	.8697
2	500.0000	.6250	7.5781	.0601	16.2485	13.0900	.8527
3	480.0000	.7500	9.0938	.0693	18.7183	12.5664	.8186
4	470.0000	.8125	9.8516	.0735	19.8557	12.3046	.8015
5	450.0000	.9375	11.3672	.0812	21.9355	11.7810	.7674
6	430.0000	.9375	11.3672	.0776	20.9606	11.2574	.7333
7	420.0000	1.0625	12.8828	.0859	23.2028	10.9956	.7163
8	410.0000	1.1875	14.3984	.0937	25.3152	10.7338	.6992
9	400.0000	1.3125	15.9141	.1010	27.2975	10.4720	.6821
10	390.0000	1.4375	17.4297	.1079	29.1498	10.2102	.6651
11	380.0000	1.3750	16.6719	.1005	27.1675	9.9484	.6480
12	380.0000	1.5625	18.9453	.1142	30.8721	9.9484	.6480
13	380.0000	1.4375	17.4297	.1051	28.4024	9.9484	.6480
14	350.0000	1.8125	21.9766	.1220	32.9844	9.1630	.5969
15	350.0000	1.9375	23.4922	.1305	35.2592	9.1630	.5969
16	340.0000	1.7500	21.2188	.1145	30.9371	8.9012	.5798
17	330.0000	2.0625	25.0078	.1309	35.3892	8.6394	.5628
18	330.0000	1.9375	23.4922	.1230	33.2444	8.6394	.5628
19	330.0000	1.8750	22.7344	.1190	32.1720	8.6394	.5628
20	320.0000	2.1875	26.5234	.1347	36.3966	8.3776	.5457
21	300.0000	2.0625	25.0078	.1190	32.1720	7.8540	.5116
22	300.0000	2.6875	32.5859	.1551	41.9211	7.8540	.5116
23	300.0000	2.5625	31.0703	.1479	39.9713	7.8540	.5116
24	300.0000	2.5625	31.0703	.1479	39.9713	7.8540	.5116
25	300.0000	2.1875	26.5234	.1263	34.1218	7.8540	.5116
26	290.0000	2.4375	29.5547	.1360	36.7541	7.5922	.4946
27	280.0000	2.6875	32.5859	.1448	39.1264	7.3304	.4775
28	240.0000	2.9375	35.6172	.1356	36.6566	6.2832	.4093
29	230.0000	2.4375	29.5547	.1079	29.1498	6.0214	.3922
30	225.0000	3.3125	40.1641	.1434	38.7527	5.8905	.3837
31	200.0000	3.9375	47.7422	.1515	40.9462	5.2360	.3411
32	130.0000	3.8125	46.2266	.0953	25.7701	3.4034	.2217
33	100.0000	.6875	8.3359	.0132	3.5747	2.6180	.1705

Z	= 10 blades	N	in rpm
Q <sub>s</sub>	= 400 gpm	F	in lbs
H <sub>s</sub>	= 3.4095 ft	T	in lb-in
H <sub>nd</sub>	= 3.6595 ft	P <sub>o</sub>	in hp
z	= 12.125 inches	E <sub>o</sub>	in percent
P <sub>i</sub>	= 0.3700 hp	U <sub>1</sub>	in fps
V <sub>1</sub>	= 15.3515 fps	U <sub>1</sub> /V <sub>1</sub>	is dimensionless
σ <sub>1</sub>	= 0.8455		

TABLE IV  
PERFORMANCE DATA FOR THE 10-BLADE  
RUNNER AT 500 GPM

	N	F	T	P <sub>o</sub>	E	U <sub>1</sub>	U <sub>1</sub> /V <sub>1</sub>
1	460.0000	1.7500	21.2188	.1549	26.0018	12.0428	.6913
2	460.0000	1.9375	23.4922	.1715	28.7877	12.0428	.6913
3	430.0000	2.3125	28.0391	.1913	32.1187	11.2574	.6462
4	400.0000	2.5000	30.3125	.1924	32.3004	10.4720	.6011
5	390.0000	2.7500	33.3438	.2063	34.6422	10.2102	.5861
6	360.0000	2.9375	35.6172	.2034	34.1577	9.4248	.5410
7	350.0000	3.0625	37.1328	.2062	34.6220	9.1630	.5260
8	340.0000	3.3125	40.1641	.2167	36.3783	8.9012	.5109
9	330.0000	3.3750	40.9219	.2143	35.9746	8.6394	.4959
10	325.0000	3.5625	43.1953	.2227	37.3978	8.5085	.4884
11	310.0000	3.5625	43.1953	.2125	35.6718	8.1158	.4659
12	300.0000	3.6875	44.7109	.2128	35.7323	7.8540	.4508
13	300.0000	3.6875	44.7109	.2128	35.7323	7.8540	.4508
14	280.0000	3.8125	46.2266	.2054	34.4807	7.3304	.4208
15	260.0000	3.9375	47.7422	.1970	33.0675	6.8068	.3907
16	250.0000	4.4375	53.8047	.2134	35.8333	6.5450	.3757
17	230.0000	4.3125	52.2891	.1908	32.0380	6.0214	.3456
18	230.0000	4.4375	53.8047	.1964	32.9666	6.0214	.3456
19	230.0000	4.4375	53.8047	.1964	32.9666	6.0214	.3456
20	210.0000	4.6875	56.8359	.1894	31.7957	5.4978	.3156
21	200.0000	4.5625	55.3203	.1755	29.4741	5.2360	.3006
22	200.0000	4.4375	53.8047	.1707	28.6666	5.2360	.3006
23	160.0000	3.8750	46.9844	.1193	20.0262	4.1888	.2404
24	150.0000	4.9375	59.8672	.1425	23.9225	3.9270	.2254
25	150.0000	4.9375	59.8672	.1425	23.9225	3.9270	.2254

Z	= 10 blades	N	in rpm
Q <sub>s</sub>	= 500 gpm	F	in lbs
H <sub>s</sub>	= 4.4626 ft	T	in lb-in
H <sub>nd</sub>	= 4.7126 ft	P <sub>o</sub>	in hp
z	= 12.125 inches	E	in percent
P <sub>i</sub>	= 0.5956 hp	U <sub>1</sub>	in fps
V <sub>1</sub>	= 17.4211 fps	U <sub>1</sub> /V <sub>1</sub>	is dimensionless
σ <sub>1</sub>	= 0.8455		

TABLE V  
PERFORMANCE DATA FOR THE 15-BLADE  
RUNNER AT 300 GPM

	N	F	T	P <sub>o</sub>	E	U <sub>1</sub>	U <sub>1</sub> /V <sub>1</sub>
1	460.0000	.3125	3.7891	.0277	13.9927	12.0428	.9295
2	450.0000	.3750	4.5469	.0325	16.4262	11.7810	.9093
3	440.0000	.3750	4.5469	.0317	16.0612	11.5192	.8891
4	430.0000	.3750	4.5469	.0310	15.6962	11.2574	.8689
5	410.0000	.4375	5.3047	.0345	17.4605	10.7338	.8285
6	410.0000	.6250	7.5781	.0493	24.9435	10.7338	.8285
7	400.0000	.5625	6.8203	.0433	21.9016	10.4720	.8083
8	400.0000	.6250	7.5781	.0481	24.3351	10.4720	.8083
9	390.0000	.5000	6.0625	.0375	18.9814	10.2102	.7881
10	380.0000	.7500	9.0938	.0548	27.7421	9.9484	.7679
11	375.0000	.7500	9.0938	.0541	27.3770	9.8175	.7578
12	340.0000	.8125	9.8516	.0531	26.8903	8.9012	.6871
13	335.0000	.8750	10.6094	.0564	28.5330	8.7703	.6770
14	320.0000	.8750	10.6094	.0539	27.2554	8.3776	.6466
15	300.0000	1.0000	12.1250	.0577	29.2022	7.8540	.6062
16	300.0000	1.1250	13.6406	.0649	32.8524	7.8540	.6062
17	290.0000	1.1875	14.3984	.0663	33.5217	7.5922	.5860
18	270.0000	1.1250	13.6406	.0584	29.5672	7.0686	.5456
19	270.0000	1.4375	17.4297	.0747	37.7803	7.0686	.5456
20	260.0000	1.6875	20.4609	.0844	42.7082	6.8068	.5254
21	250.0000	1.6875	20.4609	.0812	41.0656	6.5450	.5052
22	240.0000	1.7500	21.2188	.0808	40.8830	6.2832	.4850
23	220.0000	1.9375	23.4922	.0820	41.4914	5.7596	.4446
24	220.0000	1.9375	23.4922	.0820	41.4914	5.7596	.4446
25	210.0000	2.0000	24.2500	.0808	40.8830	5.4978	.4244
26	210.0000	2.0625	25.0078	.0833	42.1606	5.4978	.4244
27	190.0000	2.0625	25.0078	.0754	38.1453	4.9742	.3839
28	160.0000	2.6875	32.5859	.0827	41.8564	4.1888	.3233

Z	= 15 blades	N	in rpm
Q <sub>s</sub>	= 300 gpm	F	in lbs
H <sup>nd</sup>	= 2.3563 ft	T	in lb-in
H <sup>nd</sup>	= 2.6063 ft	P <sub>o</sub>	in hp
z	= 12.125 inches	E <sup>o</sup>	in percent
P <sub>i</sub>	= 0.1976 hp	U <sub>1</sub>	in fps
V <sub>1</sub>	= 12.9555 fps	U <sub>1</sub> /V <sub>1</sub>	is dimensionless
σ <sub>1</sub>	= 1.2682		

TABLE VI  
PERFORMANCE DATA FOR THE 15-BLADE  
RUNNER AT 400 GPM

	N	F	T	P <sub>o</sub>	E	U <sub>1</sub>	U <sub>1</sub> /V <sub>1</sub>
1	480.0000	1.0625	12.8828	.0981	26.5175	12.5664	.8186
2	480.0000	1.0625	12.8828	.0981	26.5175	12.5664	.8186
3	470.0000	1.0625	12.8828	.0961	25.9651	12.3046	.8015
4	440.0000	1.2500	15.1563	.1058	28.5973	11.5192	.7504
5	440.0000	1.2500	15.1563	.1058	28.5973	11.5192	.7504
6	430.0000	1.3750	16.6719	.1137	30.7421	11.2574	.7333
7	410.0000	1.4375	17.4297	.1134	30.6447	10.7338	.6992
8	400.0000	1.0000	12.1250	.0770	20.7981	10.4720	.6821
9	400.0000	1.6250	19.7031	.1250	33.7969	10.4720	.6821
10	400.0000	1.6250	19.7031	.1250	33.7969	10.4720	.6821
11	390.0000	1.6875	20.4609	.1266	34.2193	10.2102	.6651
12	390.0000	1.7500	21.2188	.1313	35.4867	10.2102	.6651
13	370.0000	1.8750	22.7344	.1335	36.0717	9.6866	.6310
14	370.0000	1.8125	21.9766	.1290	34.8693	9.6866	.6310
15	360.0000	2.0000	24.2500	.1385	37.4365	9.4248	.6139
16	350.0000	2.0000	24.2500	.1347	36.3966	9.1630	.5969
17	350.0000	2.0000	24.2500	.1347	36.3966	9.1630	.5969
18	330.0000	2.3750	28.7969	.1508	40.7512	8.6394	.5628
19	330.0000	2.0625	25.0078	.1309	35.3892	8.6394	.5628
20	330.0000	2.3750	28.7969	.1508	40.7512	8.6394	.5628
21	320.0000	2.3125	28.0391	.1424	38.4764	8.3776	.5457
22	320.0000	2.3125	28.0391	.1424	38.4764	8.3776	.5457
23	310.0000	2.3750	28.7969	.1416	38.2814	8.1158	.5287
24	300.0000	2.5625	31.0703	.1479	39.9713	7.8540	.5116
25	290.0000	2.4375	29.5547	.1360	36.7541	7.5922	.4946
26	290.0000	2.7500	33.3438	.1534	41.4662	7.5922	.4946
27	290.0000	2.7500	33.3438	.1534	41.4662	7.5922	.4946
28	280.0000	2.6875	32.5859	.1448	39.1264	7.3304	.4775
29	280.0000	2.9375	35.6172	.1582	42.7660	7.3304	.4775
30	280.0000	2.9375	35.6172	.1582	42.7660	7.3304	.4775
31	270.0000	2.8125	34.1016	.1461	39.4838	7.0686	.4604
32	260.0000	3.0625	37.1328	.1532	41.4012	6.8068	.4434
33	250.0000	3.1875	38.6484	.1533	41.4337	6.5450	.4263
34	250.0000	3.1875	38.6484	.1533	41.4337	6.5450	.4263
35	250.0000	3.1250	37.8906	.1503	40.6212	6.5450	.4263
36	250.0000	3.1875	38.6484	.1533	41.4337	6.5450	.4263
37	230.0000	3.1875	38.6484	.1410	38.1190	6.0214	.3922
38	230.0000	3.5000	42.4375	.1549	41.8561	6.0214	.3922
39	220.0000	3.3125	40.1641	.1402	37.8915	5.7596	.3752
40	210.0000	3.3125	40.1641	.1338	36.1691	5.4978	.3581
41	210.0000	3.5625	43.1953	.1439	38.8989	5.4978	.3581

Z	= 15 blades	N	in rpm
Q <sub>s</sub>	= 400 gpm	F	in lbs
H <sub>s</sub>	= 3.4095 ft	T	in lb-in
H <sub>nd</sub>	= 3.6595 ft	P <sub>o</sub>	in hp
z	= 12.125 inches	E <sub>o</sub>	in percent
P <sub>i</sub>	= 0.3700 hp	U <sub>1</sub>	in fps
V <sub>1</sub>	= 15.3515 fps	U <sub>1</sub> /V <sub>1</sub>	is dimensionless
σ <sub>1</sub>	= 1.2682		

TABLE VII  
PERFORMANCE DATA FOR THE 15-BLADE  
RUNNER AT 500 GPM

	N	F	T	P <sub>o</sub>	E	U <sub>1</sub>	U <sub>1</sub> /V <sub>1</sub>
1	650.0000	.9375	11.3672	.1172	19.6831	17.0170	.9768
2	570.0000	1.5000	18.1875	.1645	27.6168	14.9226	.8566
3	525.0000	1.8750	22.7344	.1894	31.7957	13.7445	.7890
4	520.0000	1.8750	22.7344	.1876	31.4929	13.6136	.7814
5	490.0000	2.2500	27.2813	.2121	35.6112	12.8282	.7364
6	480.0000	2.2500	27.2813	.2078	34.8844	12.5664	.7213
7	460.0000	2.5625	31.0703	.2268	38.0741	12.0428	.6913
8	460.0000	2.6875	32.5859	.2378	39.9314	12.0428	.6913
9	450.0000	3.0625	37.1328	.2651	44.5140	11.7810	.6763
10	420.0000	3.1875	38.6484	.2576	43.2422	10.9956	.6312
11	410.0000	3.1250	37.8906	.2465	41.3849	10.7338	.6161
12	410.0000	3.0625	37.1328	.2416	40.5572	10.7338	.6161
13	400.0000	3.4375	41.6797	.2645	44.4131	10.4720	.6011
14	380.0000	3.6875	44.7109	.2696	45.2609	9.9484	.5711
15	370.0000	3.5625	43.1953	.2536	42.5760	9.6866	.5560
16	370.0000	3.4375	41.6797	.2447	41.0821	9.6866	.5560
17	370.0000	3.6250	43.9531	.2580	43.3229	9.6866	.5560
18	360.0000	3.7500	45.4688	.2597	43.6055	9.4248	.5410
19	350.0000	3.8125	46.2266	.2567	43.1008	9.1630	.5260
20	350.0000	3.8750	46.9844	.2609	43.8074	9.1630	.5260
21	350.0000	3.7500	45.4688	.2525	42.3943	9.1630	.5260
22	350.0000	3.8750	46.9844	.2609	43.8074	9.1630	.5260
23	350.0000	4.4375	53.8047	.2988	50.1666	9.1630	.5260
24	350.0000	3.8750	46.9844	.2609	43.8074	9.1630	.5260
25	350.0000	4.6875	56.8359	.3156	52.9928	9.1630	.5260
26	350.0000	3.8125	46.2266	.2567	43.1008	9.1630	.5260
27	350.0000	3.8750	46.9844	.2609	43.8074	9.1630	.5260
28	350.0000	3.9375	47.7422	.2651	44.5140	9.1630	.5260
29	330.0000	4.0625	49.2578	.2579	43.3027	8.6394	.4959
30	330.0000	4.1250	50.0156	.2619	43.9689	8.6394	.4959
31	330.0000	4.1250	50.0156	.2619	43.9689	8.6394	.4959
32	320.0000	4.1875	50.7734	.2578	43.2825	8.3776	.4809
33	320.0000	4.4375	53.8047	.2732	45.8666	8.3776	.4809
34	310.0000	4.3125	52.2891	.2572	43.1816	8.1158	.4659
35	310.0000	4.4375	53.8047	.2646	44.4332	8.1158	.4659
36	310.0000	4.4375	53.8047	.2646	44.4332	8.1158	.4659
37	290.0000	4.5625	55.3203	.2545	42.7375	7.5922	.4358
38	270.0000	4.6875	56.8359	.2435	40.8802	7.0686	.4058
39	270.0000	4.8125	58.3516	.2500	41.9703	7.0686	.4058
40	260.0000	5.3125	64.4141	.2657	44.6149	6.8068	.3907
41	240.0000	4.9375	59.8672	.2280	38.2760	6.2832	.3607
42	230.0000	5.0625	61.3828	.2240	37.6098	6.0214	.3456
43	200.0000	5.6875	68.9609	.2188	36.7417	5.2360	.3006
44	175.0000	6.1875	75.0234	.2083	34.9753	4.5815	.2630

Z	= 15 blades	N	in rpm
Q <sub>s</sub>	= 500 gpm	F	in lbs
H <sub>nd</sub> <sup>s</sup>	= 4.4626 ft	T	in lb-in
H <sub>nd</sub>	= 4.7126 ft	P <sub>o</sub>	in hp
ℓ	= 12.125 inches	E <sup>o</sup>	in percent
P <sub>i</sub>	= 0.5956 hp	U <sub>1</sub>	in fps
V <sub>i</sub> <sup>1</sup>	= 17.4211 fps	U <sub>1</sub> /V <sub>1</sub>	is dimensionless
σ <sub>1</sub>	= 1.2682		



TABLE VIII  
 PERFORMANCE DATA FOR THE 20-BLADE  
 RUNNER AT 300 GPM

	N	F	T	P <sub>o</sub>	E	U <sub>1</sub>	U <sub>1</sub> /V <sub>1</sub>
1	510.0000	.3125	3.7891	.0307	15.5137	13.3518	1.0306
2	490.0000	.3750	4.5469	.0354	17.8863	12.8282	.9902
3	480.0000	.4375	5.3047	.0404	20.4415	12.5664	.9700
4	480.0000	.4375	5.3047	.0404	20.4415	12.5664	.9700
5	480.0000	.4375	5.3047	.0404	20.4415	12.5664	.9700
6	460.0000	.5000	6.0625	.0442	22.3883	12.0428	.9295
7	450.0000	.5625	6.8203	.0487	24.6393	11.7810	.9093
8	430.0000	.6250	7.5781	.0517	26.1603	11.2574	.8689
9	400.0000	.8125	9.8516	.0625	31.6357	10.4720	.8083
10	380.0000	.8750	10.6094	.0640	32.3657	9.9484	.7679
11	375.0000	.9375	11.3672	.0676	34.2213	9.8175	.7578
12	350.0000	1.0000	12.1250	.0673	34.0692	9.1630	.7073
13	340.0000	1.1875	14.3984	.0777	39.3013	8.9012	.6871
14	320.0000	1.2500	15.1563	.0770	38.9362	8.3776	.6466
15	320.0000	1.2500	15.1563	.0770	38.9362	8.3776	.6466
16	315.0000	1.3125	15.9141	.0795	40.2442	8.2467	.6365
17	300.0000	1.3750	16.6719	.0794	40.1530	7.8540	.6062
18	260.0000	1.8750	22.7344	.0938	47.4535	6.8068	.5254
19	250.0000	1.9375	23.4922	.0932	47.1493	6.5450	.5052
20	225.0000	2.4375	29.5547	.1055	53.3852	5.8905	.4547
21	210.0000	2.5000	30.3125	.1010	51.1038	5.4978	.4244
22	190.0000	3.3125	40.1641	.1211	61.2637	4.9742	.3839
23	140.0000	3.4375	41.6797	.0926	46.8452	3.6652	.2829

Z	= 20 blades	N	in rpm
Q <sub>s</sub>	= 300 gpm	F	in lbs
H <sub>s</sub>	= 2.3563 ft	T	in lb-in
H <sub>nd</sub>	= 2.6063 ft	P	in hp
ℓ	= 12.125 inches	E <sub>o</sub>	in percent
P <sub>i</sub>	= 0.1976 hp	U <sub>1</sub>	in fps
V <sub>1</sub>	= 12.9555 fps	U <sub>1</sub> /V <sub>1</sub>	is dimensionless
σ <sub>1</sub>	= 1.6910		

TABLE IX  
PERFORMANCE DATA FOR THE 20-BLADE  
RUNNER AT 400 GPM

	N	F	T	$P_o$	E	$U_1$	$U_1/V_1$
1	490.0000	1.0625	12.8828	.1002	27.0700	12.8282	.8356
2	440.0000	1.3125	15.9141	.1111	30.0272	11.5192	.7504
3	420.0000	1.5000	18.1875	.1212	32.7570	10.9956	.7163
4	410.0000	1.6250	19.7031	.1282	34.6418	10.7338	.6992
5	390.0000	1.7500	21.2188	.1313	35.4867	10.2102	.6651
6	365.0000	2.0625	25.0078	.1448	39.1426	9.5557	.6225
7	350.0000	2.2500	27.2813	.1515	40.9462	9.1630	.5969
8	330.0000	2.5000	30.3125	.1587	42.8960	8.6394	.5628
9	315.0000	2.7500	33.3438	.1667	45.0408	8.2467	.5372
10	310.0000	2.7500	33.3438	.1640	44.3259	8.1158	.5287
11	290.0000	3.1250	37.8906	.1743	47.1206	7.5922	.4946
12	290.0000	3.1250	37.8906	.1743	47.1206	7.5922	.4946
13	265.0000	3.3125	40.1641	.1689	45.6420	6.9377	.4519
14	255.0000	3.5625	43.1953	.1748	47.2344	6.6759	.4349
15	240.0000	4.0625	49.2578	.1876	50.6953	6.2832	.4093
16	210.0000	4.1875	50.7734	.1692	45.7233	5.4978	.3581
17	195.0000	4.1875	50.7734	.1571	42.4573	5.1051	.3325

Z	= 20 blades	N	in rpm
$Q_s$	= 400 gpm	F	in lbs
$H_s$	= 3.4095 ft	T	in lb-in
$H_{nd}$	= 3.6595 ft	$P_o$	in hp
$\ell$	= 12.125 inches	E	in percent
$P_i$	= 0.3700 hp	$U_1$	in fps
$V_{\sigma 1}$	= 15.3515 fps	$U_1/V_1$	is dimensionless
$\sigma_1$	= 1.6910		

TABLE X  
PERFORMANCE DATA FOR THE 20-BLADE  
RUNNER AT 500 GPM

---

	N	F	T	P <sub>o</sub>	E	U <sub>1</sub>	U <sub>1</sub> /V <sub>1</sub>
1	510.0000	2.0625	25.0078	.2024	33.9760	13.3518	.7664
2	470.0000	3.0625	37.1328	.2769	46.4924	12.3046	.7063
3	460.0000	2.4375	29.5547	.2157	36.2168	12.0428	.6913
4	440.0000	2.9375	35.6172	.2487	41.7483	11.5192	.6612
5	420.0000	3.1875	38.6484	.2576	43.2422	10.9956	.6312
6	390.0000	3.4375	41.6797	.2579	43.3027	10.2102	.5861
7	380.0000	3.9375	47.7422	.2879	48.3295	9.9484	.5711
8	335.0000	4.1875	50.7734	.2699	45.3114	8.7703	.5034
9	325.0000	4.4375	53.8047	.2775	46.5832	8.5085	.4884
10	320.0000	4.9375	59.8672	.3040	51.0346	8.3776	.4809
11	305.0000	5.0000	60.6250	.2934	49.2581	7.9849	.4583
12	300.0000	4.6875	56.8359	.2705	45.4224	7.8540	.4508
13	300.0000	4.8125	58.3516	.2778	46.6337	7.8540	.4508
14	260.0000	4.8125	58.3516	.2407	40.4159	6.8068	.3907
15	250.0000	5.4375	65.9297	.2615	43.9084	6.5450	.3757
16	230.0000	5.6875	68.9609	.2517	42.2530	6.0214	.3456
17	230.0000	5.8750	71.2344	.2600	43.6459	6.0214	.3456
18	180.0000	6.5625	79.5703	.2273	38.1548	4.7124	.2705

Z	= 20 blades	N	in rpm
Q <sub>s</sub>	= 500 gpm	F	in lbs
H <sub>s</sub>	= 4.4626 ft	T	in lb-in
H <sup>nd</sup>	= 4.7126 ft	P	in hp
i	= 12.125 inches	E <sub>o</sub>	in percent
P <sub>i</sub>	= 0.5956 hp	U <sub>1</sub>	in fps
V <sub>1</sub>	= 17.4211 fps	U <sub>1</sub> /V <sub>1</sub>	is dimensionless
σ <sub>1</sub>	= 1.6910		

---

TABLE XI  
PERFORMANCE DATA FOR THE 30-BLADE  
RUNNER AT 300 GPM

	N	F	T	P <sub>o</sub>	E	U <sub>1</sub>	U <sub>1</sub> /V <sub>1</sub>
1	480.0000	.4375	5.3047	.0404	20.4415	12.5664	.9700
2	460.0000	.6250	7.5781	.0553	27.9854	12.0428	.9295
3	450.0000	.6875	8.3359	.0595	30.1147	11.7810	.9093
4	420.0000	.7500	9.0938	.0606	30.6623	10.9956	.8487
5	420.0000	.8125	9.8516	.0657	33.2175	10.9956	.8487
6	400.0000	.8750	10.6094	.0673	34.0692	10.4720	.8083
7	390.0000	.9375	11.3672	.0703	35.5901	10.2102	.7881
8	370.0000	1.0000	12.1250	.0712	36.0160	9.6866	.7477
9	370.0000	1.1250	13.6406	.0801	40.5180	9.6866	.7477
10	360.0000	1.1250	13.6406	.0779	39.4229	9.4248	.7275
11	350.0000	1.1875	14.3984	.0800	40.4572	9.1630	.7073
12	335.0000	1.2500	15.1563	.0806	40.7614	8.7703	.6770
13	320.0000	1.3125	15.9141	.0808	40.8830	8.3776	.6466
14	310.0000	1.4375	17.4297	.0857	43.3774	8.1158	.6264
15	280.0000	1.6250	19.7031	.0875	44.2900	7.3304	.5658
16	275.0000	1.8125	21.9766	.0959	48.5182	7.1995	.5557
17	245.0000	1.9375	23.4922	.0913	46.2064	6.4141	.4951
18	235.0000	2.0625	25.0078	.0932	47.1798	6.1523	.4749
19	220.0000	2.3125	28.0391	.0979	49.5220	5.7596	.4446
20	195.0000	2.6250	31.8281	.0985	49.8262	5.1051	.3940

Z	= 30 blades	N	in rpm
Q <sub>s</sub>	= 300 gpm	F	in lbs
H <sub>s</sub>	= 2.3563 ft	T	in lb-in
H <sup>nd</sup>	= 2.6063 ft	P <sub>o</sub>	in hp
ℓ	= 12.125 inches	E <sub>o</sub>	in percent
P <sub>i</sub>	= 0.1976 hp	U <sub>1</sub>	in fps
V <sub>1</sub>	= 12.9555 fps	U <sub>1</sub> /V <sub>1</sub>	is dimensionless
σ <sub>1</sub>	= 2.5365		

TABLE XII  
PERFORMANCE DATA FOR THE 30-BLADE  
RUNNER AT 400 GPM

	N	F	T	P <sub>o</sub>	E	U <sub>1</sub>	U <sub>1</sub> /V <sub>1</sub>
1	490.0000	1.3125	15.9141	.1237	33.4394	12.8282	.8356
2	485.0000	1.3125	15.9141	.1225	33.0982	12.6973	.8271
3	475.0000	1.3750	16.6719	.1257	33.9593	12.4355	.8100
4	450.0000	1.5000	18.1875	.1299	35.0967	11.7810	.7674
5	420.0000	1.7500	21.2188	.1414	38.2165	10.9956	.7163
6	390.0000	2.0625	25.0078	.1547	41.8236	10.2102	.6651
7	365.0000	2.1875	26.5234	.1536	41.5149	9.5557	.6225
8	340.0000	2.4375	29.5547	.1594	43.0910	8.9012	.5798
9	325.0000	2.5000	30.3125	.1563	42.2461	8.5085	.5542
10	320.0000	2.7500	33.3438	.1693	45.7558	8.3776	.5457
11	310.0000	2.8125	34.1016	.1677	45.3333	8.1158	.5287
12	285.0000	3.1875	38.6484	.1748	47.2344	7.4613	.4860
13	255.0000	3.6875	44.7109	.1809	48.8917	6.6759	.4349
14	200.0000	4.3125	52.2891	.1659	44.8458	5.2360	.3411

Z	= 30 blades	N	in rpm
Q <sub>s</sub>	= 400 gpm	F	in lbs
H <sub>s</sub>	= 3.4095 ft	T	in lb-in
H <sub>nd</sub>	= 3.6595 ft	P	in hp
l	= 12.125 inches	E <sup>o</sup>	in percent
P <sub>i</sub>	= 0.3700 hp	U <sub>1</sub>	in fps
V <sub>1</sub>	= 15.3515 fps	U <sub>1</sub> /V <sub>1</sub>	is dimensionless
σ <sub>1</sub>	= 2.5365		

TABLE XIII  
PERFORMANCE DATA FOR THE 30-BLADE  
RUNNER AT 500 GPM

	N	F	T	P <sub>o</sub>	E	U <sub>1</sub>	U <sub>1</sub> /V <sub>1</sub>
1	450.0000	3.1250	37.8906	.2705	45.4224	11.7810	.6763
2	430.0000	3.6250	43.9531	.2999	50.3482	11.2574	.6462
3	420.0000	3.9375	47.7422	.3182	53.4168	10.9956	.6312
4	400.0000	3.8750	46.9844	.2982	50.0656	10.4720	.6011
5	380.0000	4.0625	49.2578	.2970	49.8637	9.9484	.5711
6	365.0000	4.3125	52.2891	.3028	50.8428	9.5557	.5485
7	350.0000	4.4375	53.8047	.2988	50.1666	9.1630	.5260
8	335.0000	4.9375	59.8672	.3182	53.4269	8.7703	.5034
9	330.0000	5.0625	61.3828	.3214	53.9619	8.6394	.4959
10	315.0000	4.9375	59.8672	.2992	50.2372	8.2467	.4734
11	310.0000	5.1875	62.8984	.3094	51.9431	8.1158	.4659
12	300.0000	5.4375	65.9297	.3138	52.6900	7.8540	.4508
13	300.0000	5.6875	68.9609	.3283	55.1126	7.8540	.4508
14	280.0000	5.3125	64.4141	.2862	48.0468	7.3304	.4208
15	265.0000	6.1875	75.0234	.3154	52.9626	6.9377	.3982
16	260.0000	6.1875	75.0234	.3095	51.9633	6.8068	.3907
17	260.0000	5.9375	71.9922	.2970	49.8637	6.8068	.3907
18	255.0000	6.0625	73.5078	.2974	49.9344	6.6759	.3832
19	240.0000	6.0625	73.5078	.2799	46.9971	6.2832	.3607
20	225.0000	6.6875	81.0859	.2895	48.6020	5.8905	.3381
21	200.0000	6.3125	76.5391	.2429	40.7793	5.2360	.3006

Z = 30 blades

Q<sub>s</sub> = 500 gpm

H<sub>s</sub> = 4.4626 ft

H<sub>nd</sub> = 4.7126 ft

z = 12.125 inches

P<sub>i</sub> = 0.5956 hp

V<sub>1</sub> = 17.4211 fps

σ<sub>1</sub> = 2.5365

N in rpm

F in lbs

T in lb-in

P<sub>o</sub> in hp

E in percent

U<sub>1</sub> in fps

U<sub>1</sub>/V<sub>1</sub> is dimensionless

TABLE XIV  
 SUMMARY OF TURBINE EFFICIENCY EQUATIONS  
 AS A FUNCTION OF ROTATIVE SPEED  
 (FIGURES 5.4 TO 5.15)

Number of Z	Supply Flow Rate $Q_s$ (gpm)	Efficiency from Curve $E_c$ %	Equation Number
6	400	$-0.0808+0.1983N-3.2554 \times 10^{-4} N^2$	(5.12)
10	300	$0.0025+0.2633N-5.7164 \times 10^{-4} N^2$	(5.13)
10	400	$-0.0076+0.2551N-4.5690 \times 10^{-4} N^2$	(5.14)
10	500	$0.0418+0.2168N-3.3474 \times 10^{-4} N^2$	(5.15)
15	300	$-0.1208+0.3123N-6.3721 \times 10^{-4} N^2$	(5.16)
15	400	$0.0267+0.2790N-4.8602 \times 10^{-4} N^2$	(5.17)
15	500	$0.0423+0.2487N-3.5002 \times 10^{-4} N^2$	(5.18)
20	300	$0.0032+0.3480N-6.5018 \times 10^{-4} N^2$	(5.19)
20	400	$0.0076+0.3292N-5.8730 \times 10^{-4} N^2$	(5.20)
20	500	$0.0253+0.2797N-4.1530 \times 10^{-4} N^2$	(5.21)
30	300	$-0.0180+0.3410N-6.2812 \times 10^{-4} N^2$	(5.22)
30	400	$0.0778+0.2963N-4.7819 \times 10^{-4} N^2$	(5.23)
30	500	$0.0380+0.3104N-4.5768 \times 10^{-4} N^2$	(5.24)

is much easier to clamp the shaft to higher shaft speeds (and get the readings) than to lower shaft speeds -- both at the same volume flowrate. The Prony brake behaved erratically when tightened to obtain slow shaft speeds making it difficult to record torque and shaft speed readings. This behavior further illustrated in the various values of torque  $T$  while rotative speed  $N$  is held at specific value. Again unsteady variations in frictional forces between the brakes and the shaft plus the highly turbulent nature of water flow play a significant role in the values of power output and efficiency. A typical example is shown in Figure 5.12.

The optimum rotative speed  $N_o$  of each equation was calculated from the differential of Equation (5.11) with respect to  $N$

$$\frac{dE}{dN} = \frac{d(P(1) + P(2)N + P(3)N^2)}{dN} = 0 \quad (5.25)$$

Thus, the maximum turbine efficiency  $E_{max}$  can be calculated by substituting the optimum rotative  $N_o$  in Equation (5.11).

In Equation (5.11),  $E$  may be expressed in terms of the velocity coefficient  $U_1/V_1$  instead of  $N$ ,

$$E = (P(1) + P(2)(U_1/V_1) + P(3)(U_1/V_1)^2) \quad (5.26)$$

The coefficient  $U_1/V_1$  was calculated from Equations (5.5) and (5.8) and are shown in the tables for each value



of  $N$ . Thus optimum velocity coefficient  $(U_1/V_1)_o$  was calculated from the derivative of Equation (5.26)

$$\frac{dE}{d(U_1/V_1)} = 0 \quad (5.27)$$

Maximum turbine efficiency based on optimum velocity coefficient can thus be calculated using Equation (5.26).

The optimum performance values of the runners are summarized in Table XV. These values are plotted in Figures 5.17, 5.18, and 5.19. Figure 5.17 shows the effect of supply flow rate  $Q_s$  on the turbine efficiency  $E$  for various runners. All runners exhibit a fairly constant efficiency for three levels of flow rates. Except for the 15-blade runner which shows a very slight increase of efficiency as flow rate rises, no significant increase or change is visible. On the other hand the graphs show an increase in efficiency of the runners as number of blades was increased. However, the 30-blade runner showed no pronounced increase compared with the 20-blade runner. So it appears that efficiency does not improve beyond that given by the 20-blade runner. Figure 5.18 shows a clearer view of the rise in efficiency up to the 20-blade runner. Figure 6.19 shows a general increase of optimum rotative speeds of the various runners as flow rate was increased. Also, an increase of the number of blades give an increase of optimum rotative speed.

TABLE X V

MAXIMUM EFFICIENCY AND CORRESPONDING OPTIMUM  
 ROTATIVE SPEED AND VELOCITY COEFFICIENT  
 OF RUNNERS AT VARIOUS FLOW RATES

Number of blades Z	Supply flow rate $Q_s$ (gpm)	Optimum rotative speed $N_o$ (rpm)	Optimum velocity coefficient $(U_1/V_1)_o$	Maximum turbine efficiency $E_{max}$
10	300	230.31	0.4657	30.32
10	400	279.22	0.4765	35.61
10	500	323.86	0.4870	35.15
15	300	245.03	0.4955	38.14
15	400	287.01	0.4898	40.06
15	500	355.26	0.5342	44.21
20	300	267.67	0.5413	46.58
20	400	280.26	0.4783	46.17
20	500	336.73	0.5064	47.11
30	300	271.46	0.5489	46.27
30	400	309.97	0.5290	46.00
30	500	339.21	0.5101	52.69

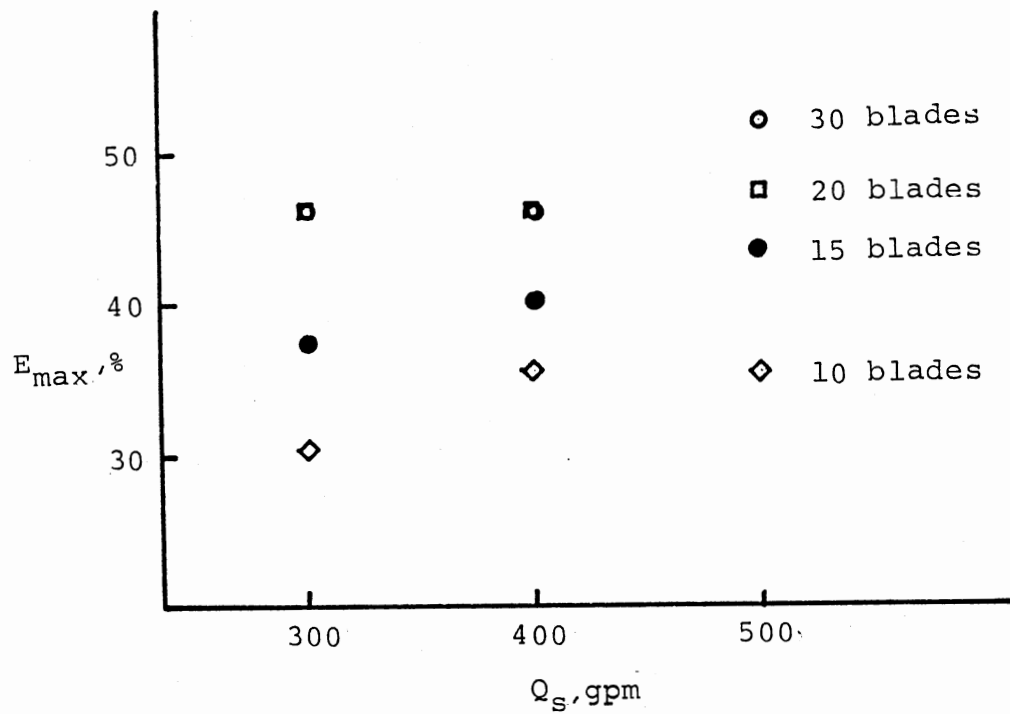


Figure 5.16. Relationship between turbine efficiency  $E$  and supply flow rate  $Q_s$  for various number of blades.

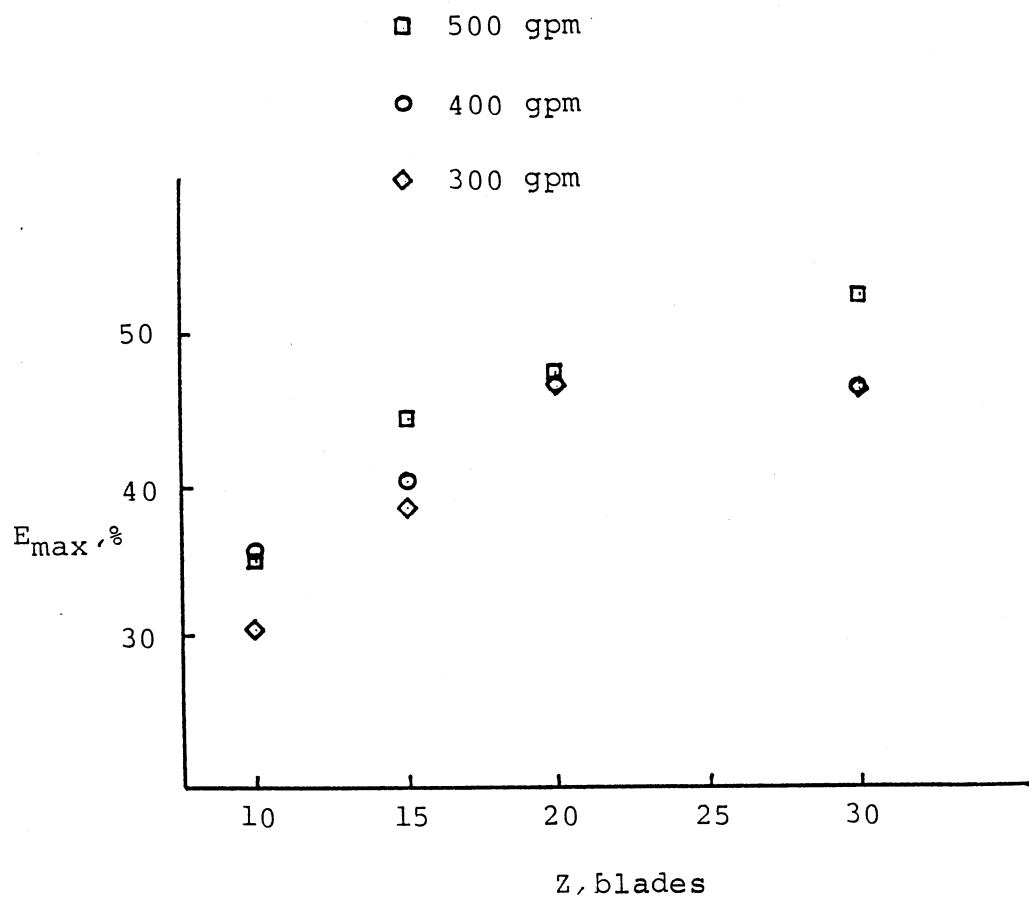


Figure 5.17. Relationship between turbine efficiency  $E$  and number of blades  $Z$  at various levels of flow rate  $Q_s$ .

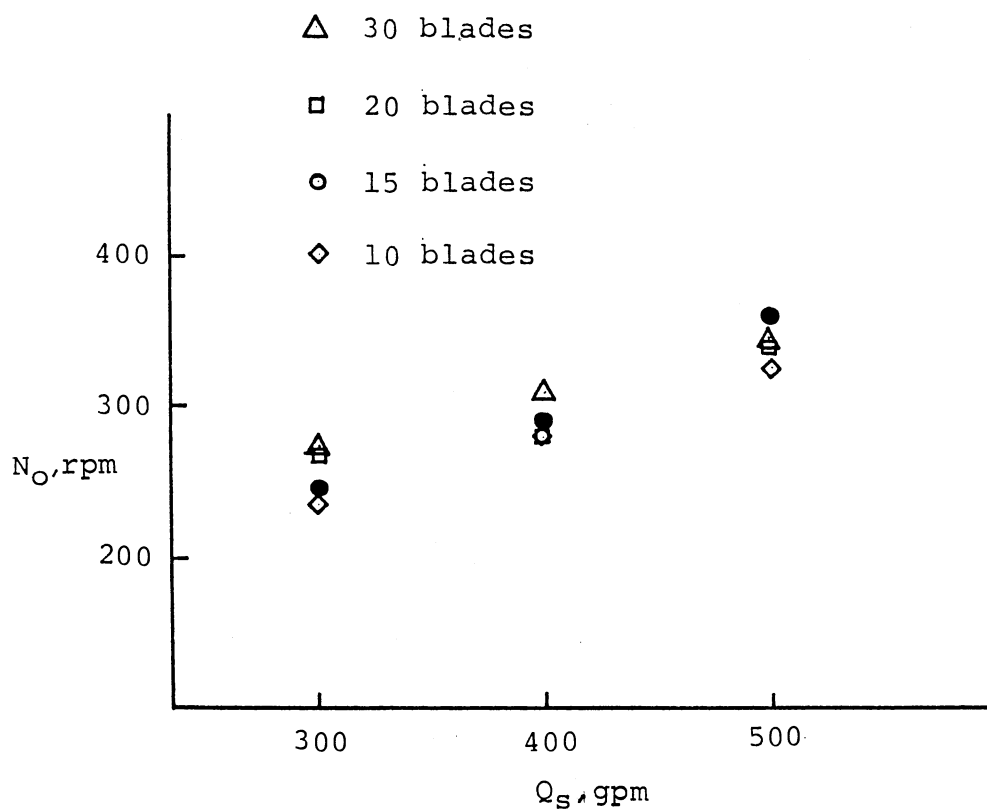


Figure 5.18. Relationship between optimum rotational speed  $N_o$  and supply flow rate  $Q_s$  for various number of blades  $Z_s$

## CHAPTER VI

### DEVELOPMENT OF A PREDICTION EQUATION

#### Selection of Pi Terms

In this chapter, performance data shown in Chapter V were further analyzed to arrive at a general output power prediction equation based on the variables involved. Dimensional analysis was used to develop the empirical prediction equation. The physical system for predicting the output power of a small crossflow turbine may be adequately described by the physical variables listed in Table XVI. It may be noted that supply flow rate  $Q_s$  nor water velocity entering the runner  $V_1$  is not included on the table. This is because total available head  $H$  increased proportionately with  $Q_s$ , as shown in Equations (5.1) and (5.2), and because  $V_1$  is a function of  $H$ , as shown in Equation (5.4).

The number of independent and dimensionless quantities necessary to adequately describe the system is equal to the number of independent physical variables minus the rank of the dimensional matrix (Langhaar, 1951). From Table XVI, the number of independent variables is 14 and the rank of the dimensional matrix is three. Therefore, the number of

TABLE XVI  
 PERTINENT VARIABLES FOR OUTPUT POWER  
 PREDICTION OF A SMALL  
 CROSSFLOW TURBINE

No	Symbol	Quantity	Unit	Dimension
1	$P_o$	Output power	$lb_f\text{-ft/sec}$	$FLT^{-1}$
2	$\Omega$	Angular velocity of runner	rad/sec	$T^{-1}$
3	H	Total available head	ft	L
4	$t_2$	Blade spacing at inner runner diameter	ft	L
5	$D_1$	Outside diameter of runner	ft	L
6	$D_2$	Inside diameter of runner	ft	L
7	$\gamma$	Specific weight of water	$lb_f/ft^3$	$FL^{-3}$
8	$\mu$	Dynamic viscosity of water	$lb_f\text{-sec}/ft^2$	$FL^{-2}T$
9	$S_o$	Width of nozzle throat	ft	L
10	$\delta$	Nozzle entry arc	rad	-
11	L	Length of runner	ft	L
12	$t_o$	Blade thickness	ft	L
13	c	Chord length of blades	ft	L
14	g	Acceleration due to gravity	$ft/sec^2$	$LT^{-2}$

the number of dimensionless groups of pi terms is 11. The following pi terms may be used:

$$\Pi_1 = \Omega (P_o/\gamma)^{0.5} (H^5 g^3)^{-0.25} \quad (6.1)$$

$$\Pi_2 = \Omega (\gamma/g) (D_1^2/\mu) \quad (6.2)$$

$$\Pi_3 = S_o(\gamma/\mu) (H/g)^{0.5} \quad (6.3)$$

$$\Pi_4 = c/t_2 \quad (6.4)$$

$$\Pi_5 = (\mu/\gamma)^2 (g/D_1^3) \quad (6.5)$$

$$\Pi_6 = S_o/L \quad (6.6)$$

$$\Pi_7 = D_2/D_1 \quad (6.7)$$

$$\Pi_8 = S_o/D_1 \quad (6.8)$$

$$\Pi_9 = t_o/D_1 \quad (6.9)$$

$$\Pi_{10} = c/D_1 \quad (6.10)$$

$$\Pi_{11} = \delta \quad (6.11)$$

It was necessary to check the independence of the pi terms. This can be shown by determining the rank of the dimensional matrix as shown in Table XVII. The rank of the matrix is 11. Therefore the pi terms are independent.

The variables of this study were  $P_o$ ,  $\Omega$ ,  $H$ , and  $t_2$ . The rest were held constant. Therefore, the variable pi terms were  $\Pi_1$ ,  $\Pi_2$ ,  $\Pi_3$ , and  $\Pi_4$  and the other pi terms were held constant throughout the duration of the study. One



TABLE XVII  
 DETERMINING THE RANK OF THE  
 DIMENSIONAL MATRIX

	$P_0$	$\Omega$	$H$	$t_2$	$D_1$	$D_2$	$\gamma$	$\mu$	$S_0$	$\delta$	$L$	$t_0$	$c$	$g$
$\pi_1$	0.5	1	-1.25				-0.5							-0.75
$\pi_2$		1			2		1	-1						-1
$\pi_3$			-0.5				-1	-1	1					-0.5
$\pi_4$				-1									1	
$\pi_5$					-3		-2	2						1
$\pi_6$									1	-1				
$\pi_7$					-1	1								
$\pi_8$					-1				1					
$\pi_9$					-1							1		
$\pi_{10}$					-1								1	
$\pi_{11}$										1				

variable was assigned to each of the four pi terms as shown in Equations (6.1) to (6.4) which made it easier to proceed with the analysis.

The general prediction equation for determining output power can now be written as:

$$\Pi_1 = \phi_1 (\Pi_2, \Pi_3, \Pi_4) \quad (6.12)$$

The actual form of the function  $\phi$  is determined by the character of the component equation. As had been found, the component equations often form as straight lines when plotted in logarithmic coordinates (Clary and Nelson, 1968). Thus Equation (6.12) may take the form

$$\Pi_1 = \phi_2 (\Pi_2)^{k_1} (\Pi_3)^{k_2} (\Pi_4)^{k_3} \quad (6.13)$$

where  $k_1$ ,  $k_2$ , and  $k_3$  are constants or slopes of straight lines in the log-log space.

#### Experimental Design and Analysis

For this analysis, the experimental design was presented in Table XVIII. The bar above the  $\bar{\Pi}$  symbol indicates that the term was held constant. As seen from Table XVIII, the analysis requires the development of three component equations:

$$\bar{\Pi}_1 = F_1 (\bar{\Pi}_2, \bar{\Pi}_3, \bar{\Pi}_4) \quad (6.14)$$

$$\bar{\Pi}_1 = F_2 (\bar{\Pi}_2, \bar{\Pi}_3, \bar{\Pi}_4) \quad (6.15)$$

TABLE XVIII  
EXPERIMENTAL PLAN

Experiment Series	$\Pi_1$	$\Pi_2$	$\Pi_3$	$\Pi_4$
1	Measure	Vary $\Omega$ or N	$\Pi_3$	$\Pi_4$
2	Measure	$\Pi_2$	Vary H or $Q_s$	$\Pi_4$
3	Measure	$\Pi_2$	$\Pi_3$	Vary $t_2$ or $Z^2$

$$\Pi_1 = F_3 (\bar{\Pi}_2, \bar{\Pi}_3, \Pi_4) \quad (6.16)$$

The following constants were substituted in order to simplify the four pi terms:

$$\gamma = 62.4 \text{ lb}_f/\text{ft}^3 \text{ of water}$$

$$g = 32.2 \text{ ft}/\text{sec}^2$$

$$\mu = 2.37 \text{ lb}_m/\text{ft-hr at } 70^\circ\text{F (Holman, 1971)}$$

$$= \frac{2.37 \text{ lb}_m}{\text{ft-hr}} \frac{(1 \text{ lb}_f \text{ sec}^2)}{32.2 \text{ lb}_m \text{ ft}} \frac{(\text{hr})}{3600 \text{ sec}}$$

$$= 2.0445 \times 10^{-5} \text{ lb}_f \text{ - sec}/\text{ft}^2$$

$$D_1 = 0.50 \text{ ft}$$

$$S_o = 0.1041 \text{ ft}$$

$$c = 0.088 \text{ ft}$$

Further, to be consistent with notations used in the previous chapters, angular velocity  $\bar{\Omega}$  was replaced with rotational speed  $N$ , total available head  $H$  was expressed in terms of supply flow rate  $Q_s$  and blade spacing  $t_2$  was replaced with number of blades  $Z$ , as follows:

$$\bar{\Omega} = 2\pi N/60 \text{ rad}/\text{sec} \quad (6.17)$$

$$H = 0.0105 Q_s - 0.5531 \text{ ft} \quad (5.1) \text{ and } (5.2)$$

$$t_2 = \frac{\Pi D_2}{Z} = \frac{\Pi (2/3 D_1)}{Z} \text{ ft} \quad (6.18)$$

where  $N$  is in revolutions per minute,  $Q_s$  is in gpm and  $D_1$  is in ft. Substituting Equations (5.1), (6.2), (6.17), and (6.18) in Equations (6.1), (6.2), (6.3) and (6.4),

$$\begin{aligned} \Pi_1 &= \frac{2\Pi N}{60} \left( \frac{550 P}{62.4} \right)^{1/2} \left( \frac{1}{H^5 32.2^3} \right)^{1/4} \\ \Pi_1 &= 6.8172 N P_o^{0.5} (Q_s - 52.5247)^{-1.25} \end{aligned} \quad (6.19)$$

$$\begin{aligned} \Pi_2 &= \frac{2\Pi N}{60} \frac{62.4}{32.2} \frac{0.5^2}{2.0445 \times 10^{-5}} \\ \Pi_2 &= 2481.4768 N \end{aligned} \quad (6.20)$$

$$\begin{aligned} \Pi_3 &= (0.1042) \frac{62.4}{2.0445 \times 10^{-5}} \left( \frac{H}{32.2} \right)^{0.5} \\ \Pi_3 &= 5749.7012 (Q_s - 52.5247)^{0.5} \end{aligned} \quad (6.21)$$

$$\begin{aligned} \Pi_4 &= \frac{0.0885}{\Pi [2/3 (0.5)]/Z} \\ \Pi_4 &= 0.0845 Z \end{aligned} \quad (6.22)$$

where  $P_o$  is in hp,  $N$  is in rpm,  $Q_s$  is in gpm, and  $Z$  is the number of blades.

Following the experimental and analysis plan in Table

XVIII  $\Pi_2$  was varied while  $\bar{\Pi}_3$  and  $\bar{\Pi}_4$  were held constant for Experiment Series Number 1.  $\Pi_1$  was calculated for each corresponding value of  $\Pi_2$ . Using  $Q_s = 400$  gpm and  $Z = 15$  blades as constants,

$$\begin{aligned}\Pi_3 &= 5749.7012 (400-52.5247)^{0.5} \\ &= 107,178.3887\end{aligned}$$

$$\begin{aligned}\Pi_4 &= 0.0845 (15) \\ &= 1.2682\end{aligned}$$

In the analysis,  $\Pi_1$  was expressed in terms of runner efficiency  $E_c$  from Equation (5.17), supply flow rate  $Q_s$  and rotative  $N$ . From previous equations

$$P_o = 2.5277 \times 10^{-6} Q_s H E \quad (5.3)$$

$$H = 0.0105 Q_s - 0.5531 \quad (5.2)$$

Substituting Equations (5.3) and (5.2) in Equation (7.19)

$$\Pi_1 = 1.1123 \times 10^{-3} N Q_s^{0.5} (Q_s - 52.5247)^{-0.75} E^{0.5} \quad (6.23)$$

At  $Q_s = 400$  gpm

$$\Pi_1 = 2.7641 \times 10^{-4} N E_c^{0.5} \quad (6.24)$$

$$\text{where } E_c = 0.0267 + 0.2790N - 4.8602 \times 10^{-4} \quad (5.17)$$

Values for  $\bar{\Pi}_2$  and  $\bar{\Pi}_1$  calculated using various values of  $N$  are shown in Table XIX. Linear regression analysis was

TABLE XIX

DATA GENERATED USING THE EMPIRICAL EFFICIENCY  
EQUATION (EQUATION (5.17) FOR THE  
15-BLADE RUNNER AT 400 GPM

	N	$E_C$	$\pi_2 \times 10^{-5}$	$\pi_1 \times 100$	LOG $\pi_2$	LOG $\pi_1$
1	25.0000	6.6975	.6204	1.7883	4.7926	-1.7475
2	50.0000	12.7604	1.2407	4.9369	5.0937	-1.3065
3	75.0000	18.2159	1.8611	8.8479	5.2698	-1.0532
4	100.0000	23.0638	2.4815	13.2746	5.3947	-.8770
5	125.0000	27.3042	3.1018	18.0543	5.4916	-.7434
6	150.0000	30.9371	3.7222	23.0614	5.5708	-.6371
7	175.0000	33.9625	4.3426	28.1899	5.6377	-.5499
8	200.0000	36.3803	4.9629	33.3440	5.6957	-.4770
9	225.0000	38.1906	5.5833	38.4340	5.7469	-.4153
10	250.0000	39.3934	6.2037	43.3718	5.7926	-.3628
11	275.0000	39.9887	6.8240	48.0680	5.8340	-.3181
12	300.0000	39.9765	7.4444	52.4298	5.8718	-.2804
13	325.0000	39.3567	8.0648	56.3570	5.9066	-.2491
14	350.0000	38.1294	8.6851	59.7383	5.9388	-.2237
15	375.0000	36.2946	9.3055	62.4464	5.9687	-.2045
16	400.0000	33.8523	9.9259	64.3293	5.9968	-.1916
17	425.0000	30.8024	10.5462	65.1983	6.0231	-.1858
18	450.0000	27.1450	11.1666	64.8057	6.0479	-.1884
19	475.0000	22.8802	11.7870	62.8027	6.0714	-.2020
20	500.0000	18.0077	12.4074	58.6482	6.0937	-.2317

used on the data to determine the slope of the curve and y-intercept in a linear space, semi-log space, and log-log space. The correlation coefficient R was highest for the log-log plot. Figure 6.1 shows the curve of  $\Pi_2$  versus  $\Pi_1$  in a log-log space. The resulting line is

$$\log \Pi_1 = 1.0529 \log \Pi_2 - \log 6.5147 \quad (6.25)$$

$$R = 0.9770$$

Therefore,

$$\Pi_1 = 3.0569 \times 10^{-7} \Pi_2^{1.0529} \quad (6.26)$$

where  $\bar{\Pi}_3$  and  $\bar{\Pi}_4$  are constants

In Experiment Series Number 2 of Table XVIII  $\Pi_2$  and  $\Pi_4$  were held constant.  $\Pi_3$  was varied using various values of  $Q_s$  and the corresponding  $\Pi_1$  was calculated. Using  $N = 300$  rpm and  $Z = 15$  blades,

$$\bar{\Pi}_2 = 2481.4768 (300) = 744443$$

$$\text{and } \bar{\Pi}_4 = 0.0845 (15) = 1.2682$$

Substituting  $N = 300$  rpm in Equation (6.23),

$$\bar{\Pi}_1 = 0.3337 Q_s^{0.5} (Q_s - 52.5247)^{-0.75} E_c^{0.5} \quad (6.27)$$

$$\text{where } E_c = 0.0288 Q_s + 26.6323 \quad (6.28)$$

Equation (6.28) is the linear equation involving calculated efficiency  $E$  and flow rate  $Q_s$  of Table XX. The linear curve



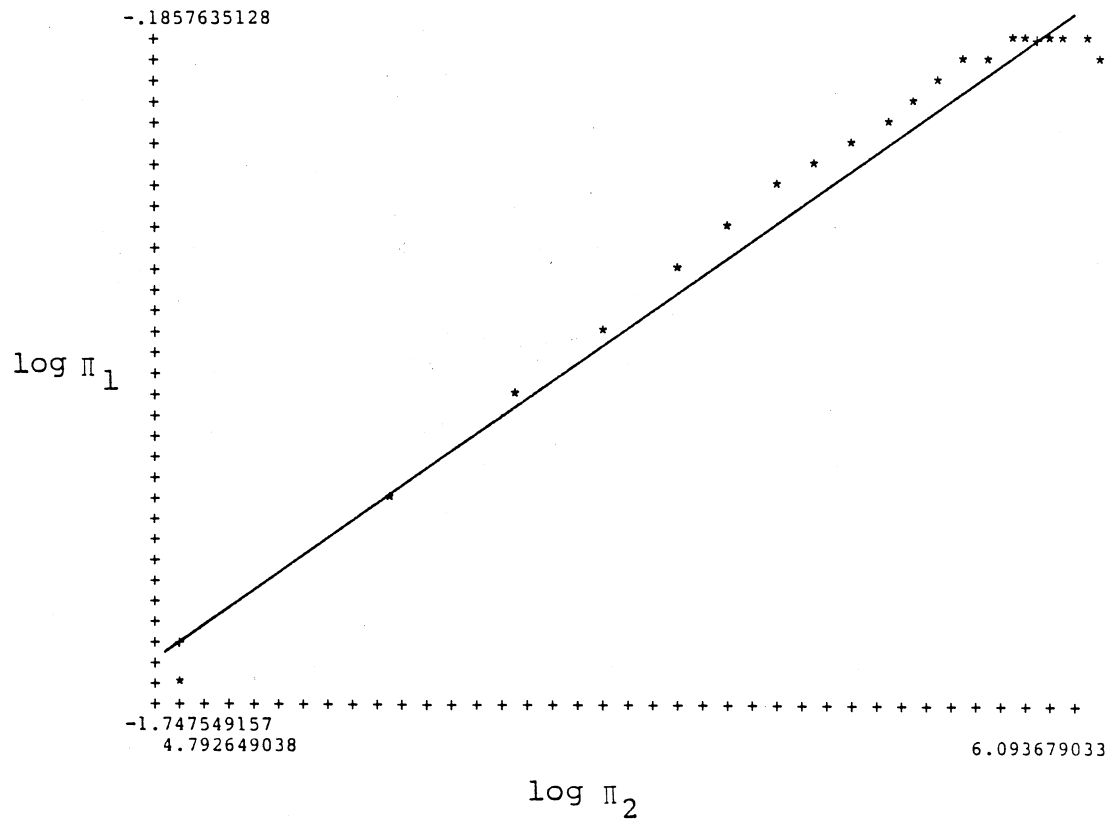


Figure 6.1. Relationship Between  $\Pi_1$  and  $\Pi_2$ ,  
With  $\Pi_3$  and  $\Pi_4$  as Constants<sup>2</sup>,

TABLE XX

PERFORMANCE DATA OF THE 15-BLADE RUNNER  
HELD AT N=300 FOR VARIOUS FLOW RATES

	Q	T	H	P <sub>i</sub>	P <sub>o</sub>	E
1	275.0000	11.6391	2.3430	.1629	.0554	34.0166
2	300.0000	15.0006	2.6063	.1976	.0714	36.1278
3	350.0000	20.9880	3.1329	.2772	.0999	36.0445
4	360.0000	23.4253	3.2382	.2947	.1115	37.8407
5	380.0000	26.1985	3.4488	.3313	.1247	37.6444
6	420.0000	33.4047	3.8701	.4109	.1590	38.7005
7	440.0000	36.3881	4.0807	.4539	.1732	38.1636
8	475.0000	45.5060	4.4493	.5342	.2166	40.5471
9	500.0000	51.9559	4.7126	.5956	.2473	41.5224

is shown in Figure 6.2. Equation (6.21) was used to calculate  $\Pi_3$  and Equation 6.27 was used to calculate  $\Pi_1$ . The  $\Pi_3$  and  $\Pi_1$  values are shown in Table XXI and plotted Figure 6.3.

The resulting curve is

$$\log \Pi_1 = -0.3969 \log \Pi_3 + \log 1.7073 \quad (6.29)$$

$$R = 0.8781$$

$$\Pi_1 = 50.9659 \Pi_3^{-0.3969} \quad (6.30)$$

where  $\Pi_2$  and  $\Pi_4$  are constants

In Experiment Series Number 3 of Table XVIII  $\Pi_2$  and  $\Pi_3$  were maintained constants.  $\Pi_4$  or Z was varied by using different runners and the corresponding  $\Pi_1$  was calculated. Using  $N = 300$  rpm and  $Q_s = 400$  gpm,

$$\Pi_2 = 744443$$

$$\Pi_3 = 107178$$

To increase the number of data points, blades were later cut out of the already tested 30-blade runner to arrive at a 6-blade runner. This increase the number of runners for the experiment to five. Thus, using Equation (6.22), and for the 6-blade runner,

$$\Pi_{4(6)} = 0.5073$$

For the 10-blade runner,

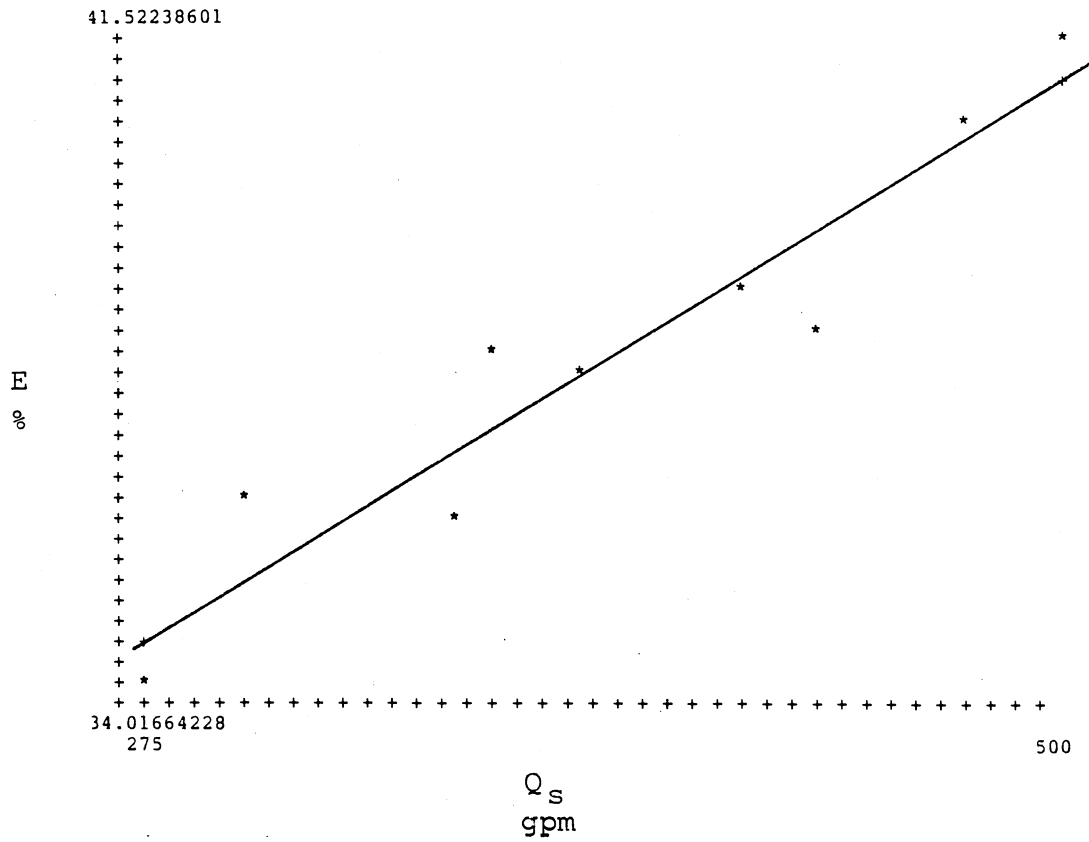


Figure 6.2. Relationship Between Runner Efficiency and Flow Rate for the 15-Blade Runner Held at 300 rpm.

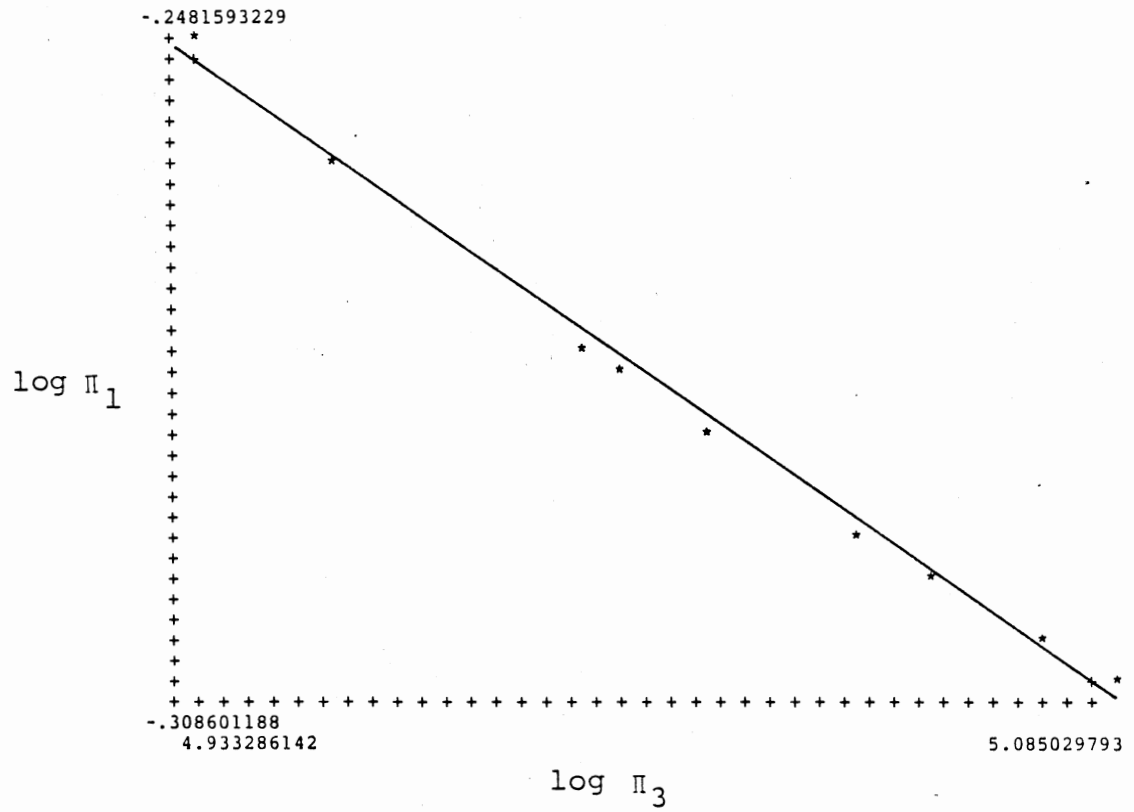


Figure 6.3. Relationship Between  $\Pi_1$  and  $\Pi_3$ ,  
With  $\Pi_2$  and  $\Pi_4$  as Constants<sup>3</sup>,

TABLE XXI

PI-TERMS FOR DATA IN TABLE XX

	Q	E	E <sub>C</sub>	$\pi_3 \times .0001$	$\pi_1$	LOG $\pi_3$	LOG $\pi_1$
1	275.0000	34.0166	34.5615	8.5760	.5647	4.9333	-.2482
2	300.0000	36.1278	35.2823	9.0451	.5502	4.9564	-.2595
3	350.0000	36.0445	36.7240	9.9168	.5282	4.9964	-.2772
4	360.0000	37.8407	37.0123	10.0821	.5246	5.0036	-.2802
5	380.0000	37.6444	37.5890	10.4048	.5181	5.0172	-.2856
6	420.0000	38.7005	38.7423	11.0220	.5071	5.0423	-.2949
7	440.0000	38.1636	39.3190	11.3179	.5026	5.0538	-.2988
8	475.0000	40.5471	40.3282	11.8181	.4956	5.0725	-.3049
9	500.0000	41.5224	41.0490	12.1627	.4914	5.0850	-.3086

$$\Pi_4(10) = 0.8455$$

For the 15-blade runner,

$$\Pi_4(15) = 1.2682$$

For the 20-blade runner,

$$\Pi_4(20) = 1.6910$$

For the 30-blade runner,

$$\Pi_4(30) = 2.5365$$

The 6-blade runner was tested and the results are tabulated in Table XXII. Calculated  $\Pi_1$  and  $\Pi_4$  values were also included.  $\Pi_1$  was calculated using Equation 6.23 (6.19) and in terms of runner efficiency  $E_c$ . At 300 rpm and 400 gpm

$$\Pi_1 = 0.0829 E_c^{0.5} \quad (6.31)$$

where, for the 6-blade runner, runner efficiency from Figure 6.4 was found to be

$$\begin{aligned} E_{c(6)} &= -0.0808 + 0.1983N - 3.2554 \times 10^{-6} N^2 \quad (5.12) \\ &= 30.1026\% \end{aligned}$$

The following efficiency equations are listed in Table XIV. For the 10-blade runner,

$$E_{c(10)} = -0.0076 + 0.2551N - 4.5690 \times 10^{-4} N^2 \quad (5.14)$$

TABLE XXII  
 PERFORMANCE DATA OF THE 6-BLADE  
 RUNNER AT 400 GPM

	N	F	T	P <sub>0</sub>	E
1	400.00000	1.16131	14.15352	.08983	24.27770
2	380.00000	1.38362	16.86286	.10167	27.47880
3	350.00000	1.58614	19.33110	.10735	29.01400
4	340.00000	1.69345	20.63896	.11134	30.09190
5	330.00000	1.73720	21.17209	.11086	29.96130
6	310.00000	1.94605	23.71747	.11666	31.52920
7	300.00000	2.04841	24.96503	.11883	32.11710
8	290.00000	2.08672	25.43196	.11702	31.62720
9	275.00000	2.17214	26.47293	.11551	31.21890
10	250.00000	2.28310	27.82525	.11037	29.83060
11	250.00000	2.34560	28.58695	.11339	30.64720
12	230.00000	2.39739	29.21817	.10663	28.81800
13	200.00000	2.38512	29.06866	.09224	24.93090
14	200.00000	2.44762	29.83039	.09466	25.58420
15	80.00000	1.43157	17.44727	.02215	5.98550



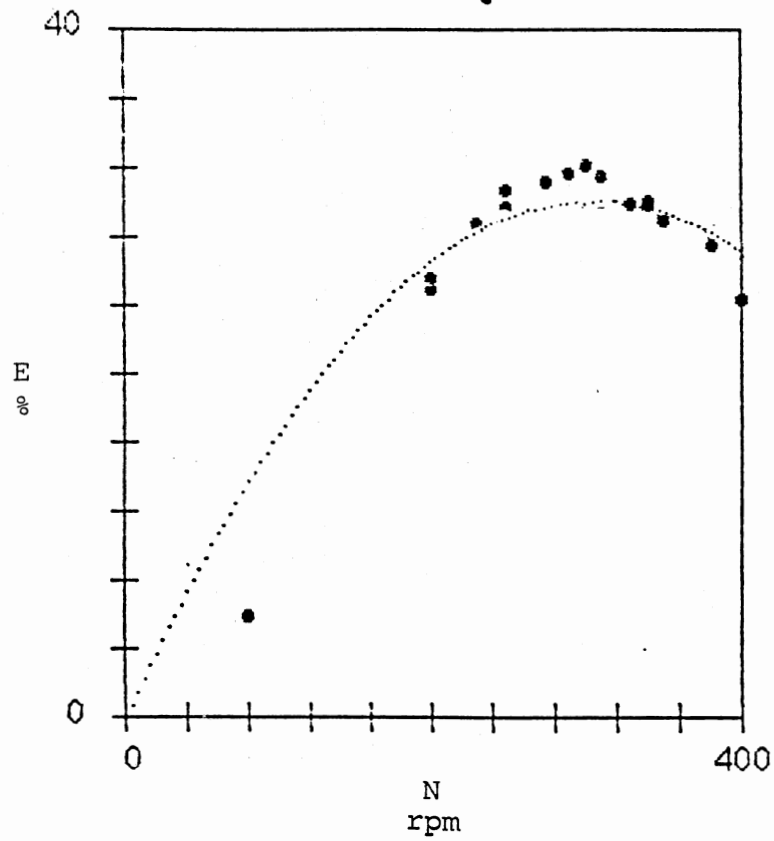


Figure 6.4. Performance Curve of the 6-Blade Runner at 400 gpm.

$$= 35.4135\%$$

For the 15-blade runner,

$$E_{C(15)} = 0.0267 + 0.2790N - 4.8602 \times 10^{-4} N^2 \quad (5.17)$$

$$= 39.97659$$

For the 20-blade runner,

$$E_{C(20)} = 0.0076 + 0.3292N - 5.8730 \times 10^{-4} N^2 \quad (5.20)$$

$$= 45.9049\%$$

For the 30-blade runner,

$$E_{C(30)} = 0.0778 + 0.2963N - 4.7819 \times 10^{-4} N^2 \quad (5.23)$$

$$= 45.7861\%$$

Therefore,  $\Pi_1(6) = 0.4549$

$$\Pi_1(10) = 0.4935$$

$$\Pi_1(15) = 0.5243$$

$$\Pi_1(20) = 0.5618$$

$$\Pi_1(30) = 0.5611$$

Plotting values of  $\Pi_4$  and  $\Pi_1$  in Figure 6.5, the following curve was derived

$$\log \Pi_1 = 0.1405 \log \Pi_4 - \log 0.2964 \quad (6.32)$$

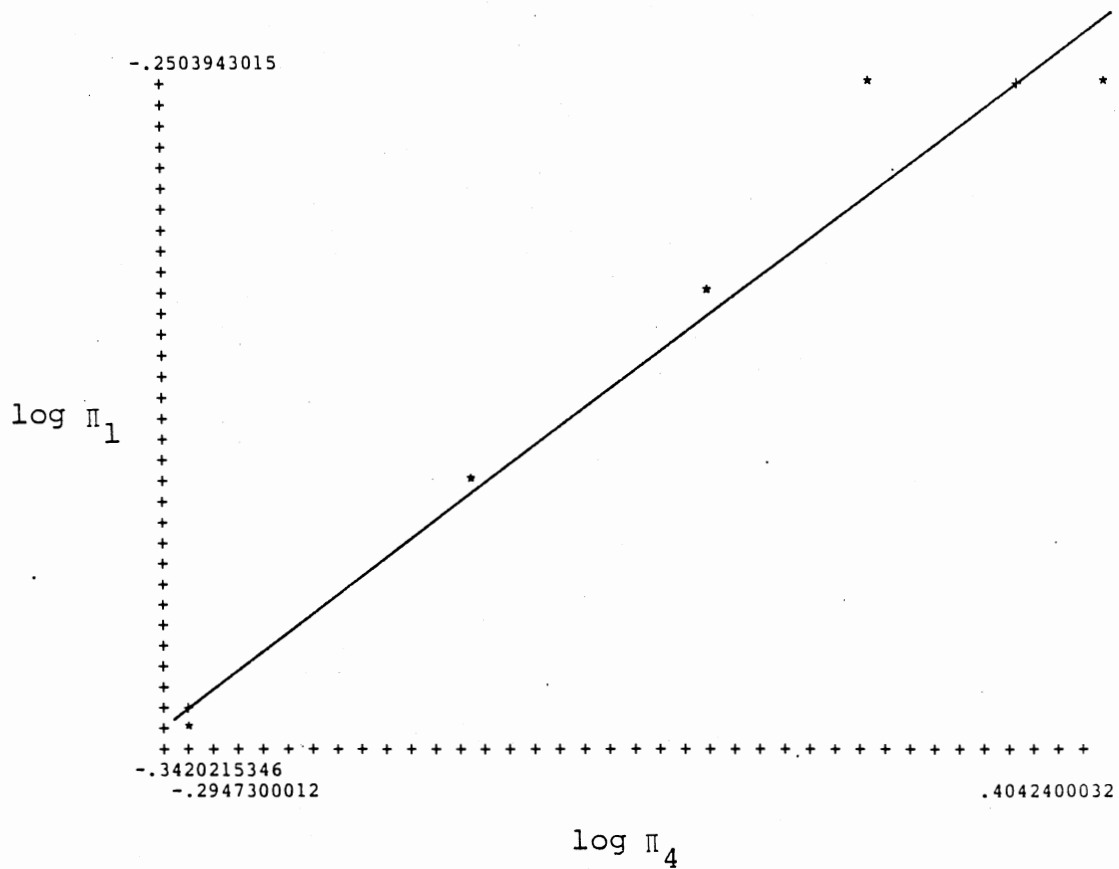


Figure 6.5. Relationship Between  $\Pi_1$  and  $\Pi_4$ ,  
With  $\Pi_2$  and  $\Pi_3$  as Constants<sup>4</sup>,

$$R = 0.9714$$

or

$$\Pi_1 = 0.5053 \Pi_4^{0.1405} \quad (6.33)$$

where  $\bar{\Pi}_2$  and  $\bar{\Pi}_3$  are constants

### The Prediction Equation

Because the component equations, that is, Equations (6.26), (6.30) and (6.33), form as straight lines in a log-log space, Murphy (1950) gave the following general prediction equation for four independent pi terms:

$$\Pi_1 = \frac{F_1(\bar{\Pi}_2, \bar{\Pi}_3, \bar{\Pi}_4) \cdot F_2(\bar{\Pi}_2, \bar{\Pi}_3, \bar{\Pi}_4) \cdot F(\bar{\Pi}_2, \bar{\Pi}_3, \bar{\Pi}_4)}{[F_4(\bar{\Pi}_2, \bar{\Pi}_3, \bar{\Pi}_4)]^2} \quad (6.34)$$

$F_4(\bar{\Pi}_2, \bar{\Pi}_3, \bar{\Pi}_4)$  may be calculated from either Equation (6.26), (6.30), or (6.33). Since they are not exactly equal, the average of the three values was used. So, using the constants  $N = 300$  rpm,  $Q = 400$  gpm, and  $Z = 15$  blades, Equation (6.26) becomes

$$\Pi_1 = 3.0569 \times 10^{-7} (744443.058)^{1.0529} = 0.4653$$

From Equation (6.30)

$$\Pi_1 = 50.9659 (107178.3887)^{-0.3969} = 0.5026$$

From Equation (6.33)

$$\Pi_1 = 0.5053 (1.2682)^{0.1405} = 0.5224$$

Therefore

$$F_4(\bar{\Pi}_2, \bar{\Pi}_3, \bar{\Pi}_4) = \frac{0.4653 + 0.5026 + 0.5224}{3}$$

$$= 0.4967$$

Equation (6.34) then becomes

$$\Pi_1 = (3.0569 \times 10^{-7} \Pi_2^{1.0529}) (50.9659 \Pi_3^{-0.3969})$$

$$(0.5053 \Pi_4^{0.1405}) / (0.4967)^2$$

or

$$\Pi_1 = 3.1897 \times 10^{-5} \Pi_2^{1.0529} \Pi_3^{-0.3969} \Pi_4^{0.1405} \quad (6.35)$$

Substituting Equations (6.19), (6.20), (6.21) and (6.22) in Equation (6.35), the predicted power output of the small crossflow water turbine is

$$P_{op} = 1.5962 \times 10^{-7} N^{0.1058}$$

$$(Q_s - 52.5247)^{2.1031} Z^{0.2811} \text{ hp} \quad (6.36)$$

Further, using Equations (5.2) and (5.3), the predicted efficiency of the turbine is

$$E_p = 0.0600 N^{0.1058} Z^{0.2811} \frac{(Q_s - 52.5247)^{1.1031}}{Q_s} \times 100\% \quad (6.37)$$

where  $P_{op}$  is in hp,  $N$  is in rpm,  $Q_s$  is in gpm,  $Z$  is the

number of blades and  $E_p$  is in percent.  $N$  and  $Q_s$  can easily be obtained using a tachometer and a flowmeter, respectively, or any similar device. Equations (6.36) and (6.37) are applicable only to the same size of turbine used throughout this experiment which include blade thickness and geometry, runner length, and nozzle design. Further, applicability of the derived equations are limited to within the normal operating range of the turbine as tested in this experiment. That is, the equations are best suited for rotative speeds up to approximately 500 rpm, for flow rates up to about 500 gpm and for number of blades of up to about 20.

Effect of Flow Rate  $Q_s$  and  
Number of Blades  $Z$

Based on the derived empirical equation (Equation (6.37)), the effect of flow rate  $Q_s$  and the number of blades  $Z$  on the efficiency of the small crossflow water turbine can also be determined.

From Equation (6.37), let

$$\frac{E_p}{K_1} = \frac{(Q_s - 52.5247)^{1.1031}}{Q_s} \quad (6.38)$$

$$\text{where } K_1 = 0.0600 N^{0.1058} Z^{0.2811} \quad (6.39)$$

Using specific values for  $N$  and  $Z$  in Equation (6.39), Equation (6.38) is plotted in Figure 6.6 for various values of  $Q_s$ . The solid curve shows the actual effect of flow on

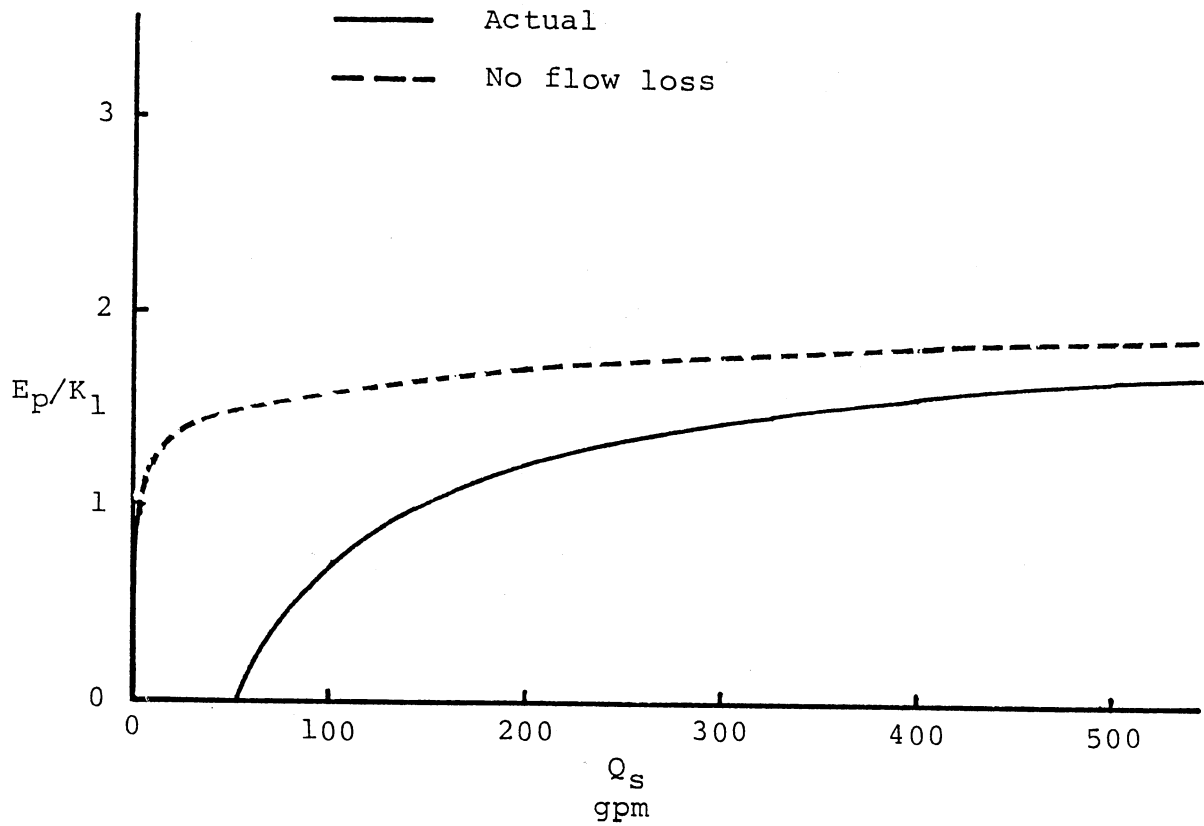


Figure 6.6. Effect of Flow Rate on Turbine Efficiency.

the turbine's performance. Note that the initial 52.52 gpm of water was unaccounted for and gave no work. The effect of flow rate is pronounced up to about 350 gpm after which it began to level off. This means that further increase of flow has no significant effect on the efficiency of the crossflow turbine. This result is reinforced by Figure 5.17. The dashed line in Figure 6.6 shows the turbine's performance if the initial 52.52 gpm were to have any effect. This way, 200 gpm and beyond give almost uniform efficiency.

Furthermore, from Equation (6.37), let

$$\frac{E_p}{K_2} = z^{0.2811} \quad (6.40)$$

$$\text{where } K_2 = 0.0600N^{0.1058} \frac{(Q_s - 52.5247)^{1.1031}}{Q_s} \quad (6.41)$$

Using specific values for  $N$  and  $Q_s$  in Equation (6.41), Equation (6.40) is plotted in Figure 6.7 for values of  $Z$ .

It appears that efficiency increases as blade number increases. In reality this is not true because the more blades there are, the lesser water flow can go through the runner. A cut-off point along the curve must be determined wherein any further increase in the number of blades gives no further significant increase in efficiency. This cut-off point may be known by drawing a series of tangent lines along the curve at uniform  $Z$ -intervals. The point of tangency on the curve, above which the curve begins to



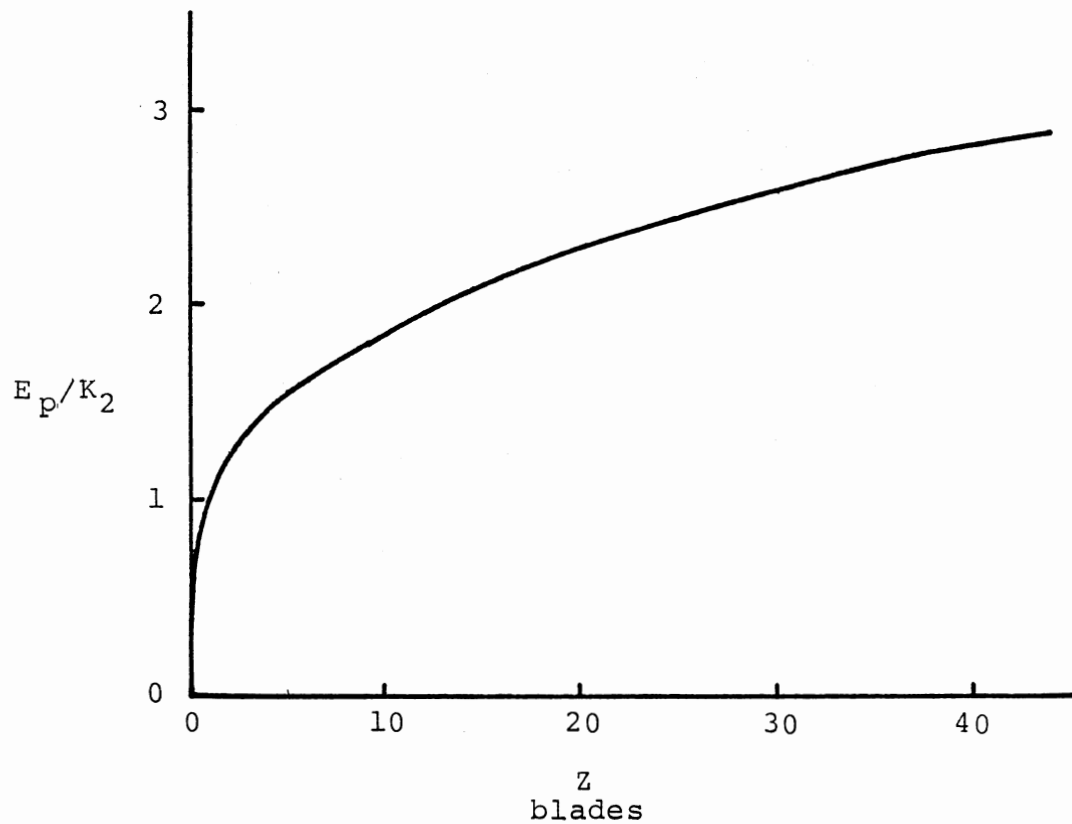


Figure 6.7. Effect of Number of Blades on Turbine Efficiency.

maintain a constant slope, is considered the optimum number of blades for this turbine. But, the derived curve has no abrupt change in slope so that pinpointing the exact optimum number of blades is rather difficult. However, the curve shows that the optimum lies between 15 to 30 blades. More than 30 blades is considered not practical because of the closeness of the blades on a 6-inch runner. Figure 6.18 helps clarify the problem. The optimum number of blades should be around 20.

#### Comparison of Theoretical and Empirical Turbine Efficiencies

Table XXIII shows a comparison of the empirical efficiency equation and the theoretical turbine efficiency equations derived by previous researchers. The theoretical turbine efficiency equations were calculated from Equations 2.1, 2.16, 2.3, 2.27 and 2.33 and the empirical efficiency was calculated from Equation 6.37. It is obvious that the empirical efficiency equation has the lowest values. Efficiency losses on the constructed turbine were due to leakage between nozzle and runner. Not all of the water entered the turbine runner. On the other hand, much power was lost due to friction in the brakes during power measurement. Other losses were due to construction quality of the blades and the runner as a whole.

TABLE XXIII  
 COMPARISON OF TURBINE EFFICIENCIES  
 FROM THEORETICAL AND EMPIRICAL  
 FORMULAS AT N=300 RPM

Number of Blades	Supply Flow Rate $\frac{Q}{S}$ (gpm)	Mockmore & Merryfield's Efficiency $E_M$ (%)	Durali's Efficiency $E_D$ (%)	Haimerl's Efficiency $E_H$ (%)	Predicted Efficiency $E_P$ (%)
6	400	87.20	96.32	83.41	28.81
10	400	87.20	96.32	83.41	33.26
10	500	87.69	74.79	64.77	35.17
15	400	87.20	96.32	83.41	37.28
15	500	87.69	74.79	64.77	39.42
20	400	87.20	96.32	83.41	40.42
20	500	87.69	74.79	64.77	42.74
30	400	87.20	96.32	83.41	45.29
30	500	87.69	74.79	64.77	47.90

## CHAPTER VII

### CONCLUSIONS AND RECOMMENDATIONS

The entire experiment demonstrated that a low-cost crossflow water turbine can be constructed from available discarded materials which in this case were aluminum. Thus, the turbine runner was sized based on the strength properties of aluminum. Because the turbine was to be constantly under stress, a 1/8-inch thick plate was used as blade and a 1-inch-diameter shaft was used to withstand centrifugal and other forces. On the other hand, the nozzle and its adaptor were constructed out of a 1/16-inch plate. Although the runner was only six inches in diameter, the 20-blade runner could easily attain 50 percent efficiency. Its maximum power potential, however, was not fully investigated because of operation problems which prevented the turbine from being tested at higher flow rates. An alarming threatening sound prevented increasing the flow rate beyond the design value of 500 gpm. Likewise brake pads burned quickly at high flow rates. Nevertheless, the 6-inch turbine prototype can be expected to deliver power of about 0.3 hp.

Of the five runners tested, the 20-blade runner appeared to be the most efficient. A further increase of

the number of blades did not proportionately increase turbine efficiency to a significant degree. On the other hand, all runners exhibited generally constant efficiency as flow rate was increased. Moreover, the optimum rotative speed increased as number of blades was increased. Increasing the flow rate set the optimum rotative speeds to higher levels as well. It may be of note also that some static pressure was present at the nozzle tip.

The empirical prediction equation for power and efficiency was developed for the actual performance of the crossflow turbine prototype in the field (Equations (6.36) and (6.37)). The inclusion of a new variable, the number of blades  $Z$ , in the prediction formula introduced some effect of this variable to the entire turbine performance equation. The usefulness of Equations (6.36) and (6.37), however, is limited only to 6-inch diameter runners with the same nozzle and runner size and geometry as the one tested. However, a proportionately bigger size turbine can be designed using the pi terms and the prediction equation as bases. A bigger turbine would undoubtedly give more power but it will likely have the same efficiency unless the scale factor is altered on some variable or variables. For example, using the same 1/8-inch blade thickness in the design of a bigger turbine would increase efficiency as well as power. On the other hand, a widely applicable prediction equation may be developed by increasing the number of variables in the equation. Thus, variables

such as nozzle entry angle, nozzle throat width, nozzle position, and runner diameter may be investigated and incorporated in the prediction equation.

A comparison of the empirically developed equation with theoretical efficiency equations produced wide differences of efficiency values. While the theoretical efficiencies were about 80 to 90 percent, the actual efficiency was only half that much. This is not surprising because many factors are involved during on-site test runs that are difficult to control as compared to assumptions developed theoretically or when the equation is developed under laboratory conditions. Heat build-up in the Prony brake was manifested by the crackling sound of water droplets when it splattered on the very hot surface of the shaft steel bushing where the brake meshes. A makeshift oil-cooling system was installed to help absorb the heat and minimize the occurrence of burning brake pads. Indeed a more efficient and appropriate Prony brake is recommended for future power measurements. Also, construction quality of the nozzle has to be improved to minimize water leakage between nozzle and runner and to minimize water turbulence.

Significantly, the crossflow turbine is an attractive choice as an alternative source of energy for rural tropical families. The turbine's low cost (using readily available discarded materials), the simplicity of its design, and the ease by which available materials can be substituted for its construction make this water turbine

ideal to provide electrical power to many rural families that have until now never enjoyed the luxury of even a single incandescent bulb.

Although this turbine is not the sole panacea to the vexing dilemma of the rural poor, it can provide a multiplier effect or even a light hope to one's perplexing fate. Hence, a crossflow water turbine with appropriate improvements should be introduced to rural areas in developing countries.

## BIBLIOGRAPHY

- Alward, R., S. Eisenbart and J. Volkman. Micro-Hydro Power: Reviewing an Old Concept. Washington, D. C.: U.S. Department of Energy, 1979.
- Arndt, R. E. A., C. Farrell and V. M. Wetzel. Hydraulic Turbines: Small and Mini Hydropower Systems. New York: McGraw Hill Book Co., 1984.
- Balje, O. E. Turbomachines: A Guide to Design Selection and Theory. New York: John Wiley & Sons Inc., 1981.
- Binder, R. C. Advanced Fluid Dynamics and Fluid Machinery. New York: Prentice-Hall, 1951.
- Clary, B. L. and G. L. Nelson. "Determining Convective Heat Transfer Coefficients from Ellipsoidal Shapes." Transactions of the ASAE, Vol. 13, No. 3, 1970, pp. 309-314.
- Doebelin, Ernest O. Measurement Systems: Application and Design. New York: McGraw-Hill Book Company, 1975.
- Durali, M. Design of Small Water Turbines for Farms and Small Communities. Cambridge, Massachusetts: Massachusetts Institute of Technology, Technology Adaptation Program Report 76-1, Spring 1976.
- Energy for Rural Development: Renewable Resources and Alternative Technologies for Developing Countries. Washington, D. C.: National Academy of Sciences, 1976.
- Gottfried, Byron S. Programming with Basic. 2nd Ed. New York: McGraw-Hill Book Company, 1982.
- Haimerl, L. A. "The Cross-Flow Turbine." Water Power, January 1960, pp. 5-13.
- Holman, J. P. Experimental Methods for Engineers. New York: McGraw-Hill Book Company, 1971.
- Inversin, Allen R. "Micro-Hydropower in Developing Countries." Alternative Sources of Energy, June/July 1986, pp. 33-36.



- Johnson, William F. "New Found Power Model and Material Testing Yields Results." Alternative Sources of Energy, May/June 1984, pp. 40-41.
- Johnson, W., R. Ely and F. White. "Design and Testing of an Inexpensive Crossflow Turbine." ASME Symposium on Small Hydro-Power Fluid Machinery, 1982, pp. 129-133.
- Langhaar, H. L. Dimensional Analysis and Theory of Models. New York: John Wiley and Sons, 1951.
- McGuigan, D. Harnessing Water Power for Home Energy. Charlotte, Vermont: Garden Way Publishing Co., 1978.
- Mockmore, C. A. and F. Merryfield. "The Banki Water Turbine." Oregon State University: Engineering Experiment Station, Bulletin No. 25, 1949.
- Mosonyi, Emil. Water Power Development: High-Head Power Plants. Vol. II. 2nd English Ed. Budapest: Akademia Kiado. 1965.
- "Mother's Microhydroelectric." Mother Earth News. January/February 1985, pp. 92-96.
- Murphy, G. Similitude in Engineering. New York: Ronald Press Co., 1950.
- Nakase, Y., J. Fukutomi, T. Watanabe, T. Suetsugu, T. Kubota and S. Kushimoto. "A Study of Cross-Flow Turbine (Effects of Nozzle Shape on its Performance)." ASME Symposium on Small Hydro-Power Fluid Machinery, 1982, pp. 13-18.
- Parker, Jerald D., J. H. Boggs and E. F. Blick. Introduction to Fluid Mechanics and Heat Transfer. Massachusetts: Addison-Wesley Publishing Company, Inc., 1970.
- Shepherd, D. G. Principles of Turbomachinery. New York: The MacMillan Co., 1956.
- Simeons, C. Hydro-Power: The Use of Water as an Alternative Source of Energy. 1st Ed. Oxford: Pergamon Press, 1980.
- Stapenhorst, F. W. E. "The Ossberger Cross-Flow Turbine." ASME Symposium on Small Hydro-Power Fluid Machinery, 1980, pp. 13-18.

Supplement to Energy for Rural Development: Renewable Resources and Alternative Technologies for Developing Countries. Washington, D. C.: National Academy Press, 1981.

Turner, Wayne C. (Ed.). Energy Management Handbook. New York: John Wiley & Sons, Inc., 1982.

Volkman, John and Bill Eastlake. The Idaho Micro Hydro Handbook. Boise, Idaho: The Idaho Department of Water Resources.

✓  
VITA

Alejandro F. Tongco

Candidate for the Degree of

Doctor of Philosophy

Thesis: FIELD TESTING OF A CROSSFLOW WATER TURBINE

Major Field: General Engineering

Biographical:

Personal Data: Born in Baybay, Leyte, Philippines, August 1, 1949, the son of Baltazar D. Tongco and Marcionila Fernandez Tongco (deceased). Married to Adeltrudis Cruz Tongco. Two children, Tara and Brent.

Education: Graduated high school from Franciscan College of the Immaculate Conception, Baybay, Leyte, Philippines in 1965; received Bachelor of Science degree in Mechanical Engineering from Colegio de San Jose-Recoletos, Cebu City, Philippines in 1973; received Master of Science degree in Agricultural Engineering from the University of the Philippines at Los Banos, Philippines in 1979; completed requirements for the degree of Doctor of Philosophy at Oklahoma State University in July, 1988.

Professional Experience: Methods Analyst, Paper Industries Corporation of the Philippines, Surigao del Sur, Philippines, 1973 to 1975. Instructor, Visayas State College of Agriculture, Baybay, Leyte, Philippines, 1976-1979. Teaching Assistant, Oklahoma State University, 1985-1987.